Chapter 3: X-ray Radiography and Computer Tomography

X-ray Physics

X-ray Physics

X-ray Generation – X-ray Tube

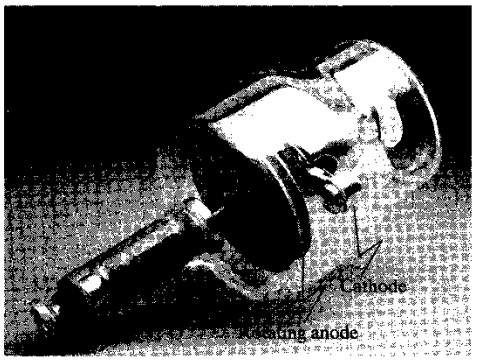

Figure 5.3
An x-ray tube.

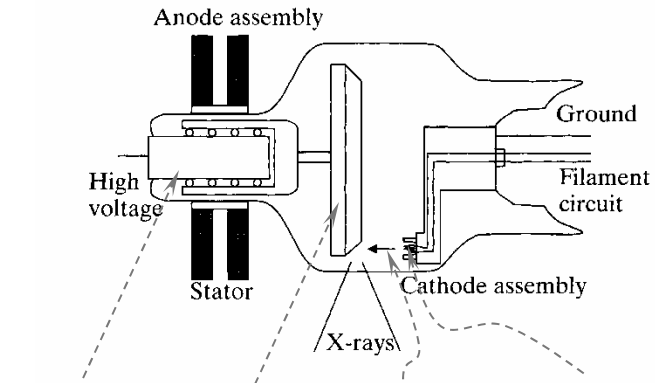

Figure 5.4
Schematic diagram of an x-ray tube.

Motor, Why?

Rotating target

Filament

Electron beam? How are electrons generated?

X-ray Generation – Bremmstrahlung

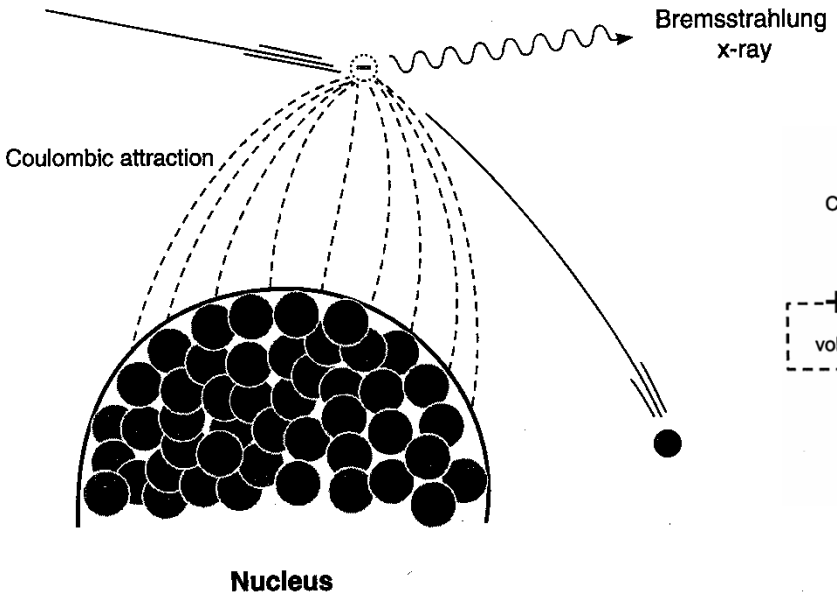

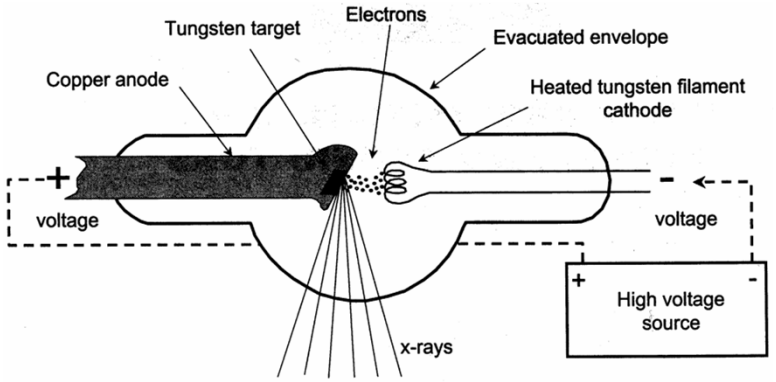

- X-rays are produced by the conversion of e^- KE into EM radiation - **Bremsstrahlung** (G: "braking radiation").
- A large potential difference is applied across the two electrodes in an evacuated envelope
- Neg. charged electrode (***cathode***): source of e^-
- Pos. charged electrode (***anode***): target of e^-

X-ray Generation – Characteristic X-rays

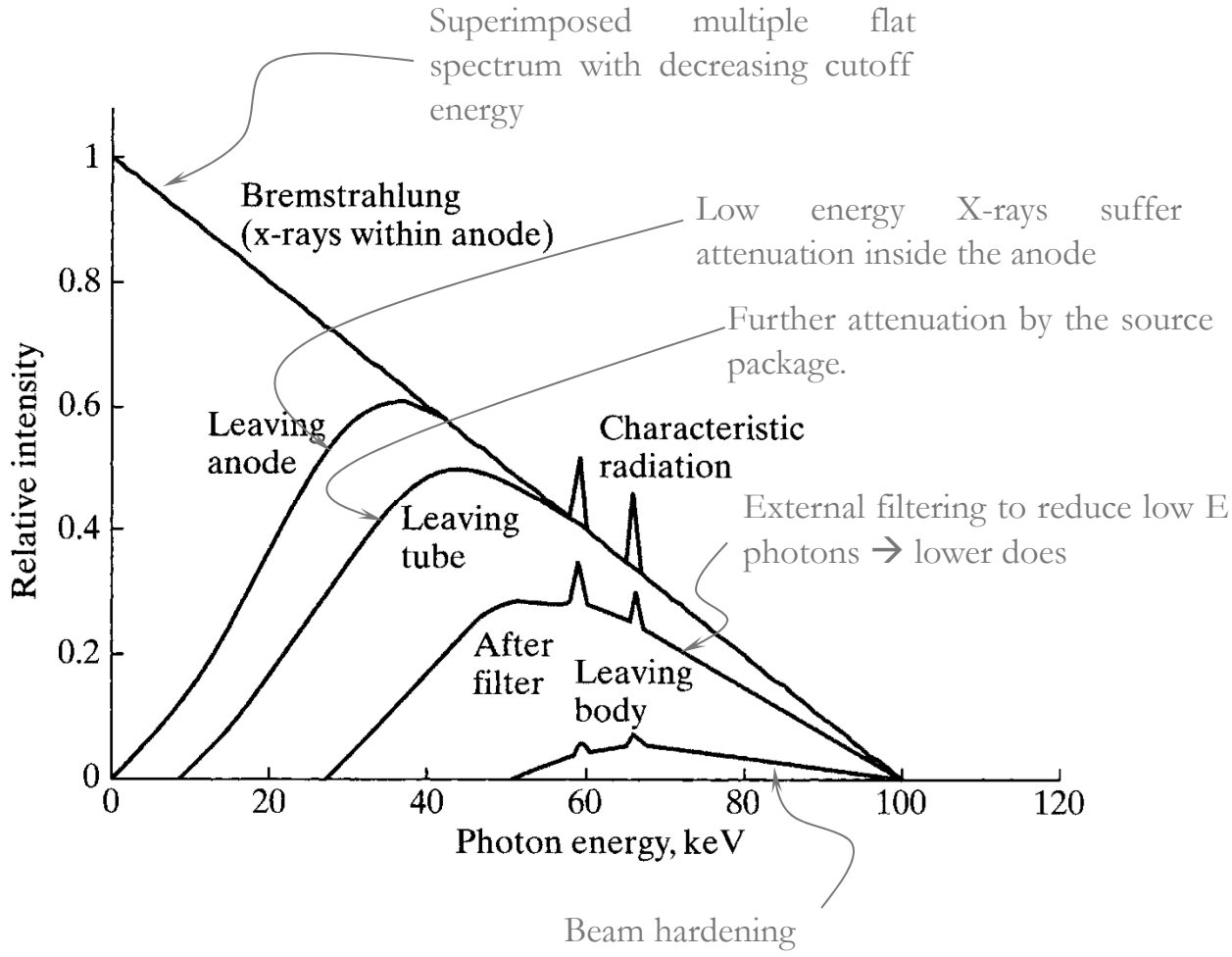

Figure 5.5
Relative intensity of x-ray photons. (Adapted from Webster, 1998. This material is used by permission of John Wiley & Sons, Inc.)

Compton Scattering

- ***Dominant interaction*** of x-rays with ***low-Z materials*** in the diagnostic range and beyond (approx. 30 keV - 30MeV)
- Occurs ***between the photon and a outer shell e$^-$***, which is considered free when E_g >> binding energy, E_b of the e$^-$.
- Encounter results in ***ionization of the atom*** and probabilistic distribution of the incident photon E to that of the scattered photon and the ejected e$^-$
- A probabilistic distribution determines the scattering angle.

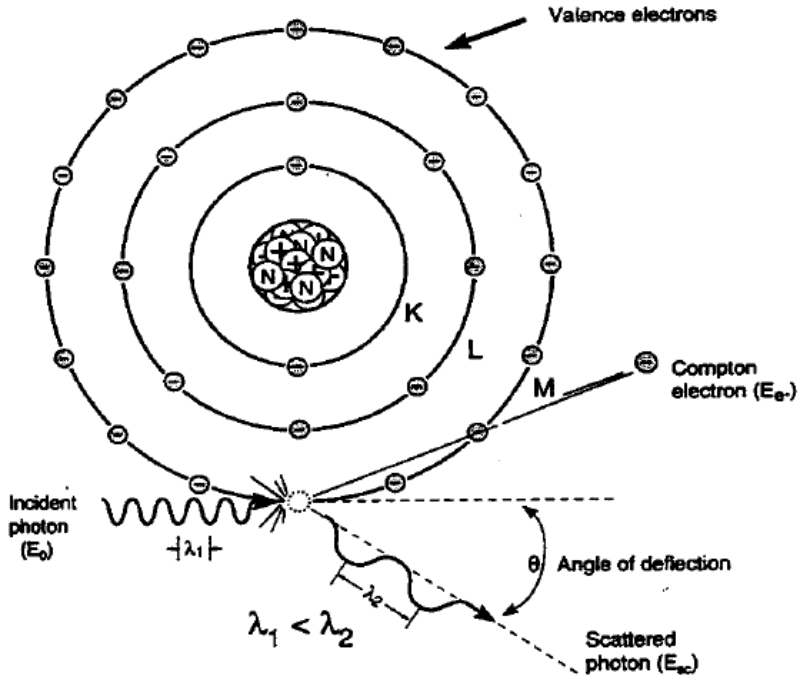

Compton Scattering

- Compton interaction probability is dependent on ***the total no. of e^- in the absorber vol.*** ($e^-/cm^3 = e^-/gm \cdot$ density) or ***electron density***
- With the exception of ^1H, e^-/gm is fairly constant for organic materials ($Z/A \cong 0.5$), thus the probability of ***Compton interaction proportional to material density (ρ)***
- ***Conservation of energy and momentum*** yield the following equations:

$$E_{h\nu'} = \frac{E_{h\nu}}{1 + \frac{E_{h\nu}}{m_e c^2}(1 - \cos\theta)},$$

where

$m_e c^2 = 511\text{keV}$

$E_{h\nu}$: energy of the incident photon

$E_{h\nu'}$: energy of the scattered photon

Photoelectric Effect

- Interaction of incident photon with ***inner shell e***$^-$, why?
- All E transferred to e^- (ejected ***photoelectron***) as kinetic energy (E_e) less the binding energy: $E_e = E_0 - E_b$
- ***Empty shell immediately filled with e***$^-$ ***from outer orbits*** resulting in the emission of characteristic x-rays (E_γ = differences in E_b of orbitals), for example, Iodine: E_K = 34 keV, E_L = 5 keV, E_M = 0.6 keV

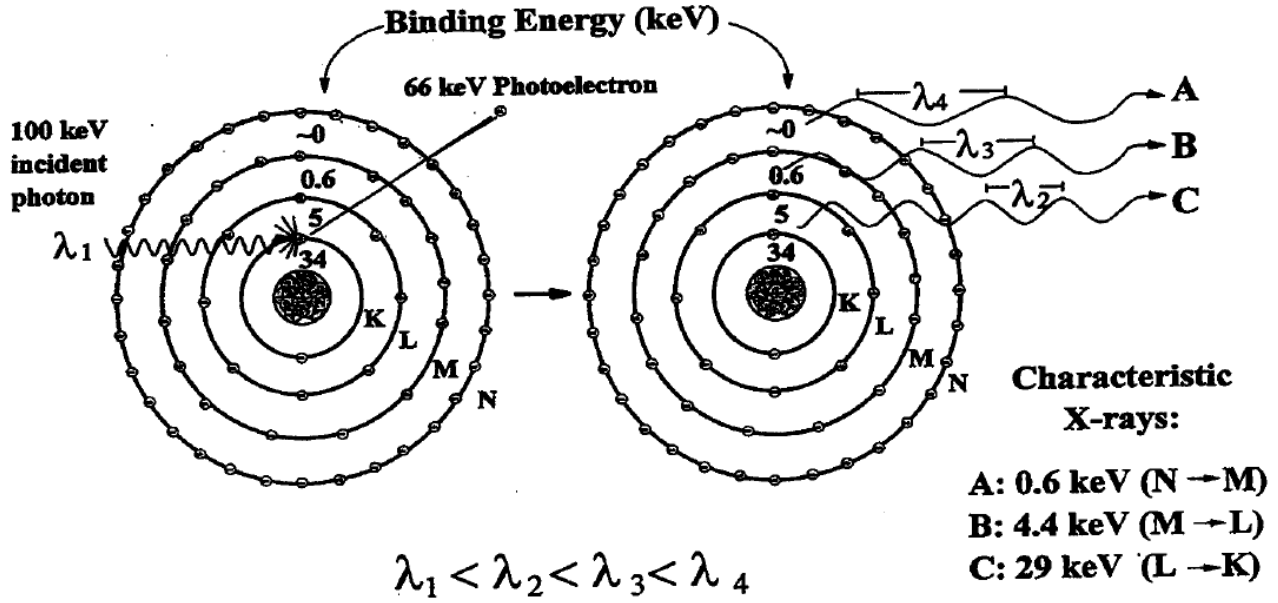

Photoelectric Effect

- Photoe$^-$ absorption is the preferred interaction for X-ray imging.
- Rem.: $E_b \propto Z^2$; characteristic x-rays and/or Auger e^- → ***preferred in high Z material***.
- Probability of photoe$^-$ absorption $\propto Z^3/E^3$ (Z = atomic no.) → ***provide contrast according to different Z***.
- Due to the absorption of the incident x-ray without scatter, maximum subject contrast arises with a photoe$^-$ effect interaction → ***No scattering contamination*** → better contrast
- Explains why contrast ↓ as higher energy x-rays are used in the imaging process
- Increased probability of photoe$^-$ absorption just above the E_b of the inner shells cause discontinuities in the ***attenuation profiles*** (e.g., K-edge)

Photoelectric Effect

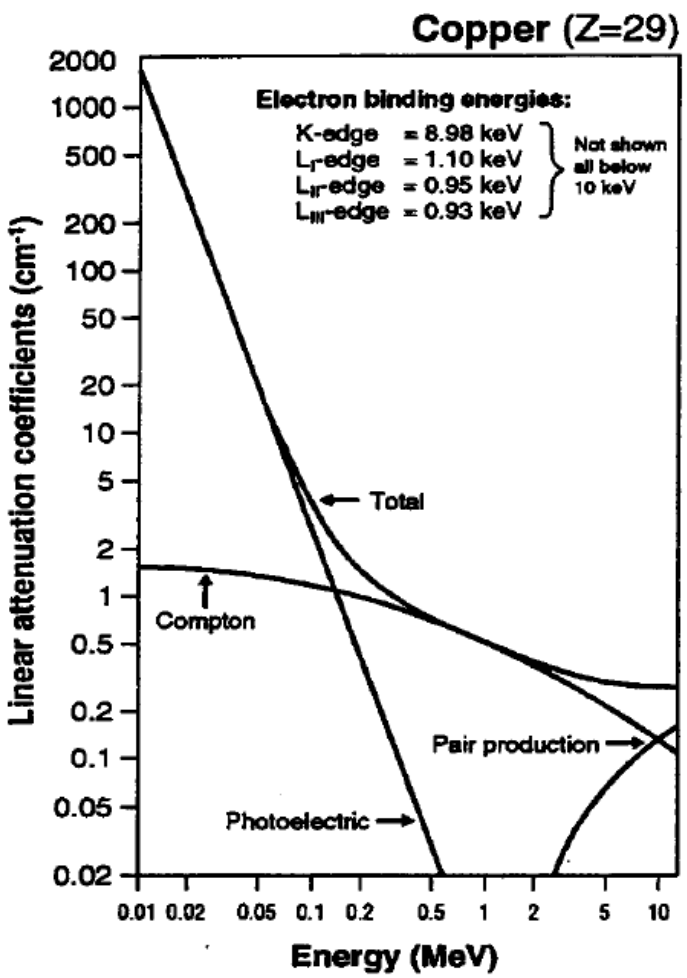

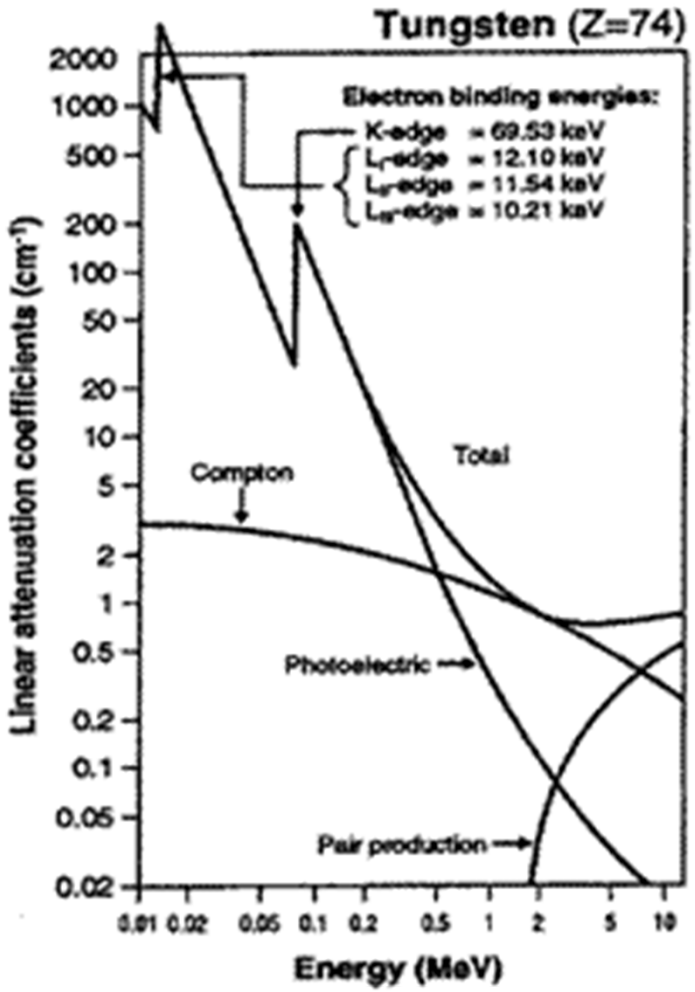

Attenuation Mechanism

- Attenuation mechanisms as a function of energy

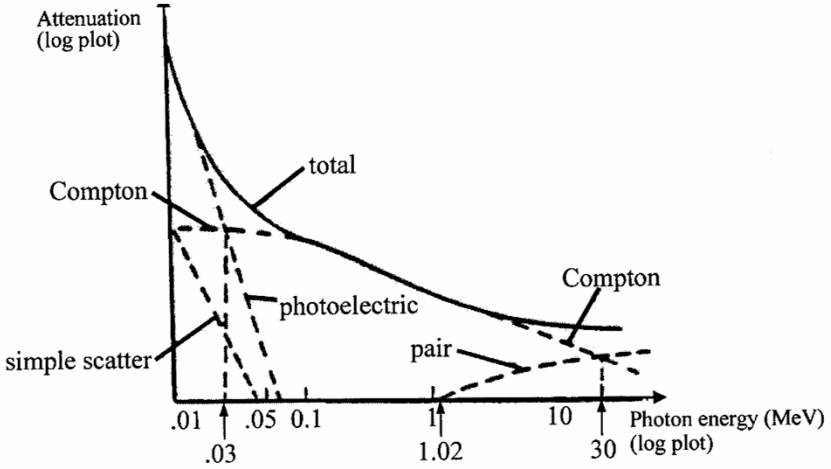

Attenuation mechanisms in water

The optimum photon energy is about 30 keV (tube voltage 80-100 kV) where the photoelectric effect dominates. The Z^3 dependence leads to good contrast:

Z_{fat}	5.9
$Z_{muscles}$	7.4
Z_{bone}	13.9

$\Rightarrow$ Photoelectric attenuation from bone is about 11x that due to soft tissue, which is dominated by Compton scattering.

Attenuation Mechanism

- Attenuation mechanisms as a function of energy

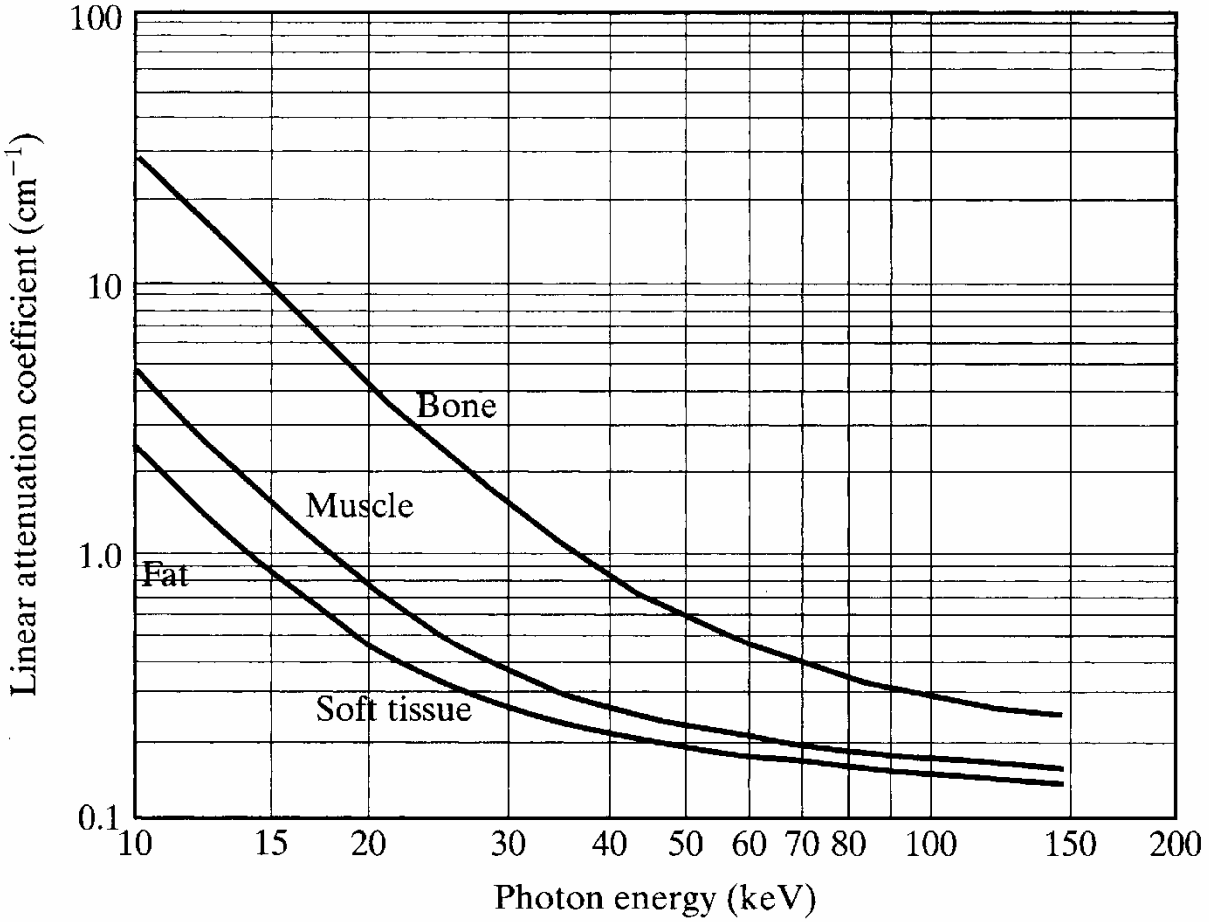

Figure 4.8
Linear attenuation coefficient for bone, muscle, and fat as a function of incident x-ray photon energy.

Photoelectric Effect

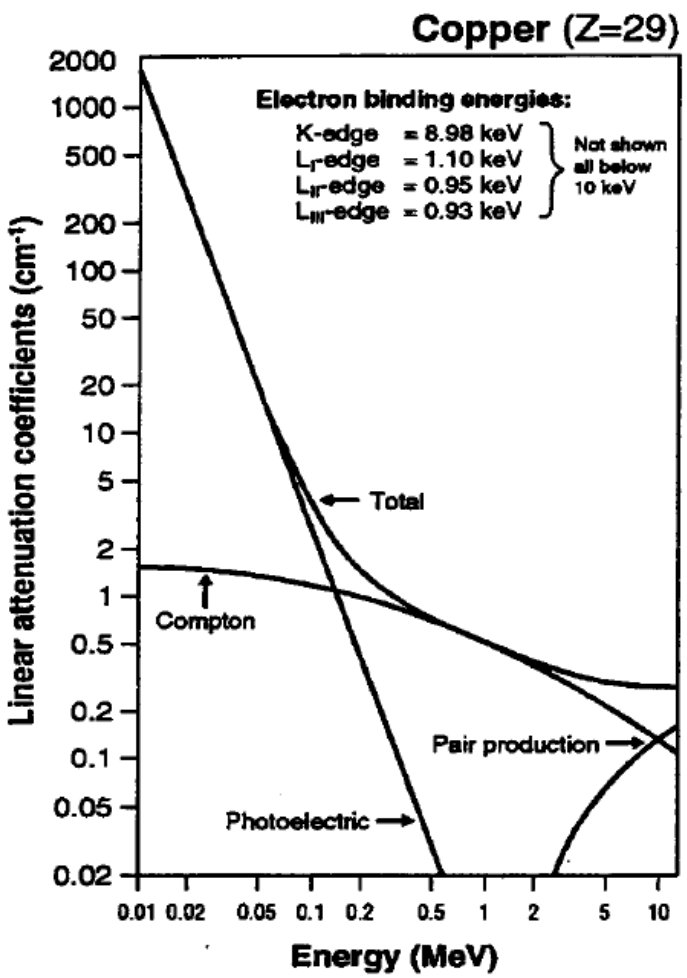

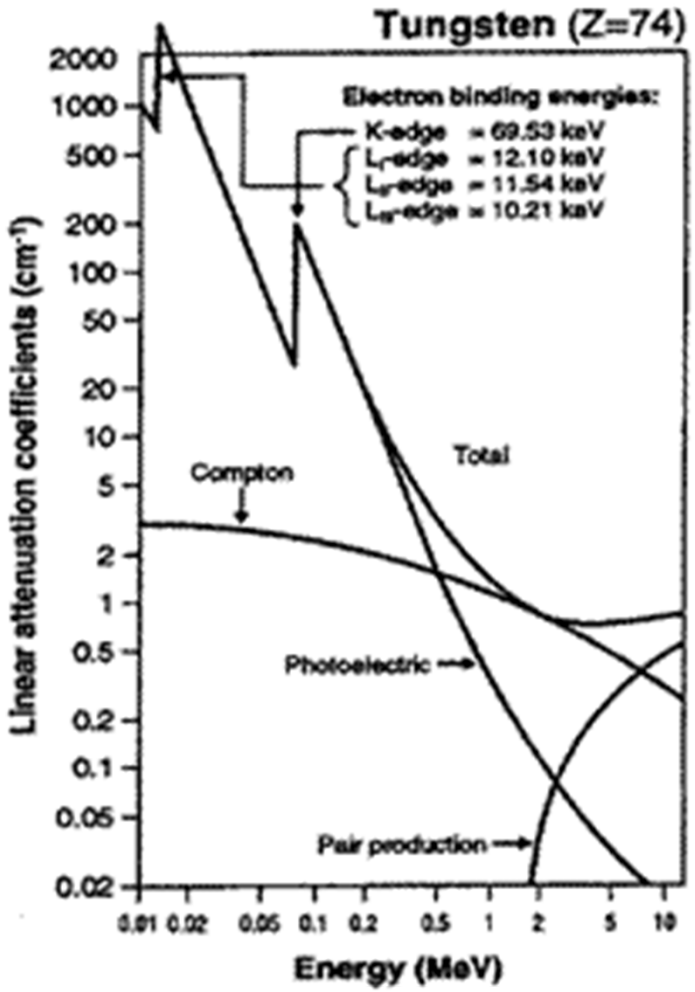

Beam Hardening Effect, Contrast Agents, and X-ray Filtration

X-ray Generation – Filtration

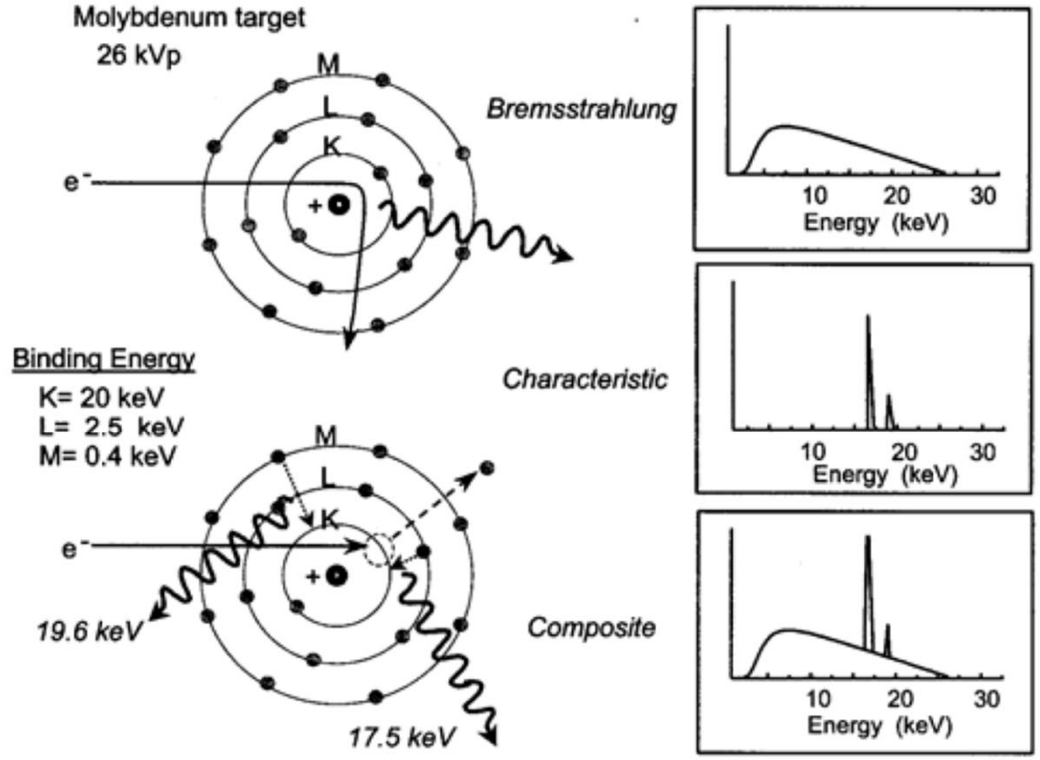

FIGURE 8-7. The output of a mammography x-ray system is composed of bremsstrahlung and characteristic radiation. The characteristic radiation energies of molybdenum (17.5 and 19.6 keV) are nearly optimal for detection of low-contrast lesions in breasts of 3- to 6-cm thickness.

Options:

Molybdenum (Mo)

Ruthenium (Ru)

Rhodium (Rh)

Palladium (Pd)

Silver (Ag)

Cadmium (Cd)

X-ray Generation – Filtration

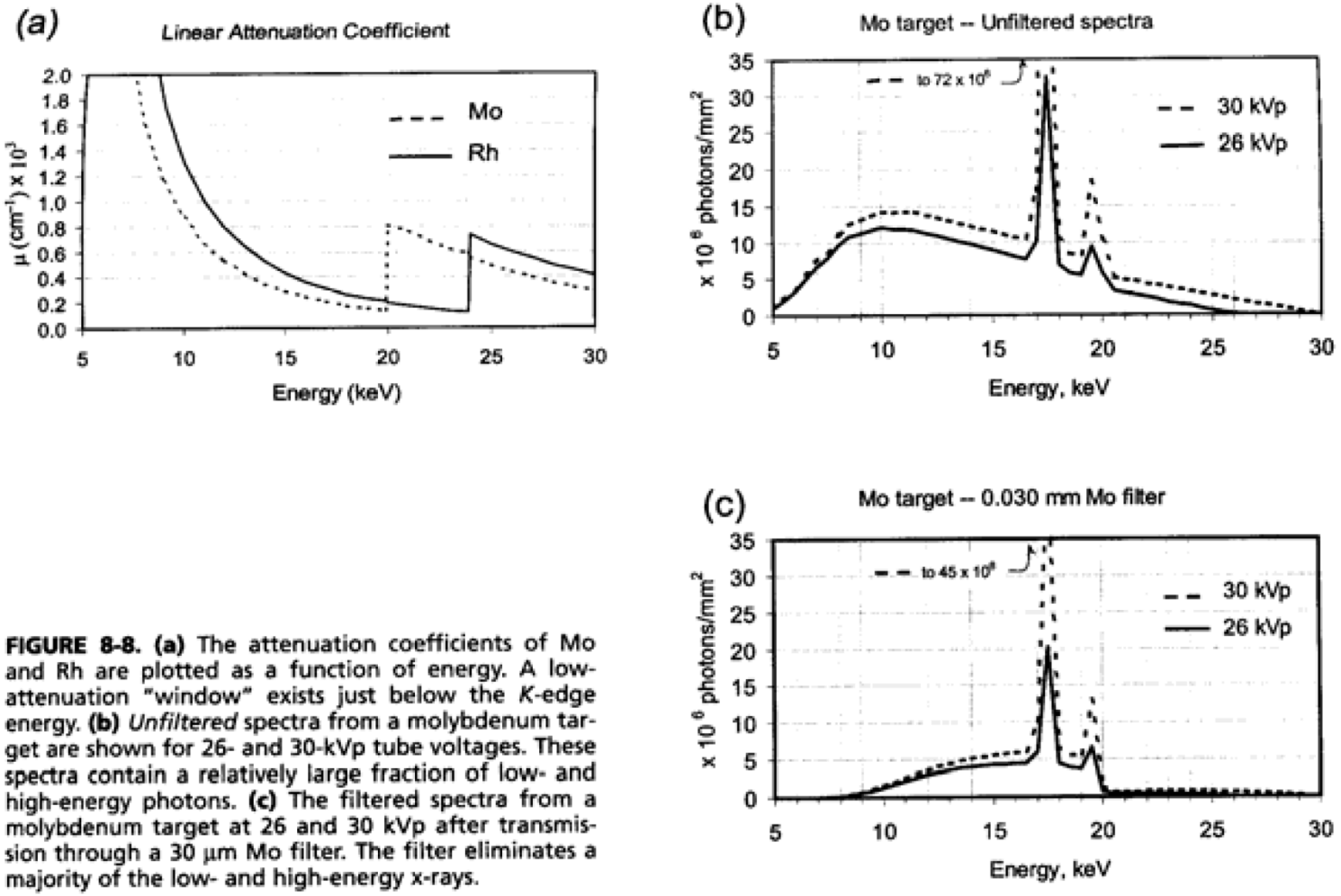

FIGURE 8-8. (a) The attenuation coefficients of Mo and Rh are plotted as a function of energy. A low-attenuation "window" exists just below the *K*-edge energy. **(b)** *Unfiltered* spectra from a molybdenum target are shown for 26- and 30-kVp tube voltages. These spectra contain a relatively large fraction of low- and high-energy photons. **(c)** The filtered spectra from a molybdenum target at 26 and 30 kVp after transmission through a 30 μm Mo filter. The filter eliminates a majority of the low- and high-energy x-rays.

X-ray Generation – Filtration

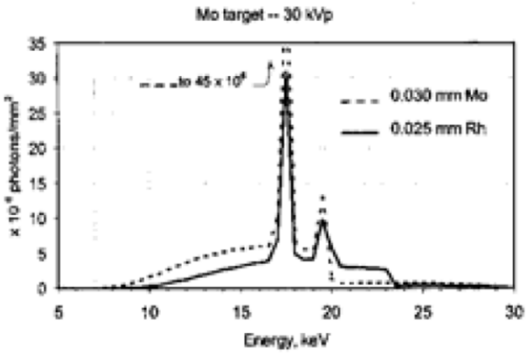

FIGURE 8-9. Output spectra from a Mo target for a 30-kVp tube voltage with a 0.030-mm Mo filter and 0.025-mm Rh filter show the relative bremsstrahlung photon transmission "windows" just below their respective *K*-edges.

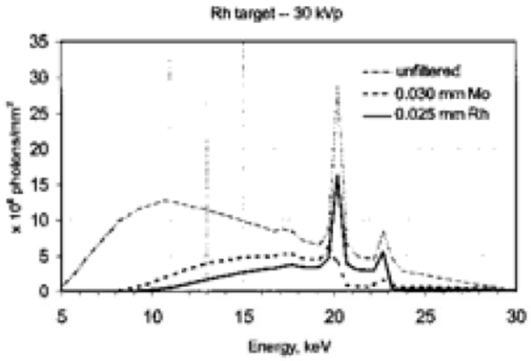

FIGURE 8-10. The rhodium target provides characteristic x-ray energies 2 to 3 keV higher than the corresponding Mo target. The unfiltered spectrum (*light dashed line*) is modified by 0.030-mm Mo (*heavy dashed line*) and 0.025-mm Rh (*solid line*) filters. A Mo filter with an Rh target inappropriately attenuates Rh characteristic x-rays.

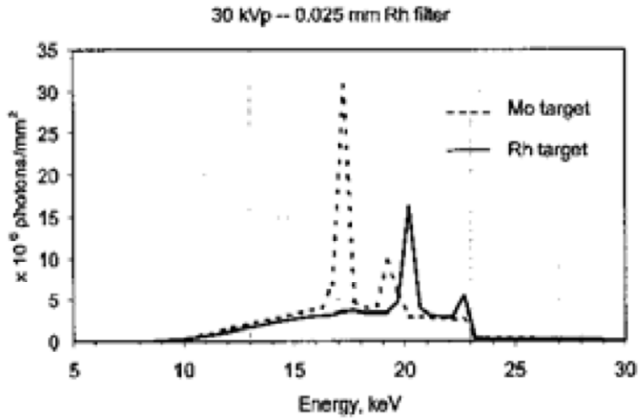

FIGURE 8-11. Spectra from beams filtered by 0.025 mm Rh are depicted for a Mo and an Rh target. The major difference is the higher energies of the characteristic x-rays generated by the Rh target, compared to the Mo target.

- filtering reduces the x-ray energy photons below the K-shell edge providing a transmission window for characteristic x-rays.

typical values – Mo target with 0.03 mm Mo filter (Mo/Mo)

- Rh target with 0.025 mm Rh filter (Rh/Rh)
- Mo target with Rh filter
- note: cannot use Rh target with Mo filter!

Ref: Bushberg

Photoelectric Effect and Absorption Edge

- Edges become significant factors for higher Z materials as the E_b are in the diagnostic energy range:
- **Contrast agents** – barium (Ba, Z=56) and iodine (I, Z=53)
- Rare earth materials used for intensifying screens – lanthanum (La, Z=57) and gadolinium (Gd, Z=64)
- **Computed radiography** (CR) and **digital radiography** (DR) acquisition – europium (Eu, Z=63) and cesium (Cs, Z=55)
- Increased absorption probabilities improve subject contrast and quantum detective efficiency
- At photon **E << 50 keV**, the photoelectric effect plays an important role in **imaging soft tissue**, amplifying small differences in tissues of slightly different Z, thus improving subject contrast (e.g., in mammography)

Example of Contrast Agents

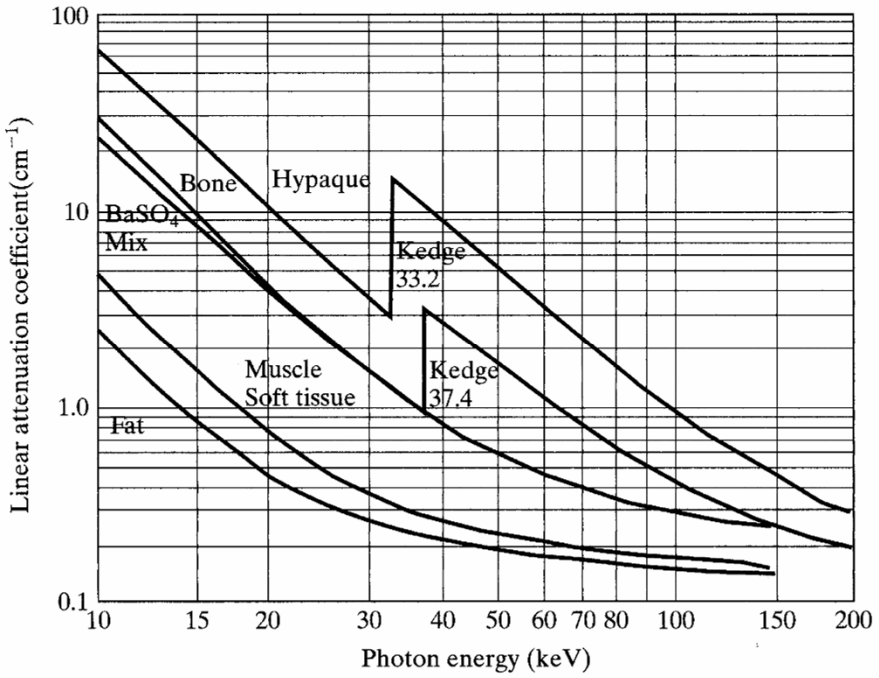

Figure 5.8
Linear attenuation coefficients of bone, muscle, fat, and two contrast agents. (From Johns and Cunningham, 1983.)

Bring out the difference between fat and soft tissues

X-ray Generation – Characteristic X-rays

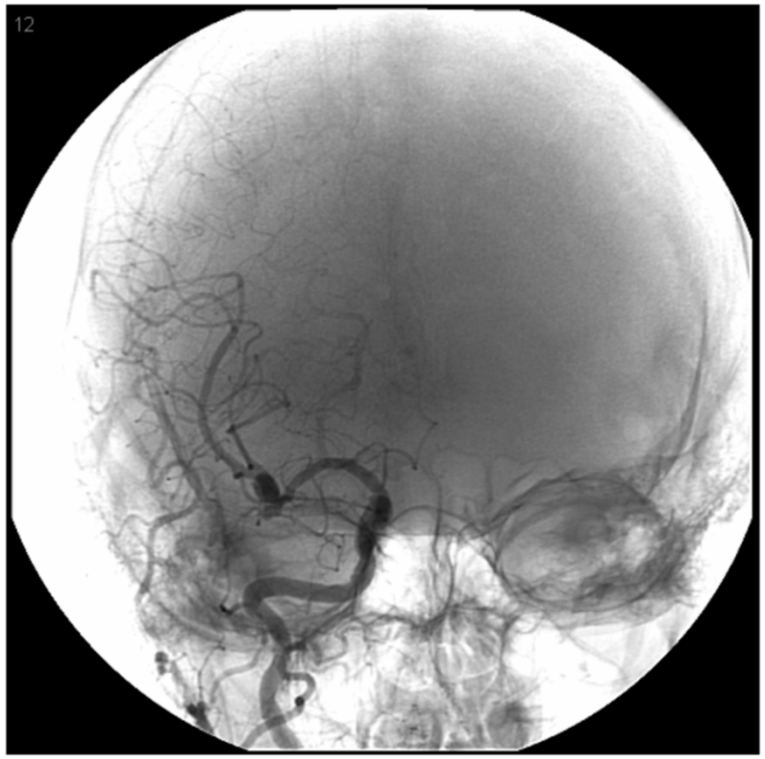

This is a mask image showing the background bone which obscures many of the smaller vessels.

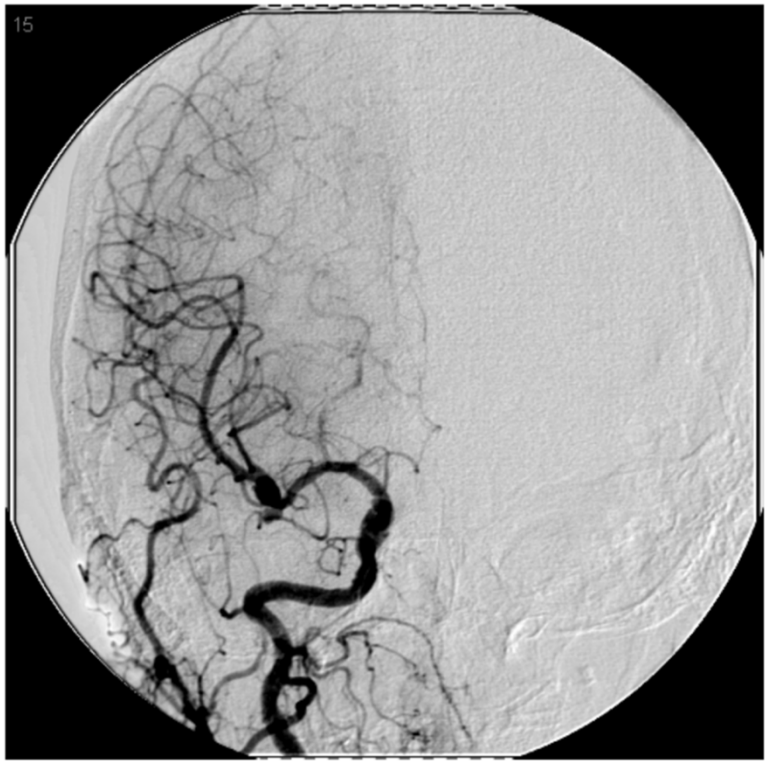

Subtracted image with the background details removed.

Both images from Bushberg et al. 2003

Beam Hardening Effect, Contrast Agents, and X-ray Filtration

X-Ray Detectors

- Film: sensitivity is very low, it would require too high a dose to the patient
- Film + screen: conventional radiography
- Image intensifier (I.I.): fluoroscopy
- Photosensitive phosphor (computed radiography)
- **Flat panel detectors**
- **Direct digital radiography (semiconductor)**

Roentgen's X-ray Setup (1895)

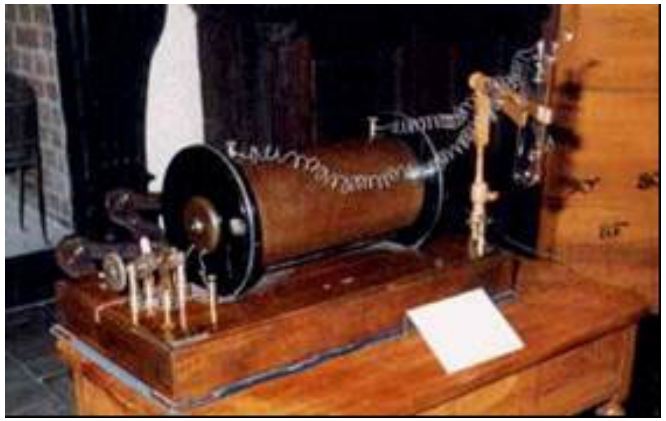

Roentgen's experimental apparatus (Crookes tube) that led to the discovery of the new radiation on 8 Nov. 1895 – he demonstrated that the radiation was not due to charged particles, but due to an as yet unknown source, hence "x" radiation or "x-rays"

German Museum, Munich

Known as "the radiograph of Bera Roentgen's hand" taken 22 Dec. 1895

X-Ray Film-screen Detectors

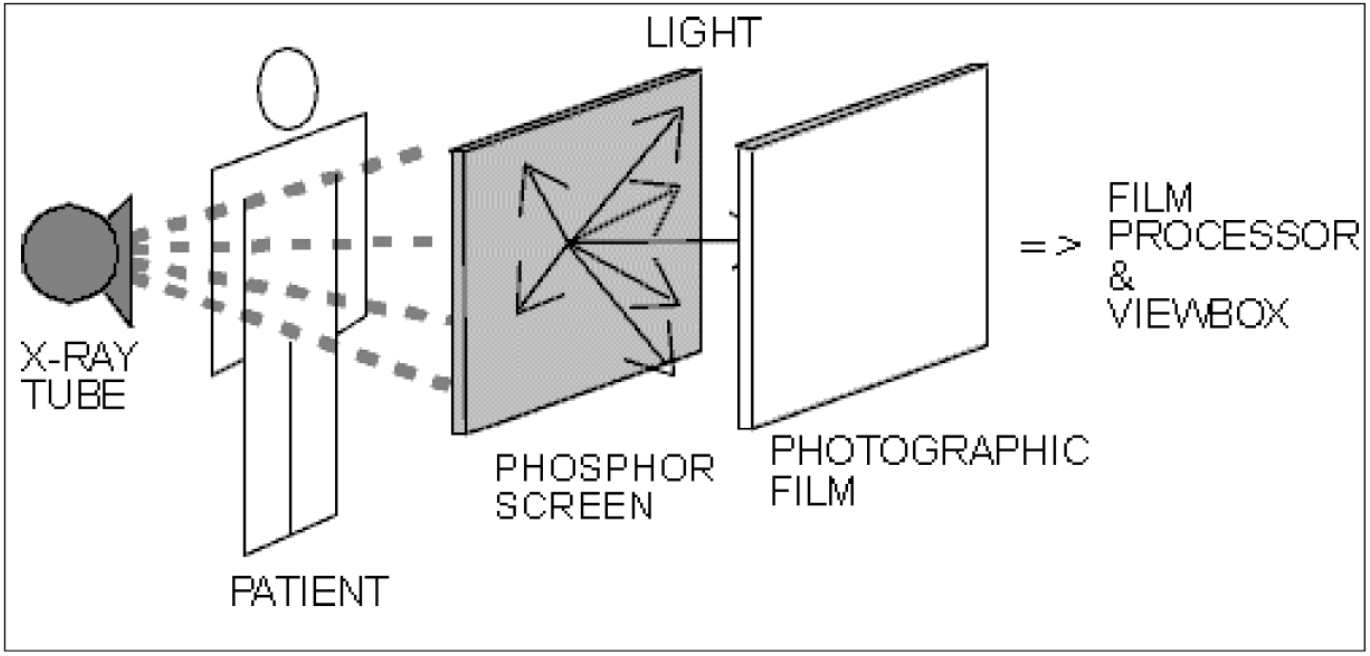

Film-Screen Radiography:

- Phosphor screen emits light in response to x-rays absorption.
- The resulting optical image is used to expose a photographic film

Currently most diagnostic radiographic systems (such as chest and breast imaging) are based on a phosphor screen.

X-Ray Film-screen Detectors

X-ray photons

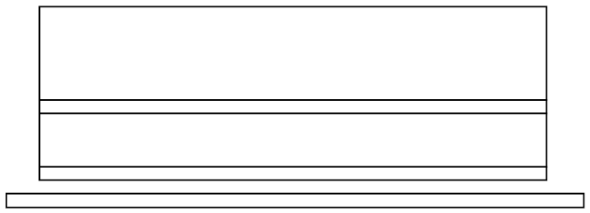

Substrate, 0.5 mm

Phosphor, 0.2 mm

Protective layer, 0.02 mm

Film

Screen Types: **$CaWO_4$, 430 nm blue**

Gd_2O_2S, 410 nm blue

Screen Sensitivity ~ thickness

Increased X-ray Absorption

=> more visible photons

Screen Resolution ~ 1/thickness

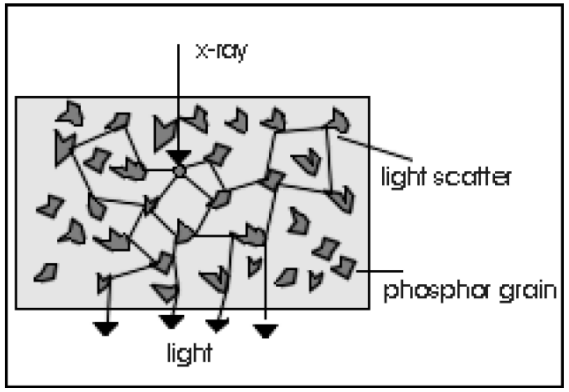

X-Ray Film-screen Detectors

Radiographic Cassettes

- Function: absorb x-rays, convert to visible or UV light which exposes the film emulsion
- Conversion efficiency of a phosphor = fraction of absorbed energy emitted as UV or visible light
- $CaWO_4$ ≈ 5% intrinsic conversion efficiency
- Gd_2O_2S:Tb ≈ 15% intrinsic conversion efficiency

  50,000 eV x-ray x 0.15 = 7500 eV

  Green light, 2.7 eV

  7500 eV / 2.7 eV/photon

  = 2,800 photons

- 200-1000 photons reach film after diffusing through phosphor layer and being reflected at the interface layers

1 X-ray photon => 20-100 silver particles to be developed.

X-ray film: dynamical range

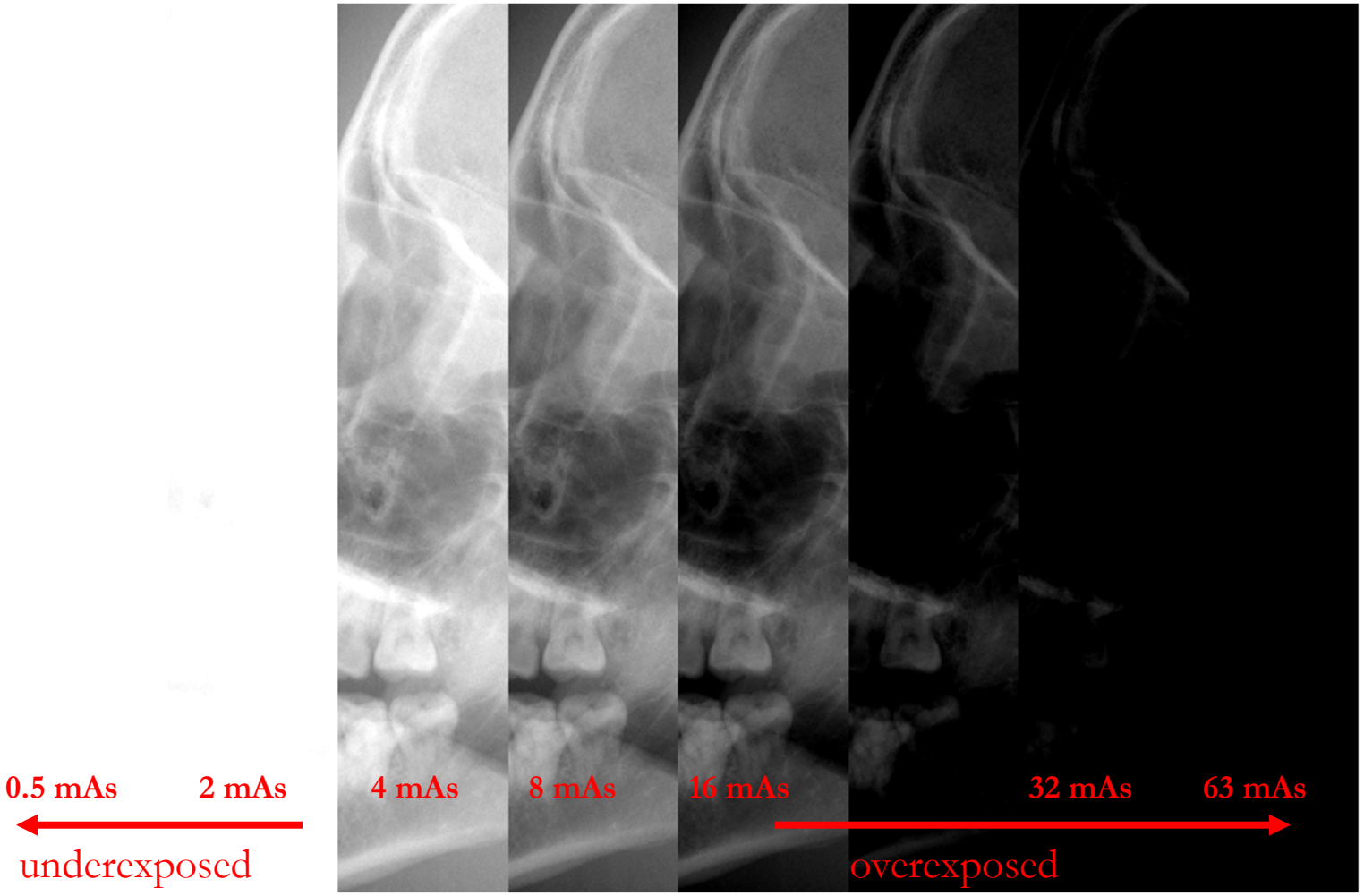

M. Overdick (PHILIPS), 11/09/2002, IWORID 2002, Amsterdam

Flat panel detector: dynamical range

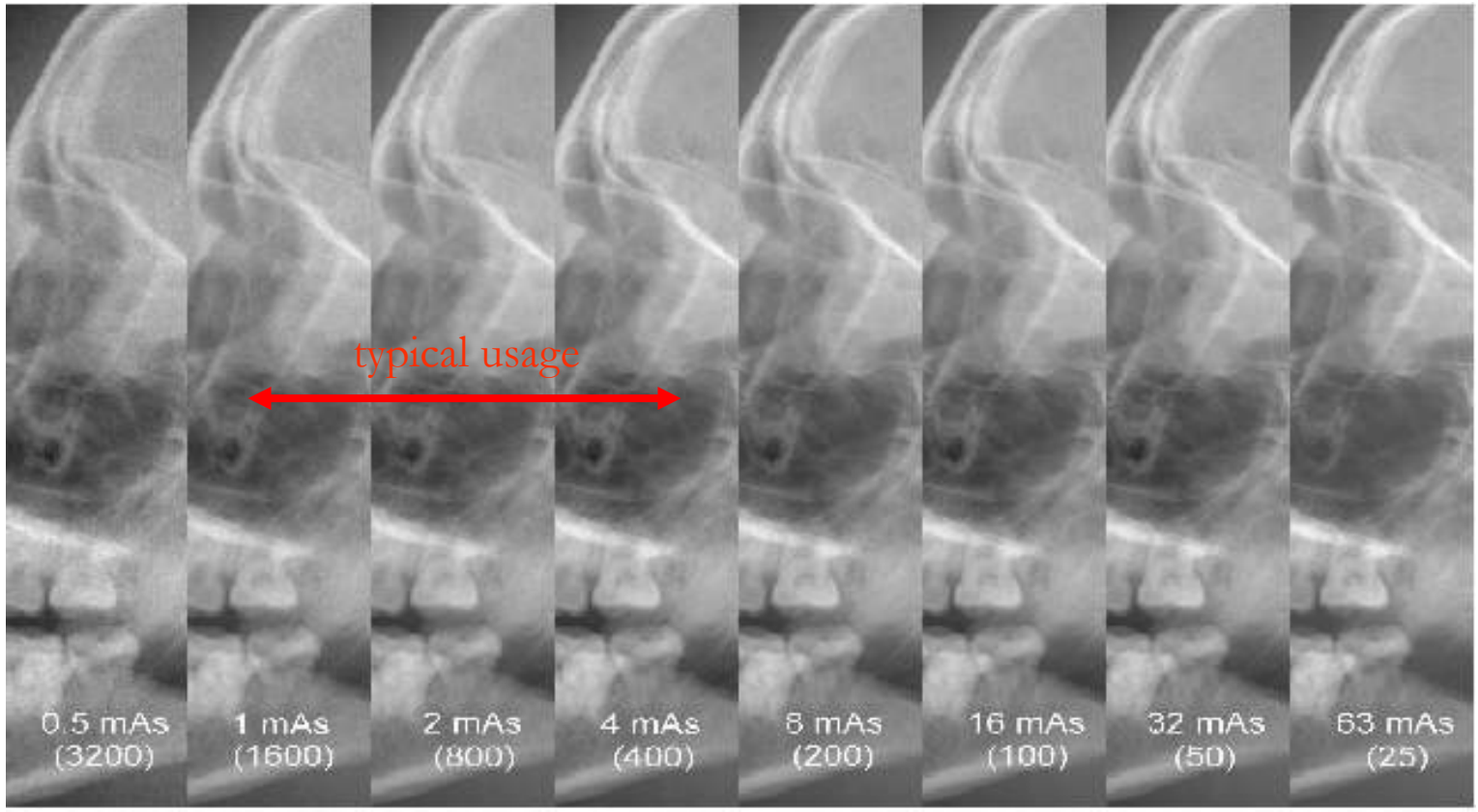

Digital Diagnost (PHILIPS) 43 cm x 43 cm, 143μm x 143 μm

M. Overdick (PHILIPS), 11/09/2002, IWORID 2002, Amsterdam

Image Plate based X-Ray Radiology

Digital X-ray image acquisition systems for projection radiography.

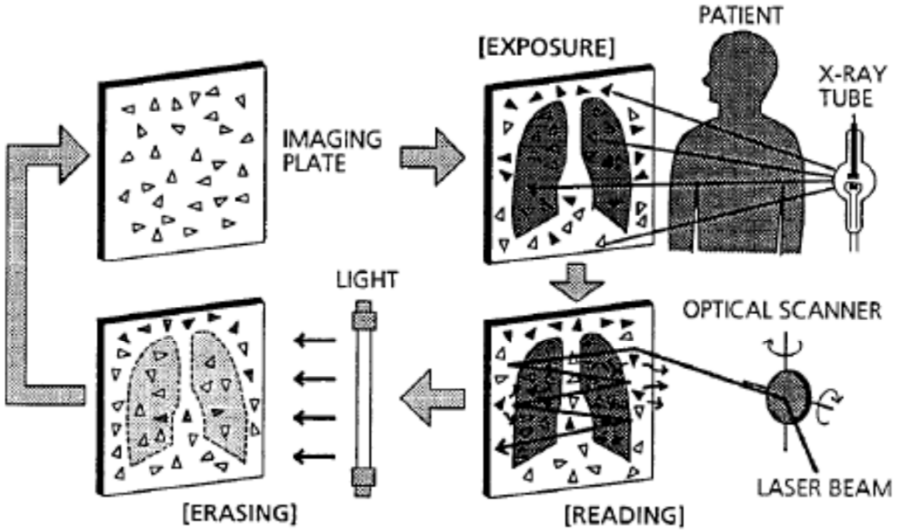

Stimulatable Phosphor System

- Imaging plate (stimulable phosphor) is exposed forming a latent image ("traps" in phosphor).
- latent image is read via laser scanning --> stored energy is released in form of "photostimulated luminescence light" proportional to the local X-ray exposure.
- The luminescence signal is converted to an electrical signal and is digitized.

Image Plate X-Ray Detector

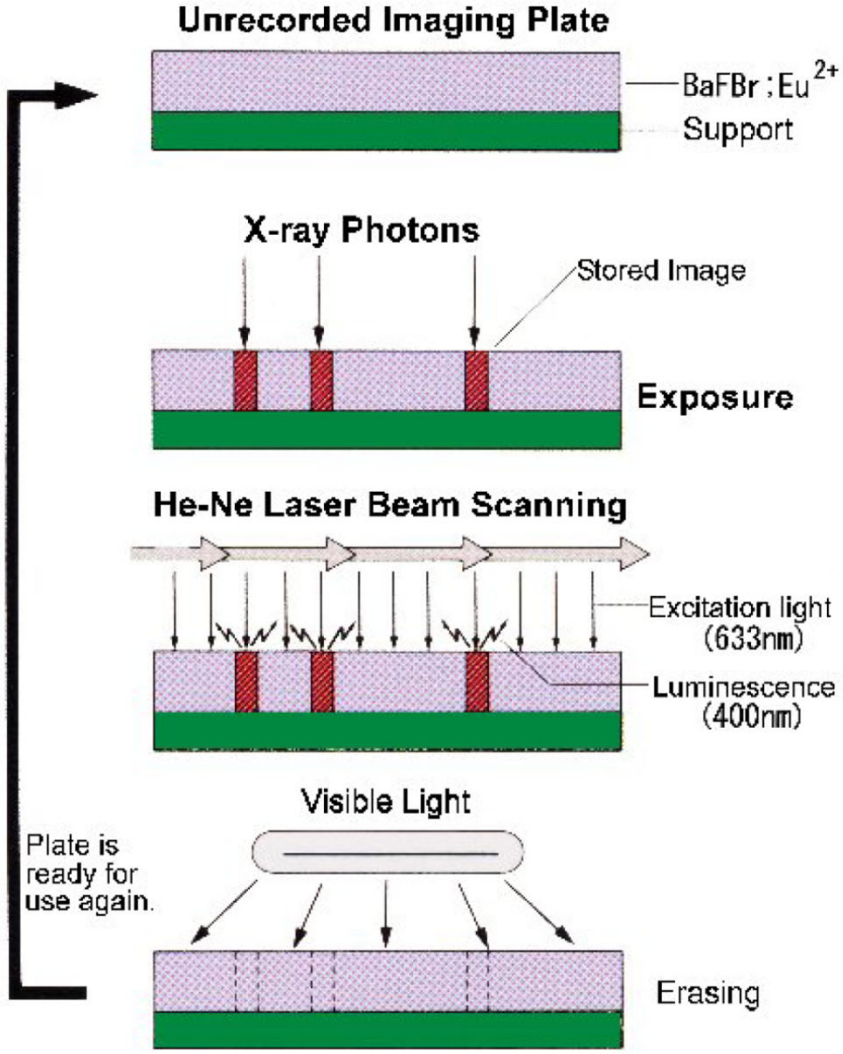

Image Plate X-Ray Detector

Success of CR:
– high dynamic range (> 104)
– digital nature
– easy to introduce
– relative low cost
– improvements for more than 25 years
– **but not for image or dose performances !**

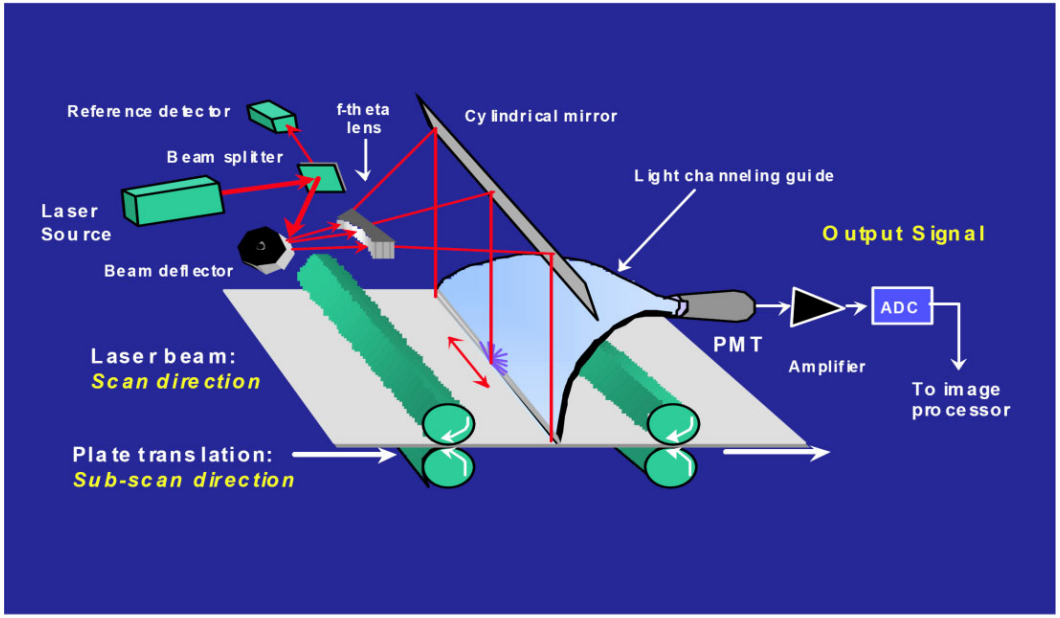

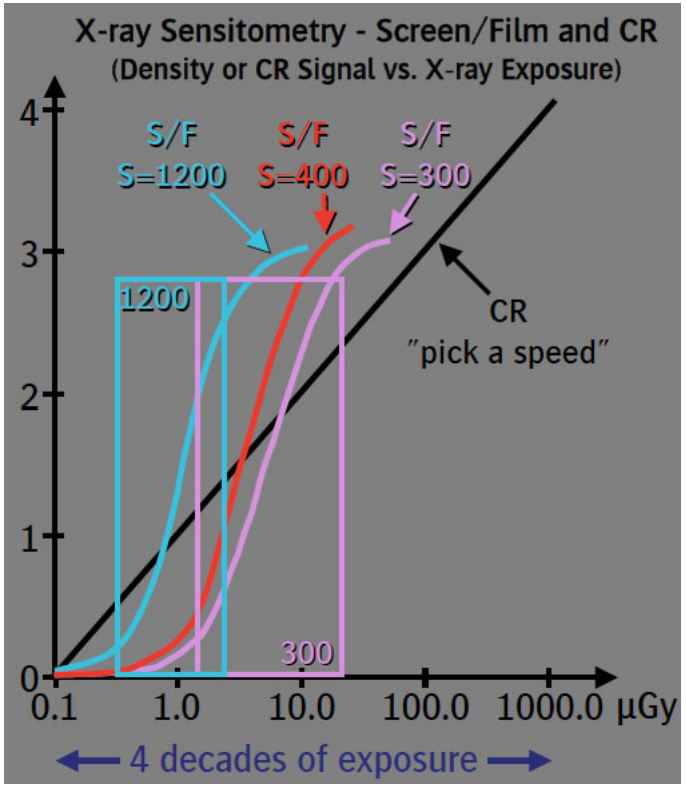

Limitation of Image Plate X-Ray Detector

Relatively small of "information carriers" created per x-ray photon.

— Low signal to noise ratio (SNR)

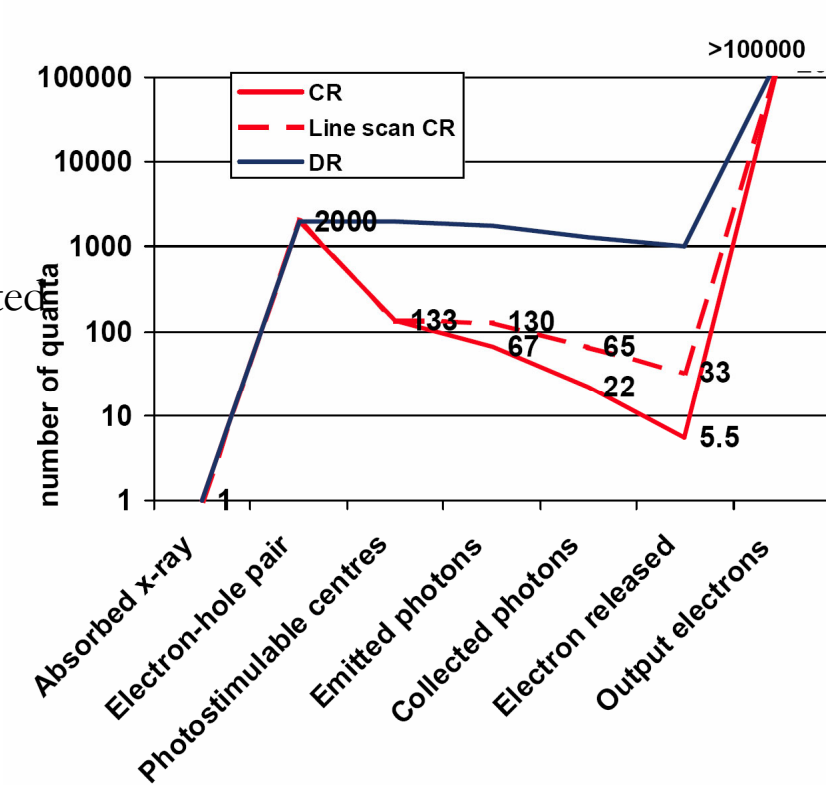

X-Ray Image Intensifier (X-ray II)

X-ray II is the standard detector for current projection radiography system

X-Ray Image Intensifier (X-ray II)

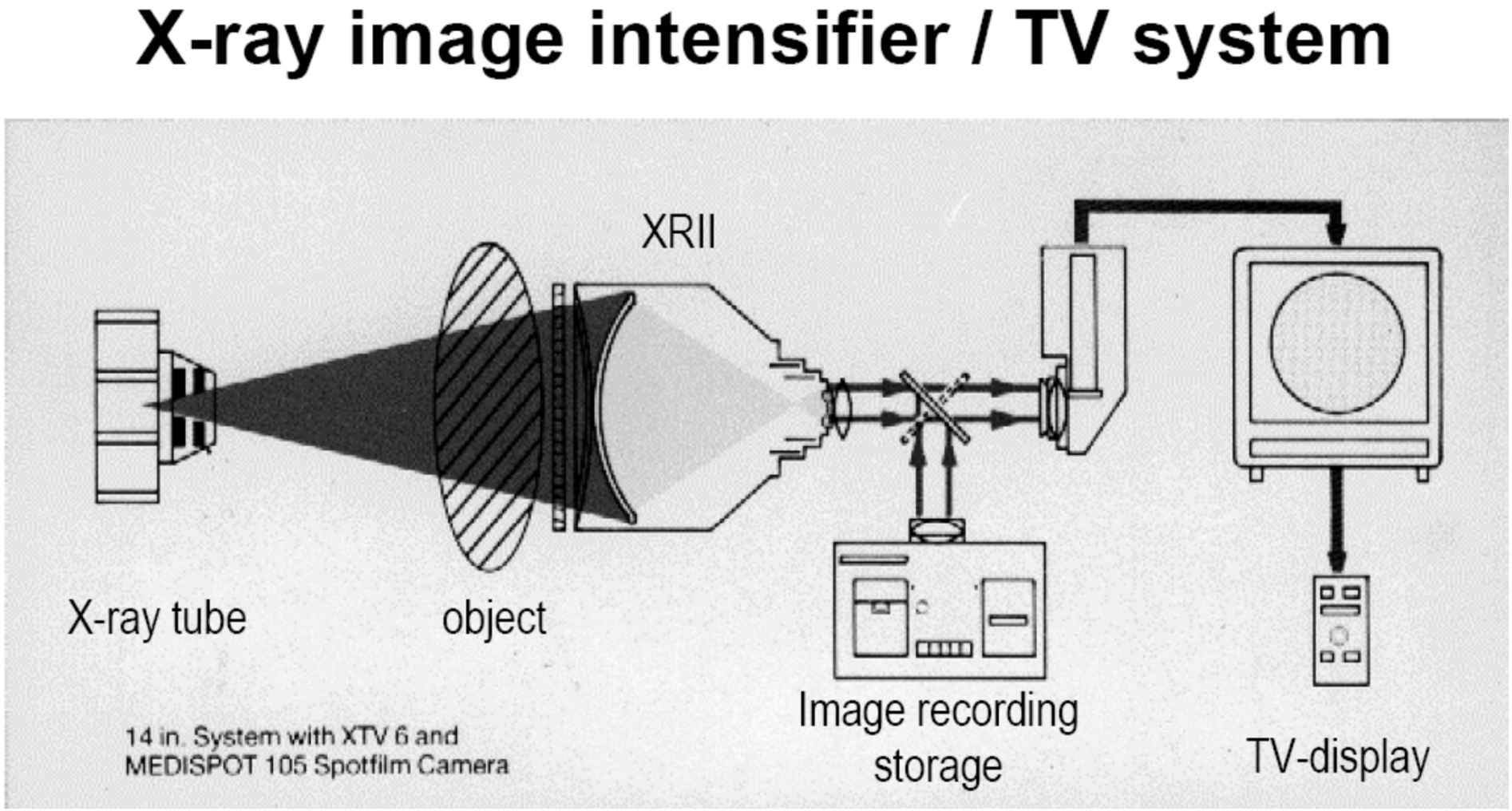

X-Ray Image Intensifier (X-ray II)

Principle Operation of XRII

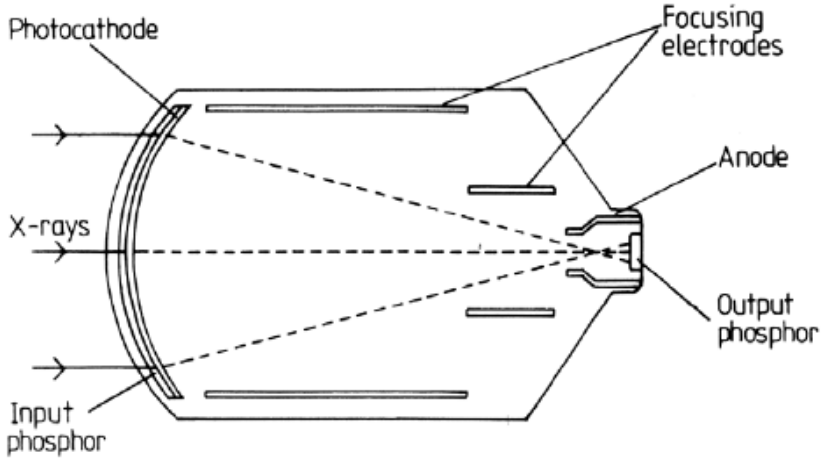

Construction of the image intensifier.

- X-rays are absorbed in CsI input phosphor.
- Emitted light is converted to electrons by photocathode.
- Electrons are focused and accelerated to output phosphor and converted to light..
- Bright light image at output window is imaged by TV-camera.

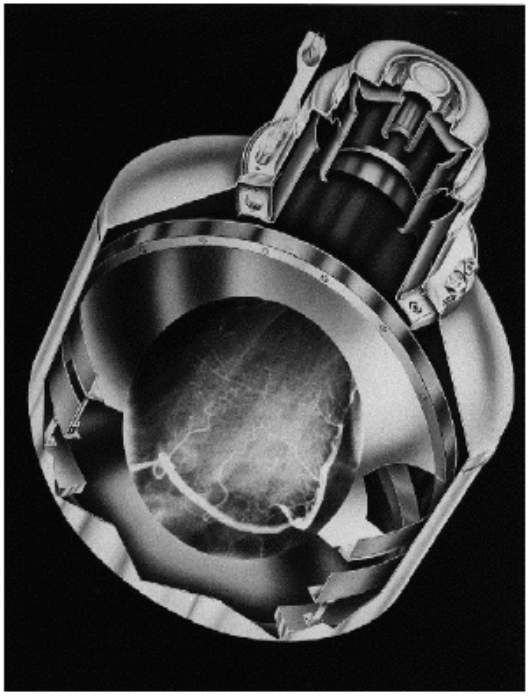

Medical Image Processing (Med Img 1) 39

Flat Panel Detectors

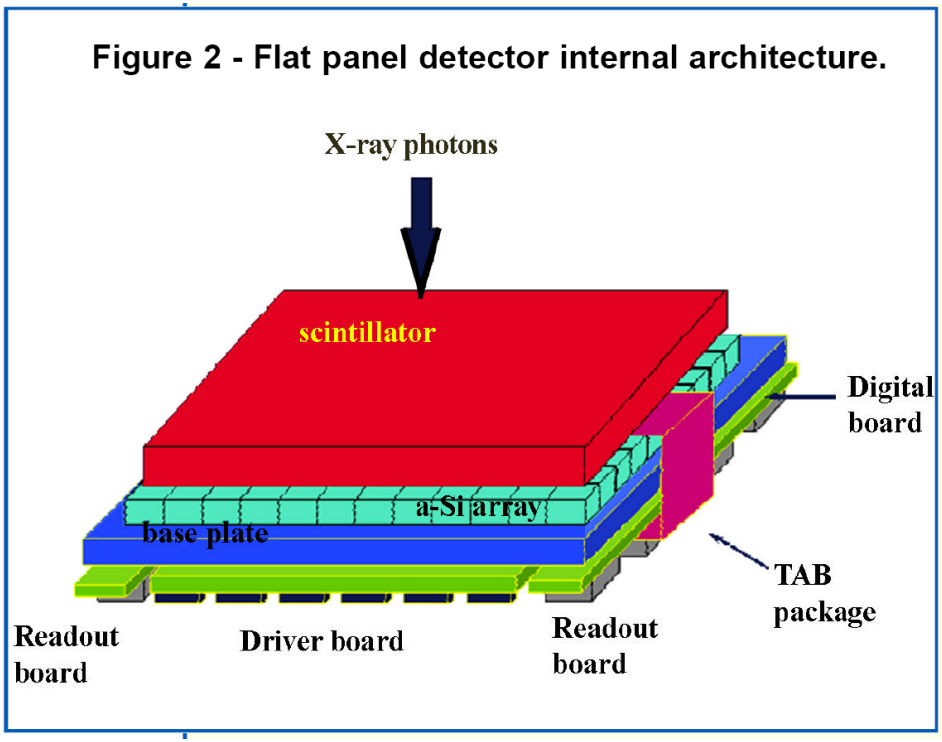

The construction of FPDs is similar in many ways to flat panel displays, and uses many of the same technologies. Figure 2 shows the construction of a typical FPD. At the core is an amorphous-silicon TFT/photodiode array. Closely coupled to the array is the X-ray scintillator.

http://www.varian.com/xray/pdf/Flat%20Panel%20Xray%20Imaging%2018-11-04.pdf

Scintillation Material as Detection Media

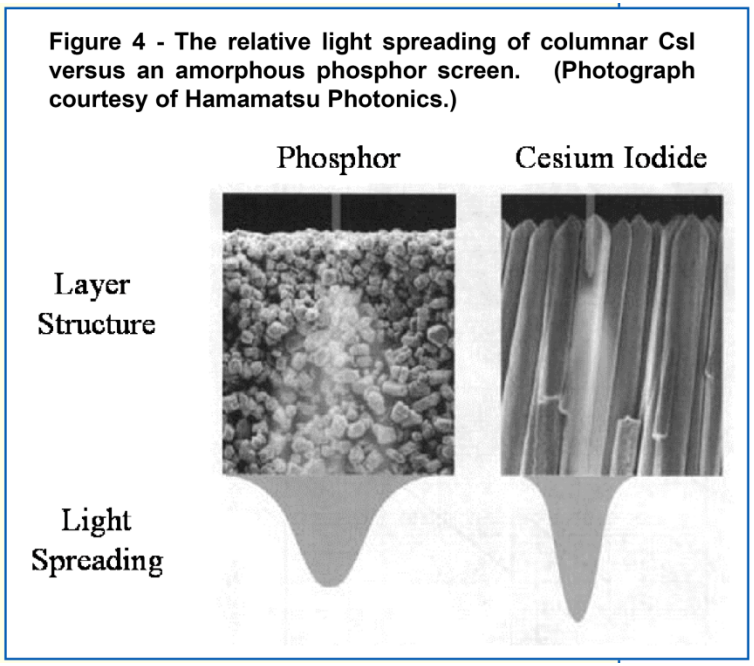

- CsI(Tl) scintillator: density 4.6g/cm^3, emission peak ~550nm.
- Columnar structure of up to 3mm thick to provide an adequate stopping power and a reduced light spread.

http://www.varian.com/xray/pdf/Flat%20Panel%20Xray%20Imaging%2018-11-04.pdf

Readout Electronics for Plat Panel Detectors

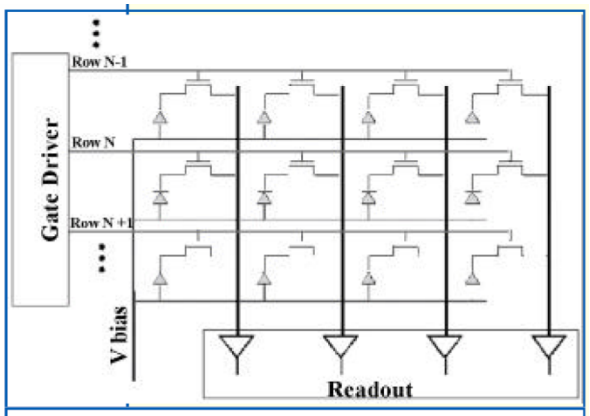

Figure 5 - TFT/Photodiode array schematic and view of a single 127μm pixel.

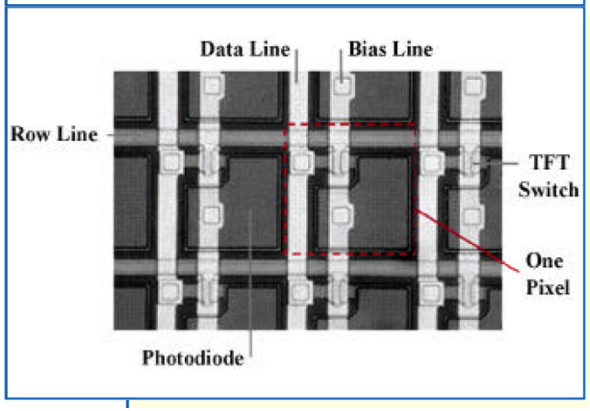

- scanned progressively, one line at a time from top to bottom. The TFTs are essentially switches.
- When a large positive voltage is applied to one of the gate lines, the switches (TFTs) in the selected row are closed, causing them to conduct electricity.
- With the TFTs energized, each pixel in the selected row discharges the stored signal electrons onto the dataline. At the end of each dataline is a charge integrating amplifier which converts the charge packet to a voltage.
- a programmable gain stage and an Analog-to-Digital Converter (ADC), which converts the voltage to a digital number.

http://www.varian.com/xray/pdf/Flat%20Panel%20Xray%20Imaging%2018-11-04.pdf

Direct Radiography (DR)

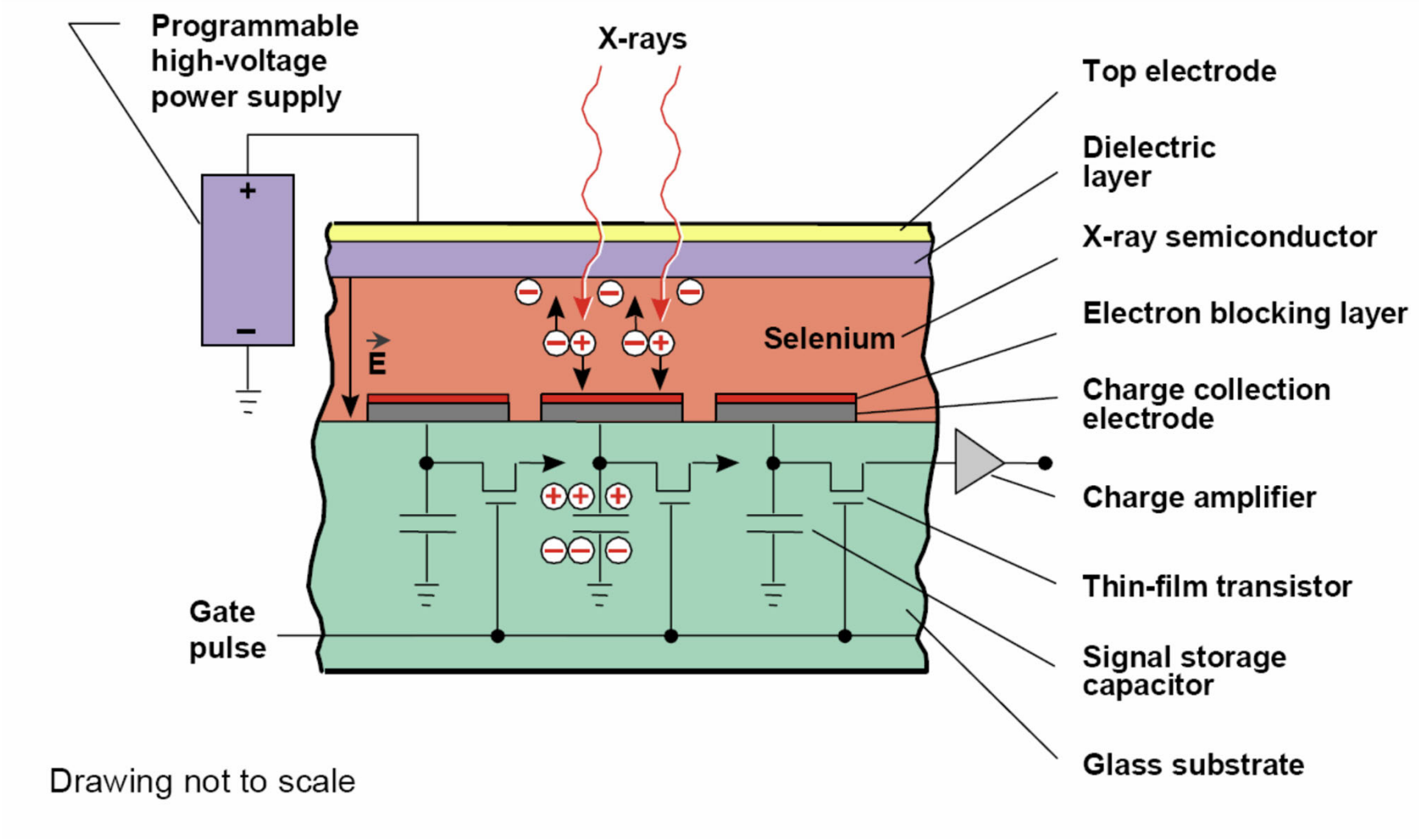

Review Slices X-ray Physics

X-ray CT

Basic Imaging Formation

Basic Principle of Planar X-ray

2 % attenuation change detectable in film

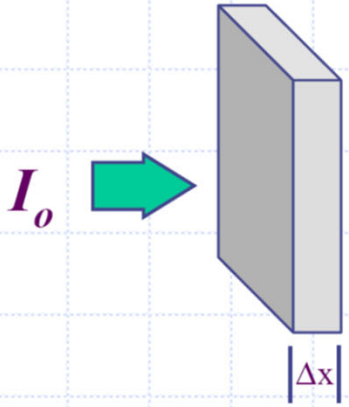

$$I = I_o e^{-\mu \Delta x}$$

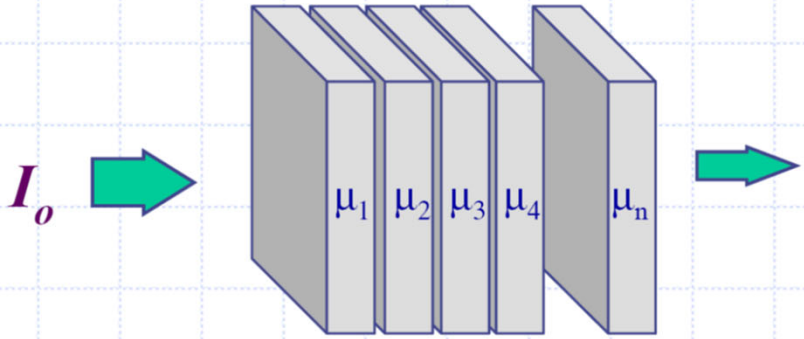

$$I = I_o e^{-\mu_1 \Delta x} e^{-\mu_2 \Delta x} \cdots e^{-}$$

$$= I_o e^{-(\mu_1 + \mu_2 + \cdots + \mu_n)\Delta x}$$

$$\Delta x \to 0, \qquad P = -\ln\left(\frac{I}{I_o}\right) = \int_{-\infty}^{\infty} \mu(x)\, dx$$

X-ray Computed Tomography (CT)

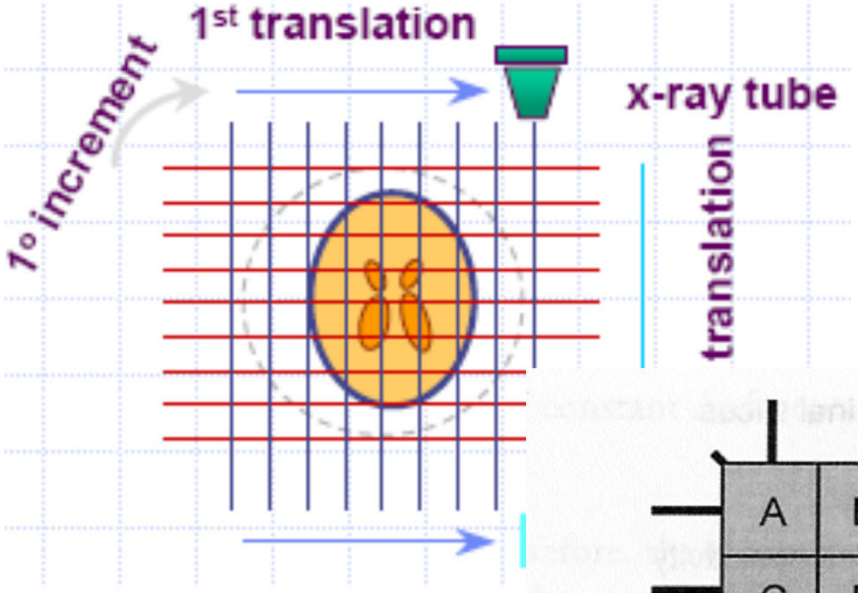

0.2 % attenuation change detectable in CT Images !!

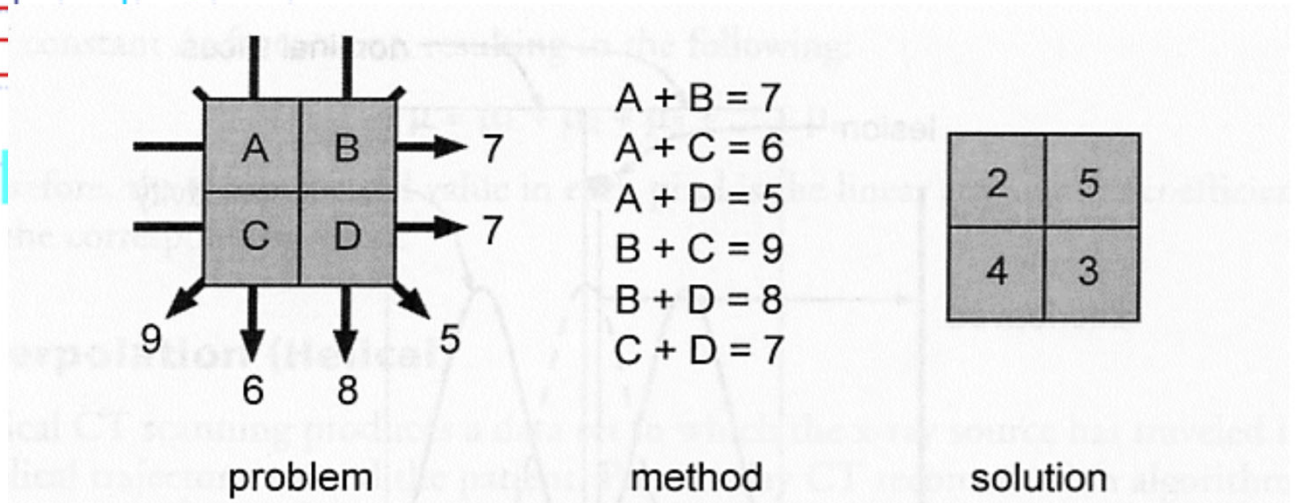

FIGURE 13-27. The mathematical problem posed by computed tomographic (CT) reconstruction is to calculate image data (the pixel values—A, B, C, and D) from the projection values *(arrows)*. For the simple image of four pixels shown here, algebra can be used to solve for the pixel values. With the six equations shown, using substitution of equations, the solution can be determined as illustrated. For the larger images of clinical CT, algebraic solutions become unfeasible, and filtered backprojection methods are used.

Review of the X-ray CT Image Formation

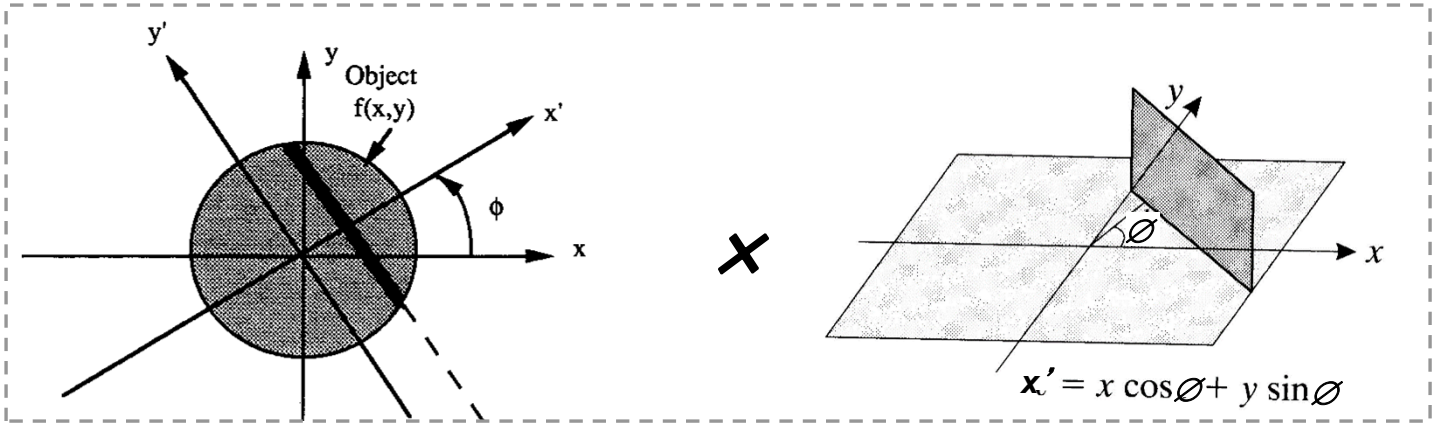

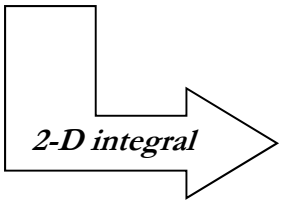

The value of the projection function $p_\phi(x')$ at this point is the integral of the function of f(x,y) along the straight line: $x' = x\cos\phi + y\sin\phi$

The integral of a line impulse function and a given 2-D signal gives the ***projection*** *data from a given view …*

$$p_\phi(x') = \int_{-\infty}^{\infty}\int_{-\infty}^{\infty} f(x,y)\delta(x\cos\phi + y\sin\phi - x')dxdy$$

Central Slice Theorem

$$F\{p(\phi, x')\} = F(r, \phi)$$

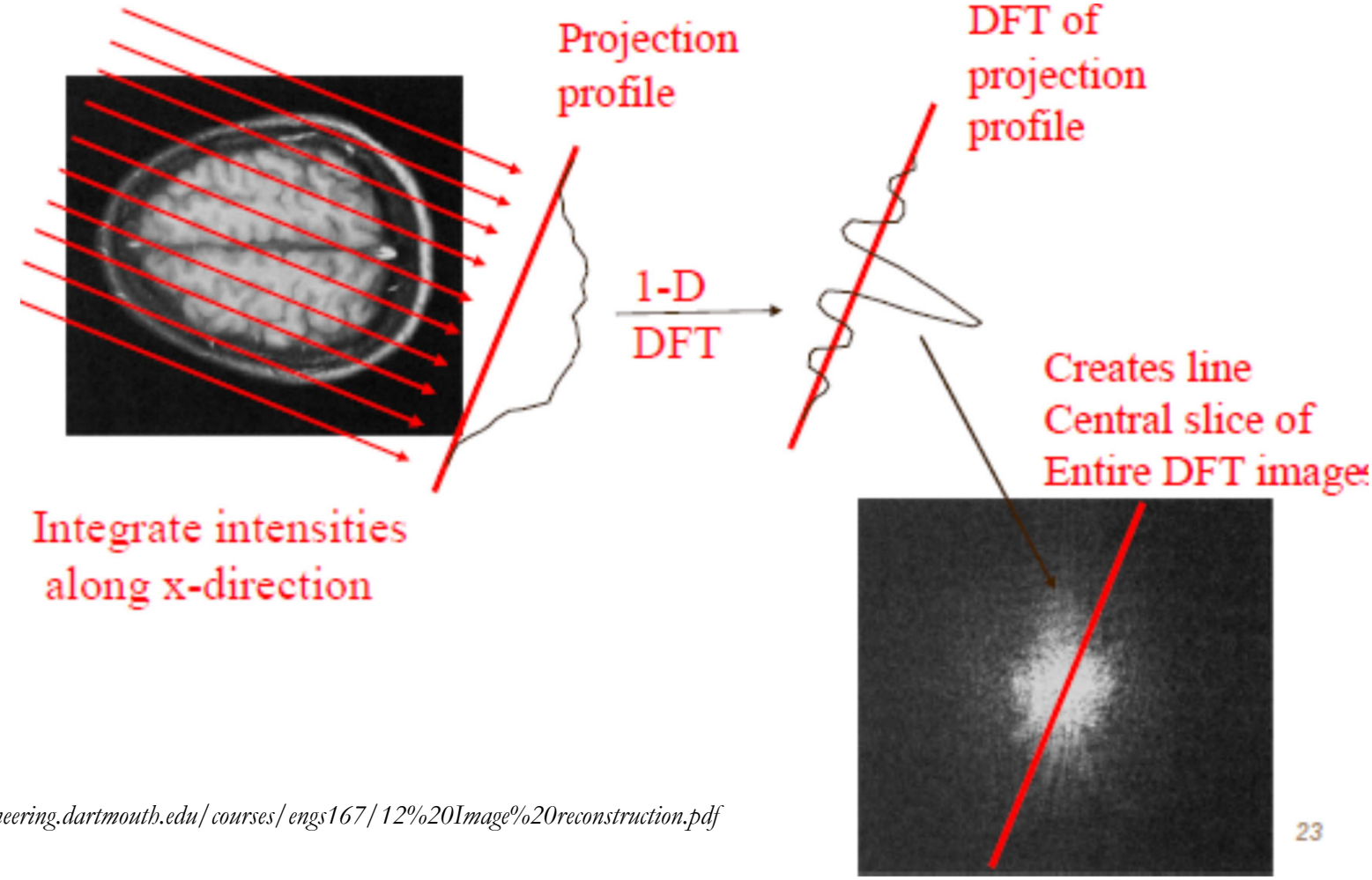

http://engineering.dartmouth.edu/courses/engs167/12%20Image%20reconstruction.pdf

Simple Back-projection and the 1/r Blurring

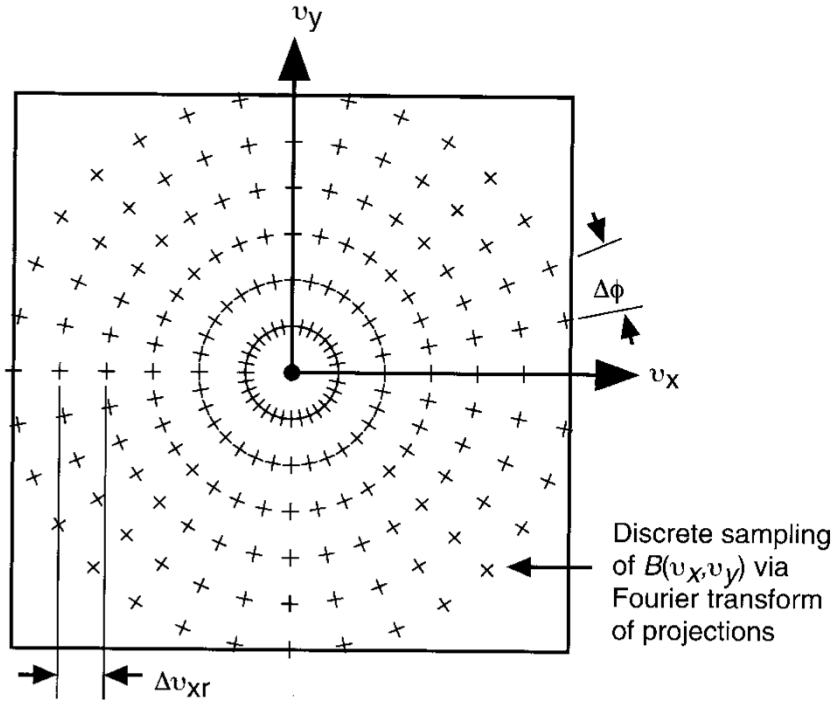

FIGURE 18 The discrete sampling pattern of $F(\upsilon_x,\upsilon_y)$ contained in $B(\upsilon_x,\upsilon_y)$, resulting from the use of discretely sampled projections.

The nature of the 1/r blurring:
Radon transform produced equally spaced radial sampling in Fourier domain.

Simple and Filtered Back-projection

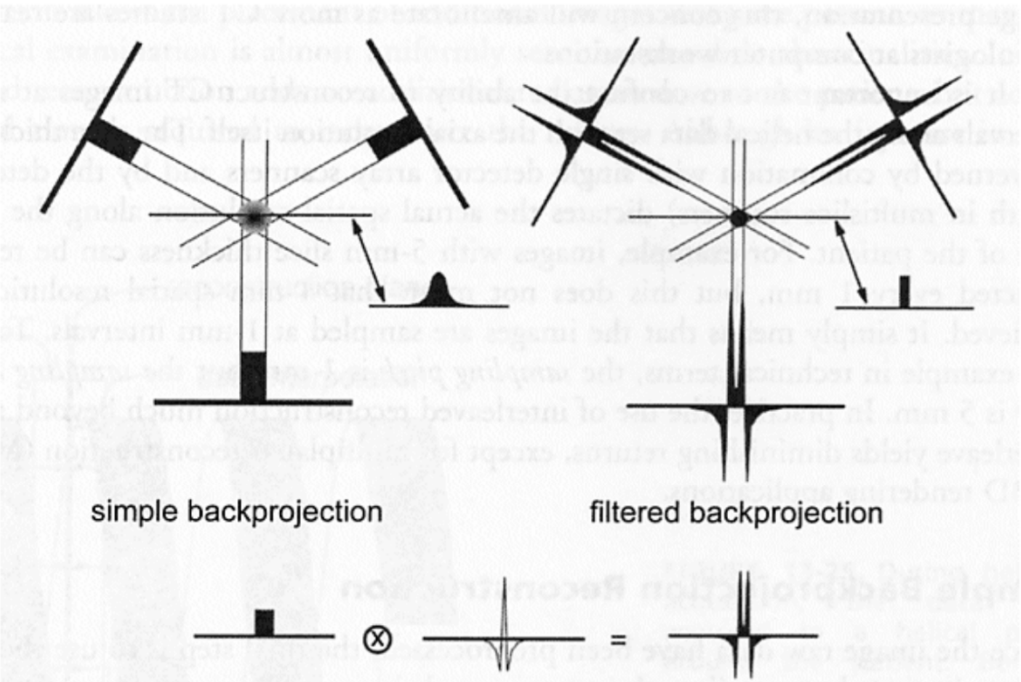

FIGURE 13-28. Simple backprojection is shown on the left; only three views are illustrated, but many views are actually used in computed tomography. A profile through the circular object, derived from simple backprojection, shows a characteristic 1/r blurring. With filtered backprojection, the raw projection data are convolved with a convolution kernel and the resulting projection data are used in the backprojection process. When this approach is used, the profile through the circular object demonstrates the crisp edges of the cylinder, which accurately reflects the object being scanned.

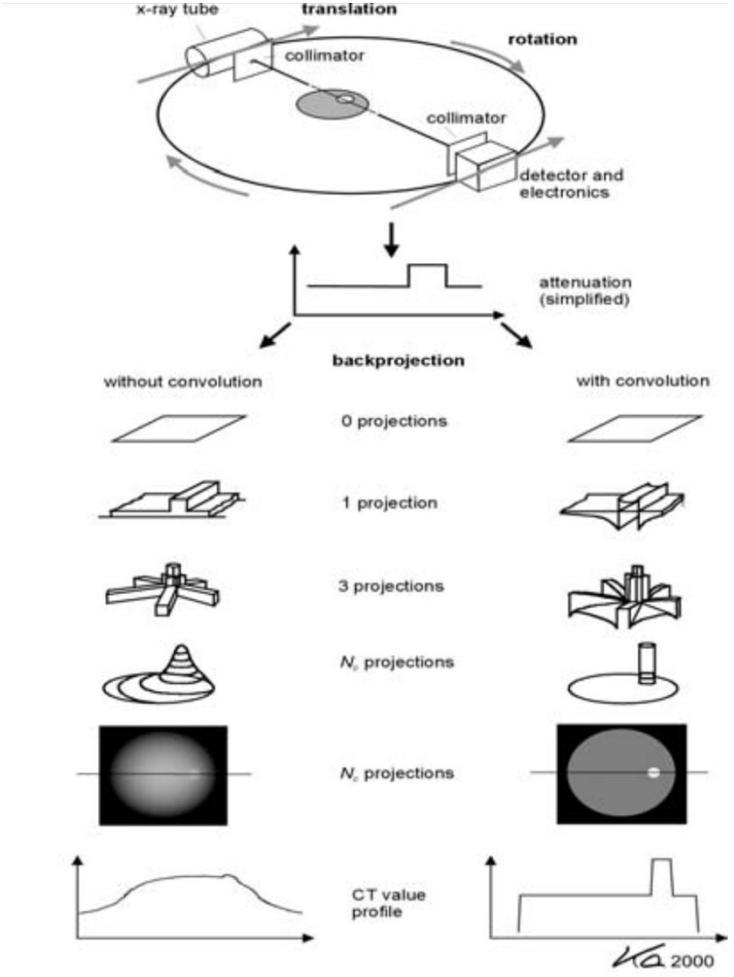

Chapters 12 & 13, The Essential Physics of Medical Imaging, Bushberg

Inside an X-ray CT System

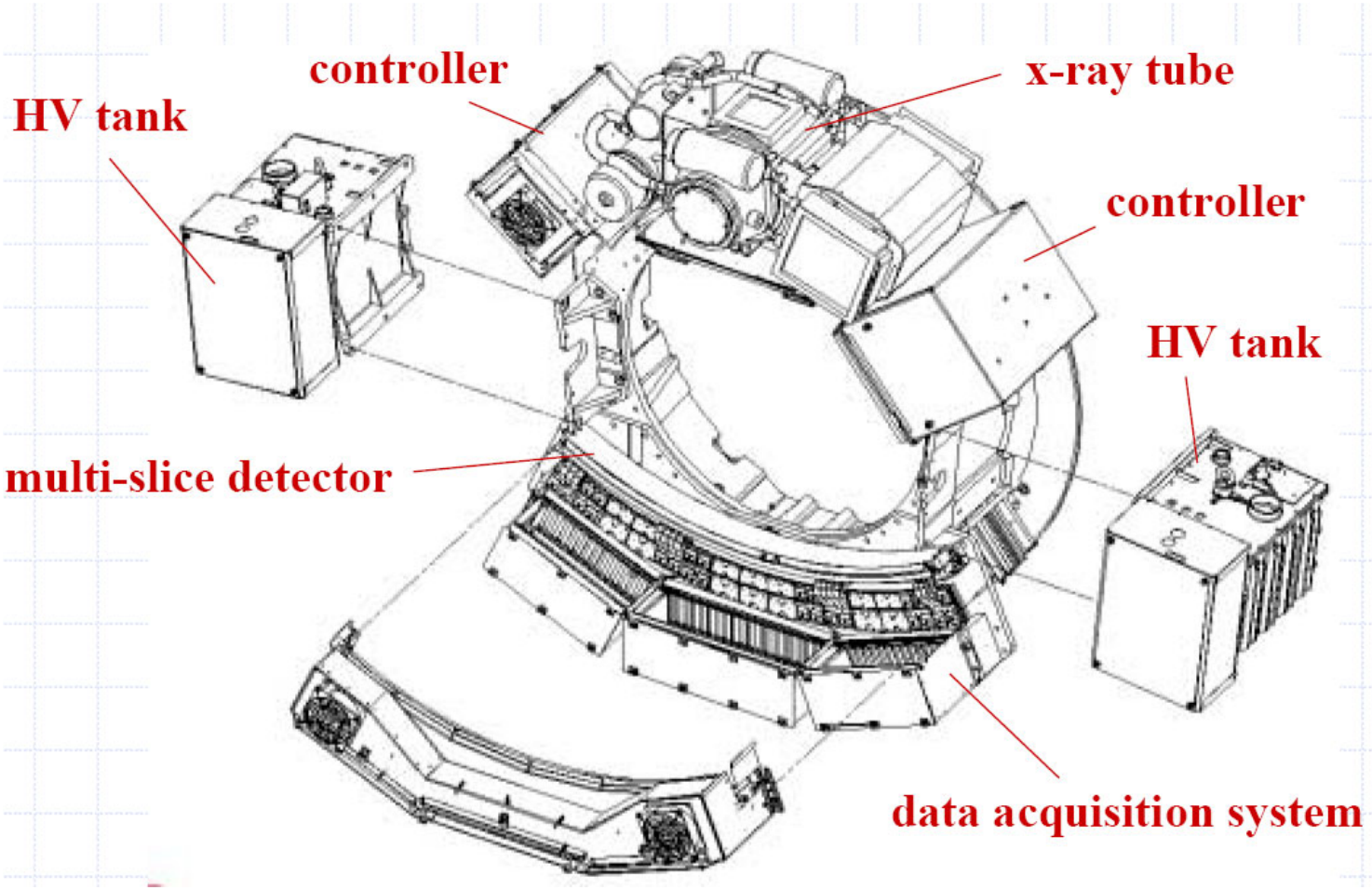

Contrast, Modulation, Modulation Transfer Function and Resolution

CT Numbers

CT Number is defined/measured as:

$$h = 1000 \times \frac{\mu - \mu_{water}}{\mu_{water}} (HU),$$ where the HU is the Houndsfield unit.

CT number → relative attenuation coefficient respect to that of water.

CT number is widely used for quality control purpose, basically,

→ The same object should appear with the same CT number in CT images taken with different scanners.

→ The a uniform object should appear to have homogeneous CT numbers across the entire reconstructed image.

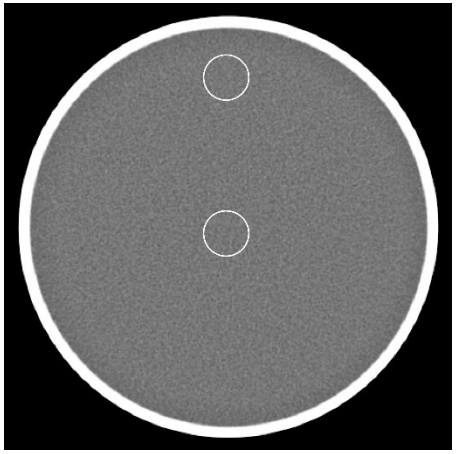

h_{air}=-1000, h_{water}=0 and h_{bone}≅1000.

Subject (or Object) Contrast

- *Difference in some aspects of the signal prior to it being recorded*
- *Consequence of fundamental differences in the object, e.g., in x-ray intensity based on attenuation*
- $C = (A-B)/A$

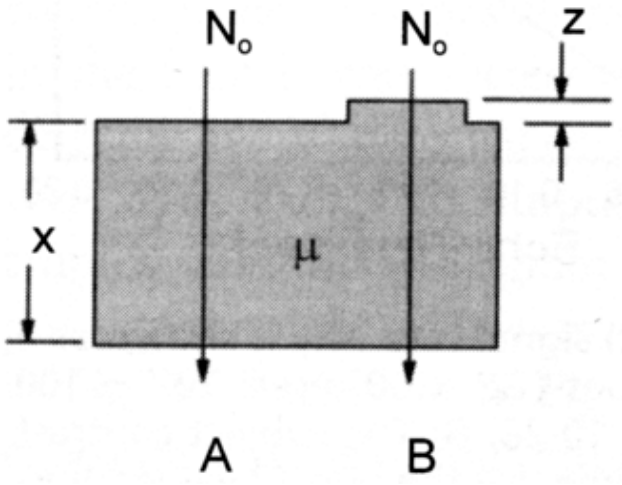

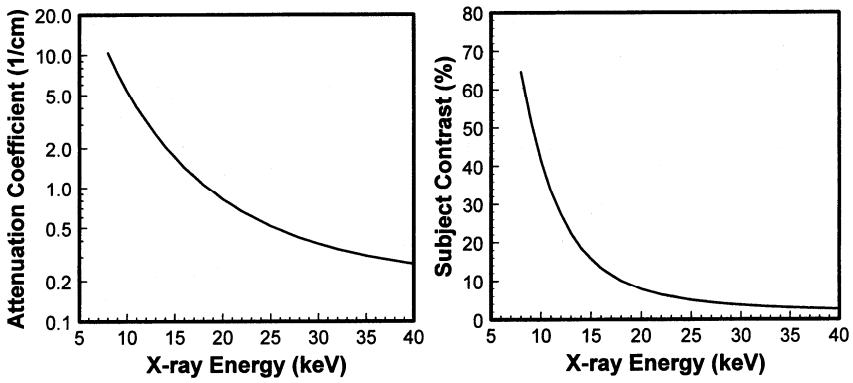

Modulation

- *The modulation m_f is an effective way to quantify the contrast of a periodic signal*

$$m_f = \frac{f_{\max} - f_{\min}}{f_{\max} + f_{\min}}.$$

- *In general, m_f is refer to as* ***the contrast of a periodic signal f(x,y) relative to its average value****.*

- *So within two signals, f(x,y) and g(x,y), with the same average value , f(x,y) is said to have* ***more contrast*** *if $m_f > m_g$.*

Modulation

- *Now let this signal to pass through an LSI imaging system. Suppose an input signal function. Since*

$$f(x, y) = A + B \sin(2\pi u_0 x) = A + \frac{B}{2j}\left[e^{j2\pi u_0 x} - e^{-j2\pi u_0 x}\right],$$

- *Suppose the system impulse response function h(x,y) is circularly symmetric,*

$$g(x, y) = AH(0, 0) + B\,|H(u_0, 0)| \sin(2\pi u_0 x)\,.$$

- *So the modulation of the output signal is*

$$m_g = \frac{B|H(u_0, 0)|}{AH(0, 0)} = m_f \frac{|H(u, 0)|}{H(0, 0)}\,.$$

In Plane Spatial Resolution

Resolution of an CT system is measured with the ***modulation transfer function*** *(MTF):*

Modulation of the output:

in Reconstructed CT image

$$H(u,v) = F\left[h(x,y)\right] = F\left\{S\left[\delta(x,y)\right]\right\},$$

$S[\ ]$ is the system operator and

$F[\ ]$ is the Fourier transform operator

$$\mathrm{MTF}(u,v) = \frac{m_g}{m_f} = \frac{|H(u,v)|}{H(0,0)},$$

Modulation of the input signal

$$f(x,y) = A + B\sin(2\pi u_0 x),$$

$$m_f = \frac{f_{\max} - f_{\min}}{f_{\max} + f_{\min}} = \frac{B}{A}.$$

For a linear and shift-invariant system

$$g_{\substack{output \\ function}}(x,y) = f(x,y) * h(x,y)$$

$$= F^{-1}\left\{F(u,v)\cdot H(u,v)\right\}$$

Modulation Transfer Function (MTF)

- *In case of non-isotropic impulse response function (h(x,y) is not circularly symmetric), the MTF can be defined as*

$$\mathrm{MTF}(u,v) = \frac{m_g}{m_f} = \frac{|H(u,v)|}{H(0,0)},$$

- *A typical MTF of an imaging system*

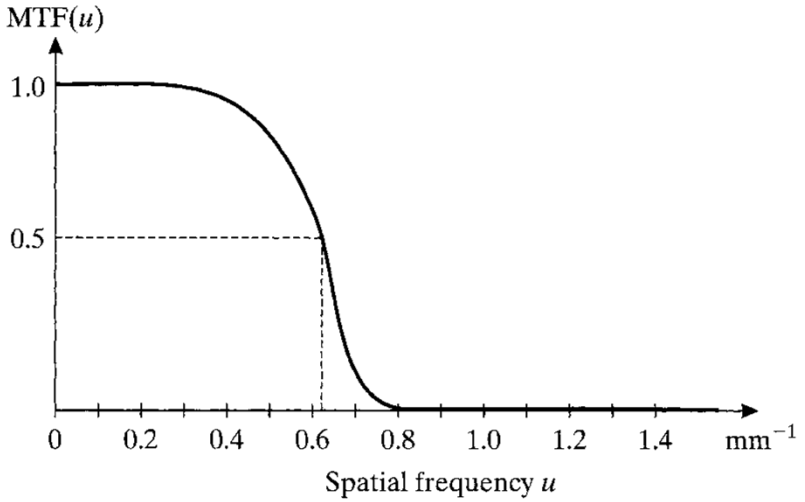

Figure 3.3
A typical MTF of a medical imaging system.

Modulation Transfer Function (MTF)

- *An example of the same signal passing through three imaging systems with decreasingly poor MTF, which leads to decreasing contrast in images*

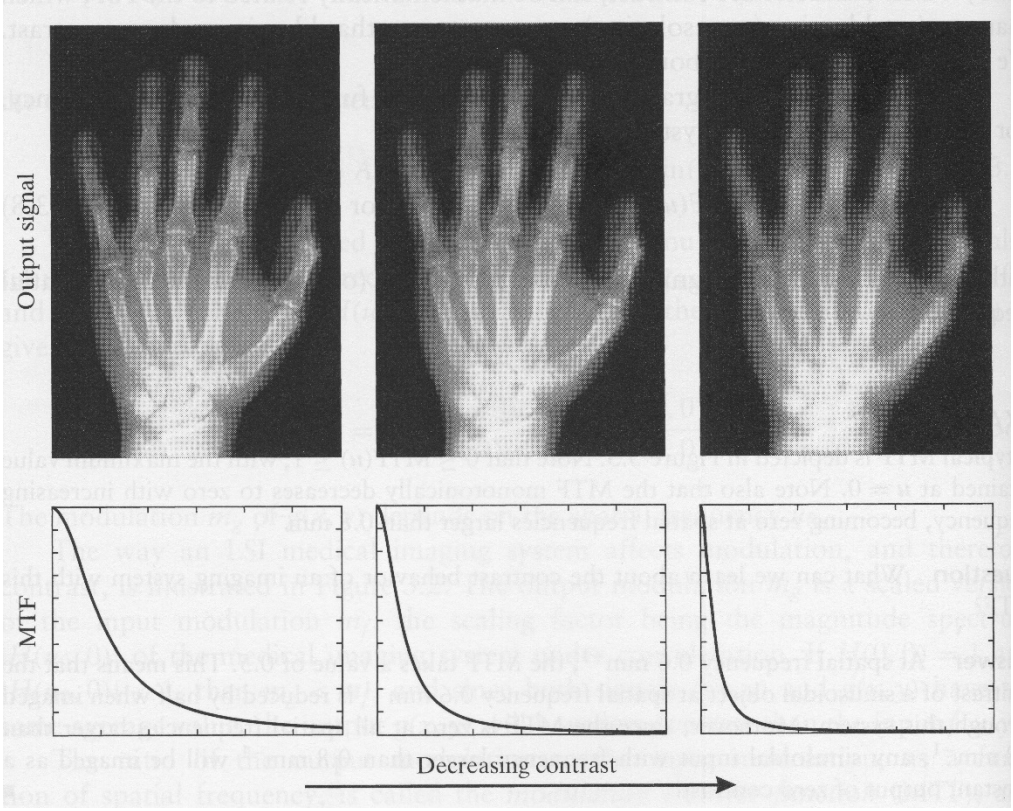

System Cascade

- *Modulation Transfer Function (MTF).*

$$g(x,y) = h_K(x,y) * \cdots * (h_2(x,y) * (h_1(x,y) * f(x,y))) .$$

- *The overall MTF is the product of the MTF for sub-systems:*

$$MTF_{total}(u) = \prod_{i=1}^{i=I} MTF_i(u)$$

- *MTF of an imaging system that can be modeled as a chain if systems is often determined by the MTF of the worst system in the cascade.*

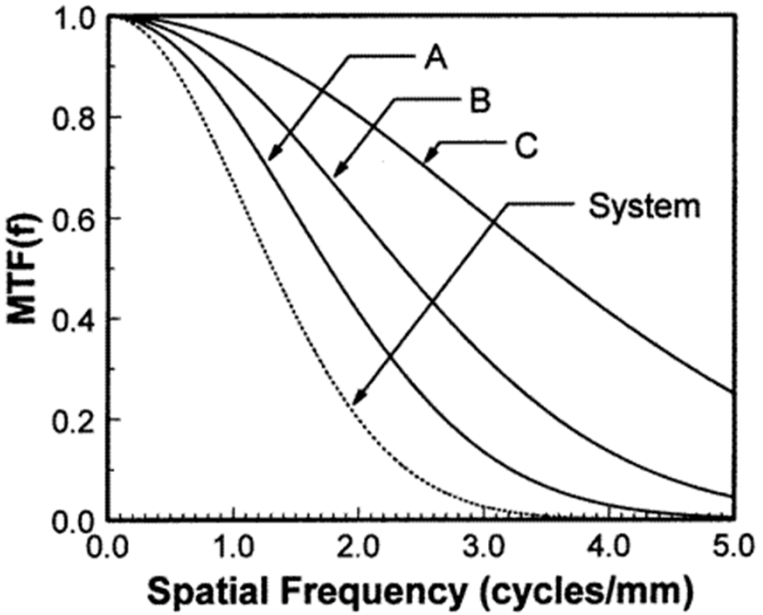

How to Measure Modulation Transfer Function

- *Modulation Transfer Function (MTF).*

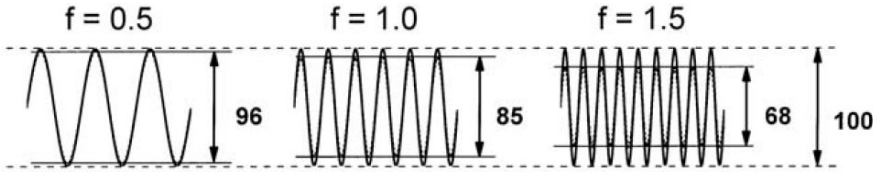

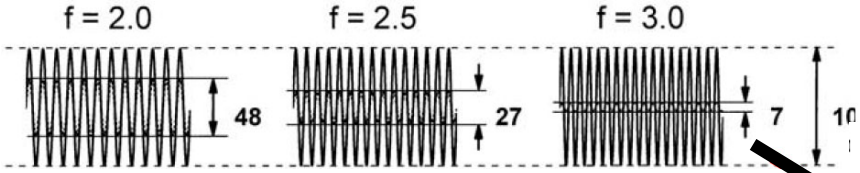

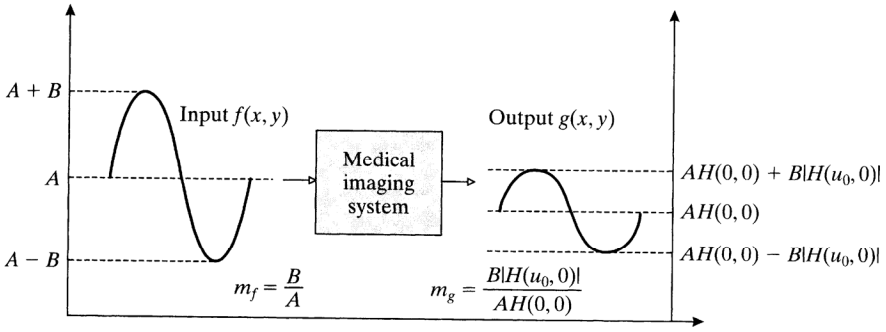

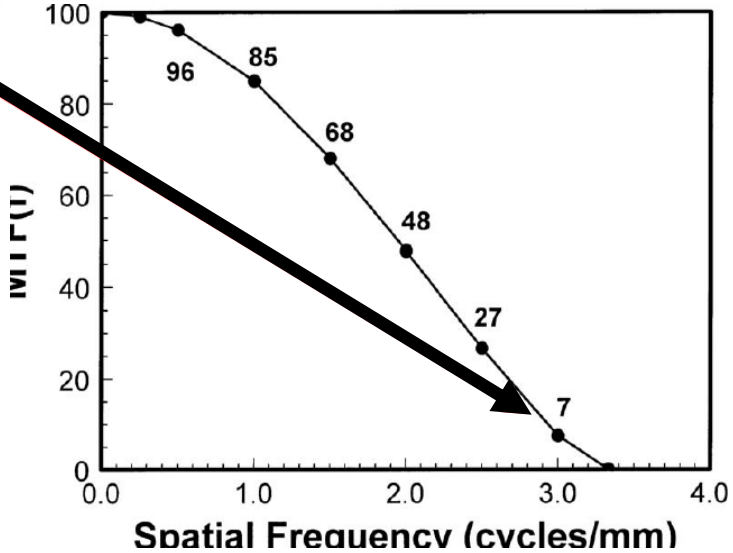

In Plane Spatial Resolution

Resolution of an CT system is measured with the ***modulation transfer function*** *(MTF):*

Modulation of the output:

in Reconstructed CT image

$$H(u,v) = F\left[h(x,y)\right] = F\left\{S\left[\delta(x,y)\right]\right\},$$

$S[\ ]$ is the system operator and

$F[\ ]$ is the Fourier transform operator

$$\mathrm{MTF}(u,v) = \frac{m_g}{m_f} = \frac{|H(u,v)|}{H(0,0)},$$

Modulation of the input signal

$$f(x,y) = A + B\sin(2\pi u_0 x),$$

$$m_f = \frac{f_{\max} - f_{\min}}{f_{\max} + f_{\min}} = \frac{B}{A}.$$

For a linear and shift-invariant system

$$S_{\substack{output \\ function}}(x,y) = f(x,y) * h(x,y)$$

$$= F^{-1}\left\{F(u,v)\cdot H(u,v)\right\}$$

In Plane Spatial Resolution

Resolution of an CT system is measured with the modulation transfer function (MTF):

$$\mathrm{MTF}(u,v) = \frac{m_g}{m_f} = \frac{|H(u,v)|}{H(0,0)},$$

- *A typical MTF of an imaging system*

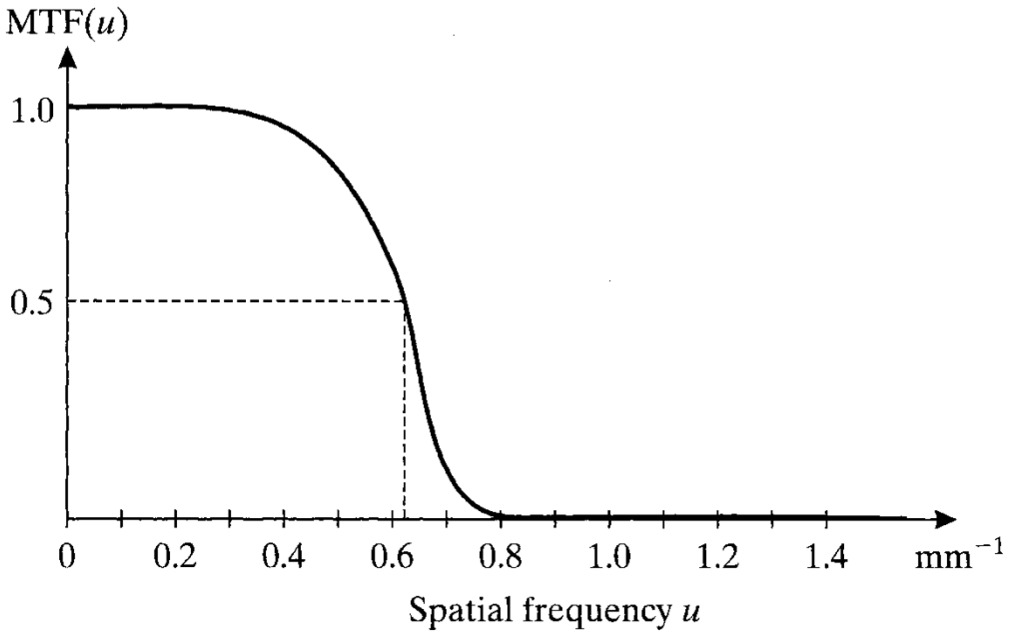

Figure 3.3
A typical MTF of a medical imaging system.

LSF and MTF

- *Modulation Transfer Function (MTF).*

$$\mathrm{MTF}(u) = \frac{m_g}{m_f} = \frac{|H(u,0)|}{H(0,0)} = \frac{|L(u)|}{L(0)}, \qquad \text{for every } u.$$

- *For a "reasonable" imaging system, the L(0)=0, so that*

$$\mathrm{MTF}(u) = L(u)$$

- *MTF is an effective way to compare two imaging systems in terms of spatial resolution and contrast.*

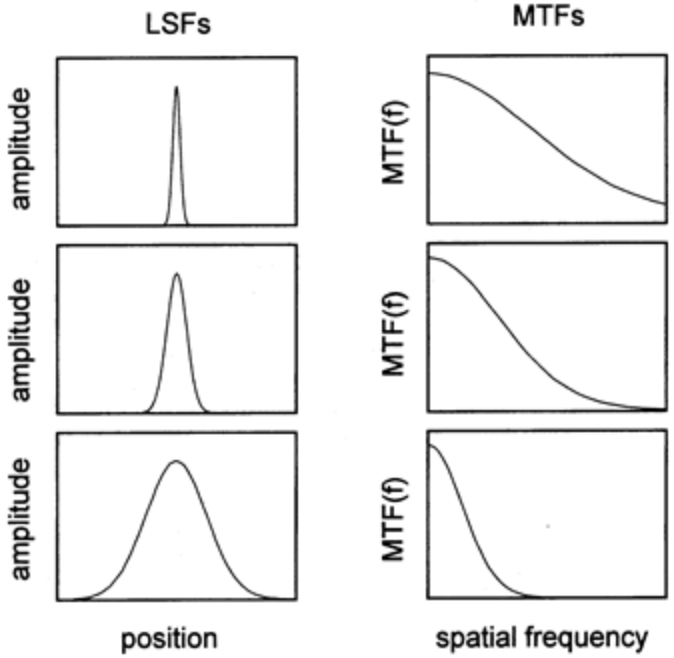

In Plane Spatial Resolution

Resolution of an CT system is measured with the modulation transfer function (MTF):

$$\mathrm{MTF}(u,v) = \frac{m_g}{m_f} = \frac{|H(u,v)|}{H(0,0)},$$

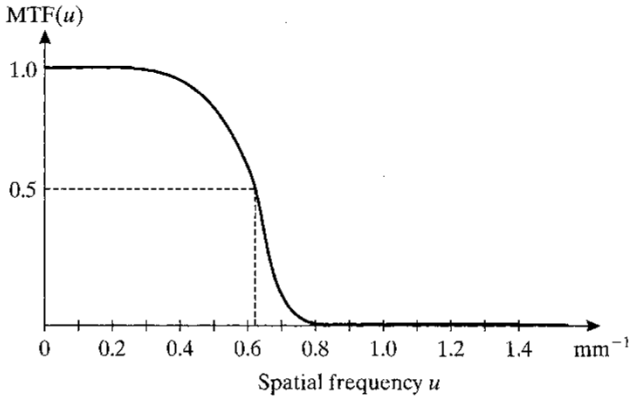

Figure 3.3
A typical MTF of a medical imaging system.

What is limiting MTF (Contrast, Resolution) of a CT System?

A Revisit to Key Image Quality Measures

Spatial Resolution

How to quantify spatial resolution?
How to measure spatial resolution?
The relationship between spatial resolution and modulation transfer function (MTF)?

Spatial Resolution

- ***Resolution****: the ability of an given imaging system to* ***accurately depict two distinct events in space, time or frequency*** *respectively.*
- *Resolution can also be thought as the* ***degree of blurring, smearing****.*

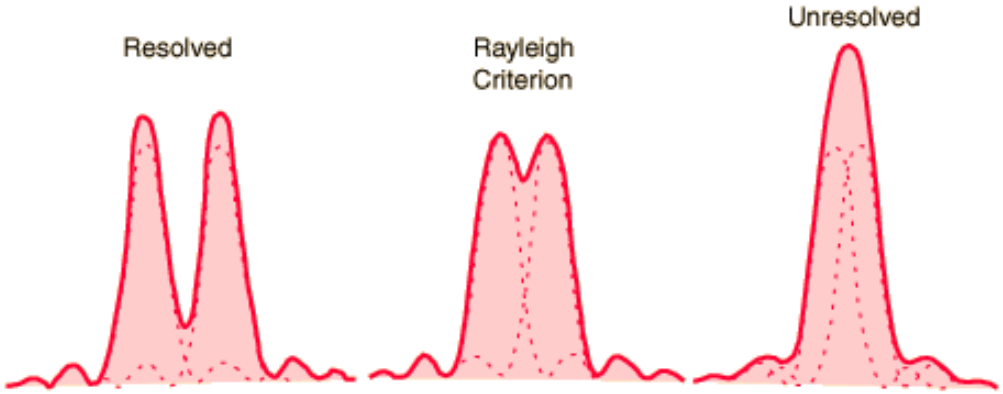

- ***Spatial resolution*** *is fully described by the* ***point-spread function*** *or* ***impulse response function, h(x,y)****.*

Stationary and Non-stationary PSF

- *Spatial variation of the PSF is another important aspect of an given imaging system.*

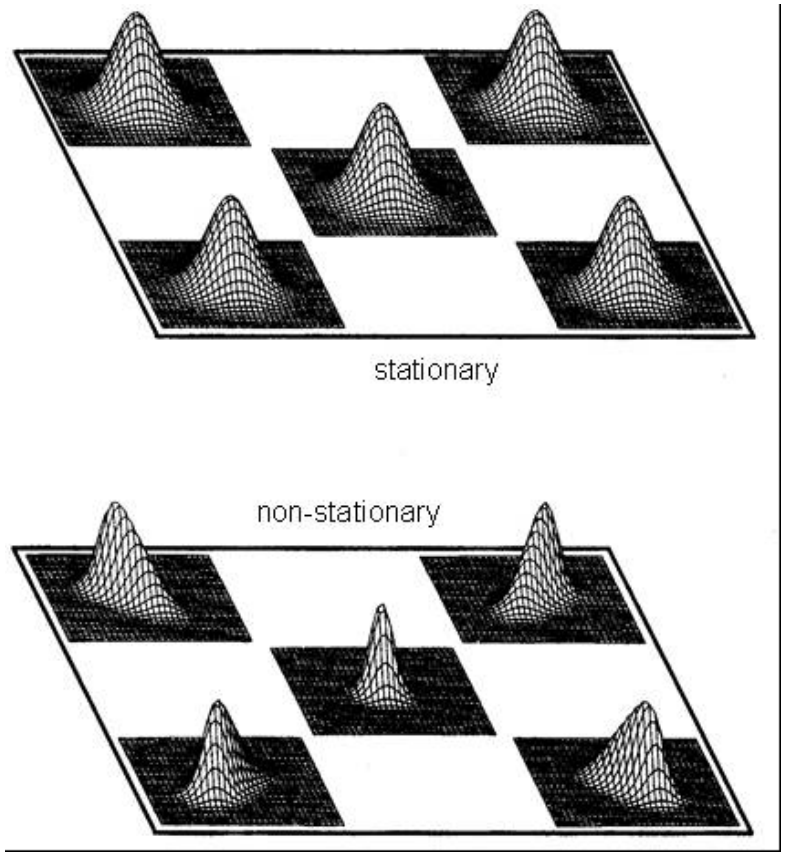

Other Ways to Measure the Spatial Resolution
Line Response Function

- *The resolution of an imaging system can also be estimated with the* ***line-spread function***
- *Given a line impulse*

$$\textit{line impulse } f(x,y) = \delta_\ell(x,y) = \delta(x\cos\theta + y\sin\theta - \ell)$$

- *Assuming the impulse response function of the imaging system h(x,y) is isotropic,* ***line response function*** *is*

$$\begin{aligned} g(x,y) &= \int_{-\infty}^{\infty}\int_{-\infty}^{\infty} h(\xi,\eta) f(x-\xi, y-\eta)\, d\xi\, d\eta\,, \\ &= \int_{-\infty}^{\infty}\left[\int_{-\infty}^{\infty} h(\xi,\eta)\delta(x-\xi)\, d\xi\right] d\eta\,, \\ &= \int_{-\infty}^{\infty} h(x,\eta)\, d\eta\,, \end{aligned}$$

Line Response Function

- *The 1-D Fourier transform of the line spread function is*

$$
\begin{aligned}
L(u) &= \mathcal{F}_{1D}[l](u)\,, \\
&= \int_{-\infty}^{\infty} l(x) e^{-j2\pi ux}\, dx\,, \\
&= \int_{-\infty}^{\infty}\int_{-\infty}^{\infty} h(x,\eta) e^{-j2\pi ux}\, dx\, d\eta\,, \\
&= H(u,0).
\end{aligned}
$$

- *So the values of the Fourier transform of the LSF crossing an horizontal line passing through the origin is sufficient for describing the LSF*

LSF and MTF

- *Modulation Transfer Function (MTF).*

$$\mathrm{MTF}(u) = \frac{m_g}{m_f} = \frac{|H(u,0)|}{H(0,0)} = \frac{|L(u)|}{L(0)}, \qquad \text{for every } u.$$

- *For a "reasonable" imaging system, the L(0)=0, so that*

$$\mathrm{MTF}(u) = L(u)$$

- *MTF is an effective way to compare two imaging systems in terms of spatial resolution and contrast.*

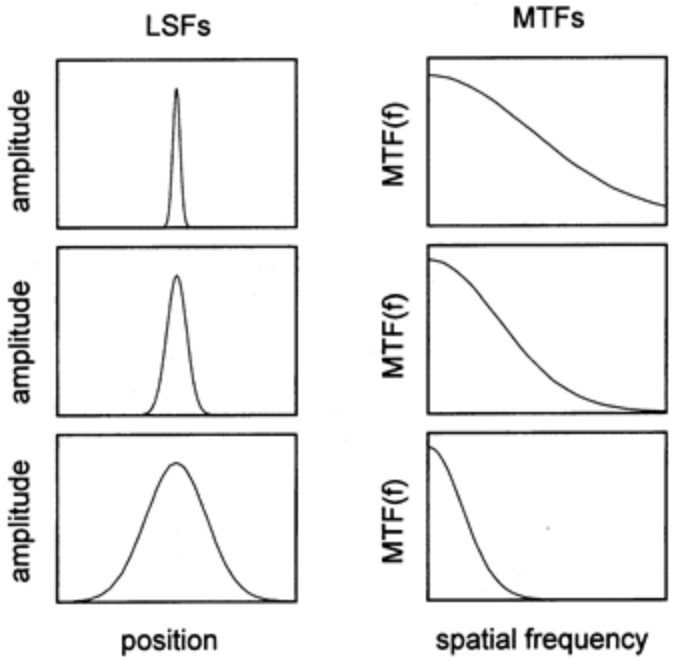

Chapter 4: Single Photon Emission Computed Tomography (SPECT)

Key concepts

Emission Tomography (ET) for Nuclear Medicine Applications

- *Tracer principle*
- *Commonly used radio-nuclides for ET.*
- *Detector technologies for ET*

A comparison between

- *Regular pinhole or multiple SPECT cameras*
- *Coded aperture*
- *Compton camera*

The Tracer Principle

What is the tracer principle?

- *Appropriately chosen radioactive compounds participate in an organism's physiological processes in the same way as non-radioactive materials.*
- *These compounds can be detected through the detecting of their radiation signatures, such as gamma rays.*

Two major attributes

- *Because one can detect even minute quantities of radioactive material, the tracer principle can be used to measure molecular concentrations with a* ***tremendous sensitivity****.*
- *Tracer measurements are* ***noninvasive*** *– the concentration of tracer is deduced from the number of gamma rays detected.*

Emission Tomography

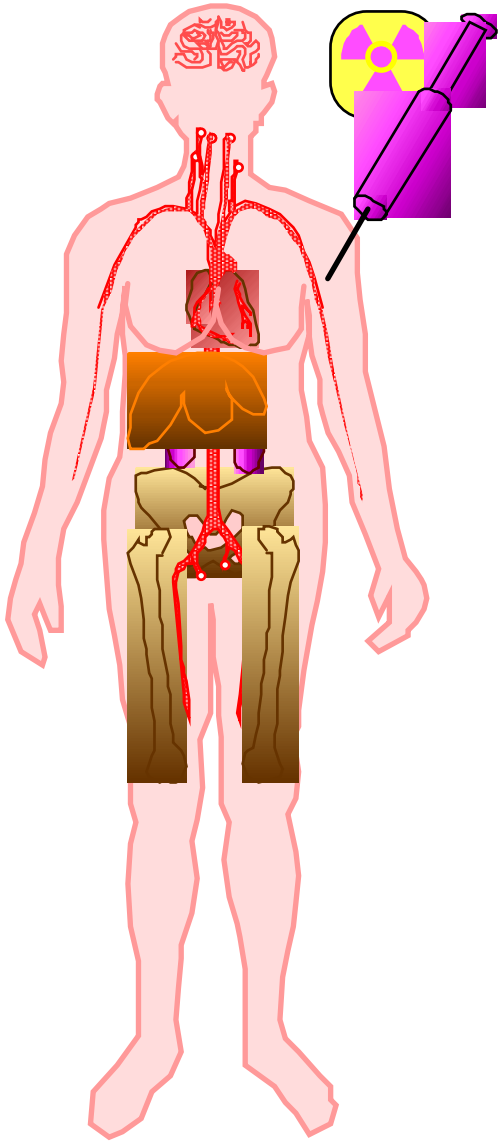

- ***Drug is labeled with radioisotopes that emit gamma rays.***
- ***Drug localizes in patient according to metabolic properties of that drug.***
- ***Trace (pico-molar) quantities of drug are sufficient.***
- ***Radiation dose fairly small (<1 rem).***

Drug Distributes in Body

Single Photon Emission Computed Tomography (SPECT)

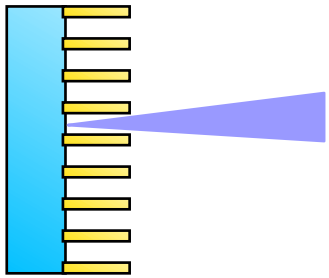

Collimator

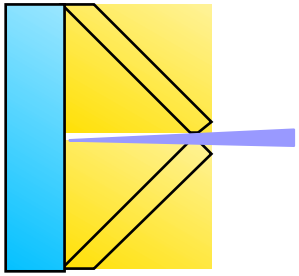

Pinhole

Collimator in front of the detector to select gamma rays from certain directions only …

Rotated around the object for collecting multiple projections …

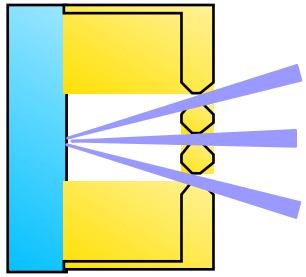

Coded Aperture

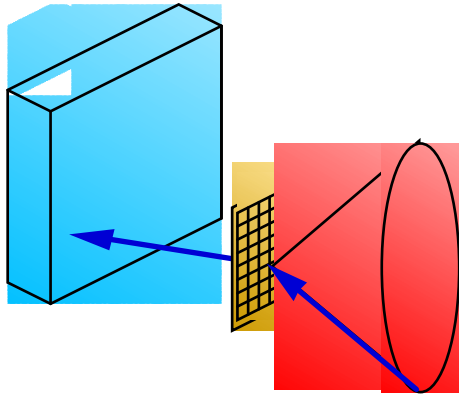

Compton

Single Photon Emission Computed Tomography (SPECT)

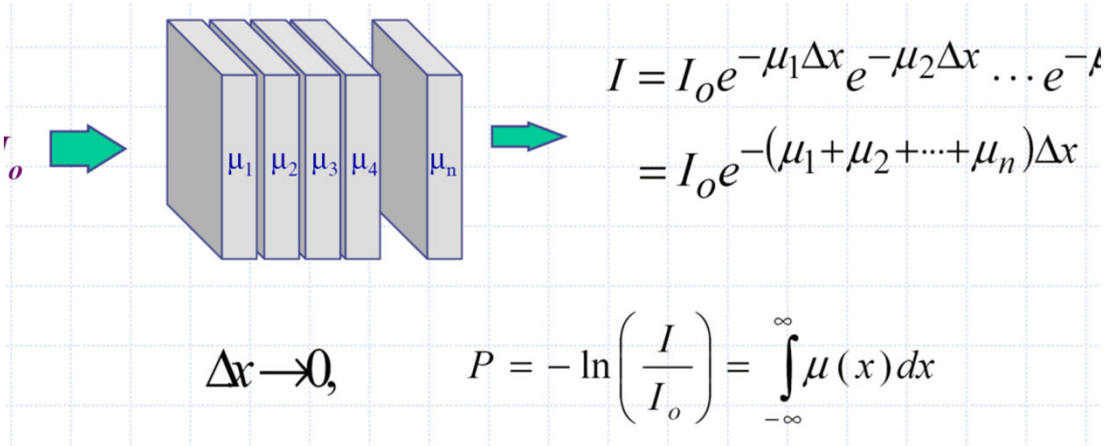

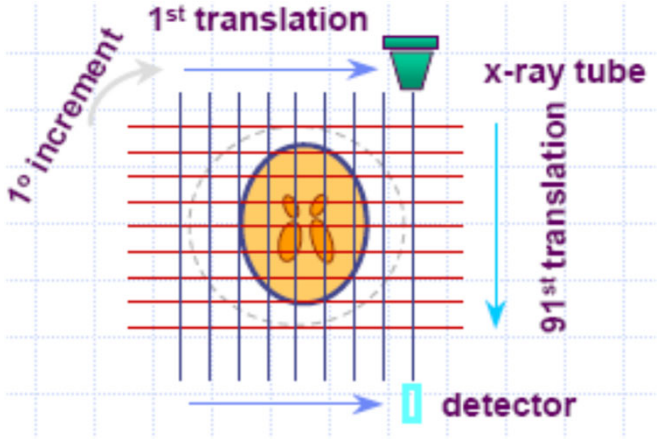

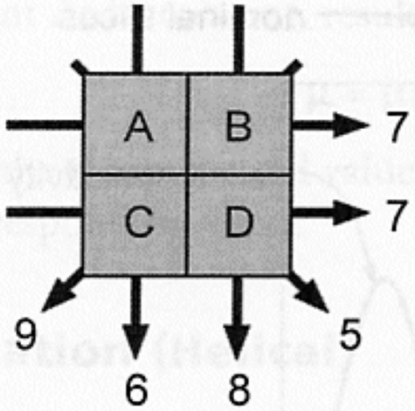

A + B = 7
A + C = 6
A + D = 5
B + C = 9
B + D = 8
C + D = 7

2	5
4	3

Tc-99m for Nuclear Medicine

The Basic Aspects:

- *99mTc (IT,γ) 99Tc - 6 hr half life (from 99Mo)*
- *Reactor produced ($^{235}U+^{1}n \rightarrow ^{137}Cs+^{99}Mo$)*
- *γ emission at 140 keV - ideal*
- *6 hr half life - ideal*
- *Readily available from a Generator*
- *90% of all nuclear medicine studies use 99mTc*

Conventional Anger Camera

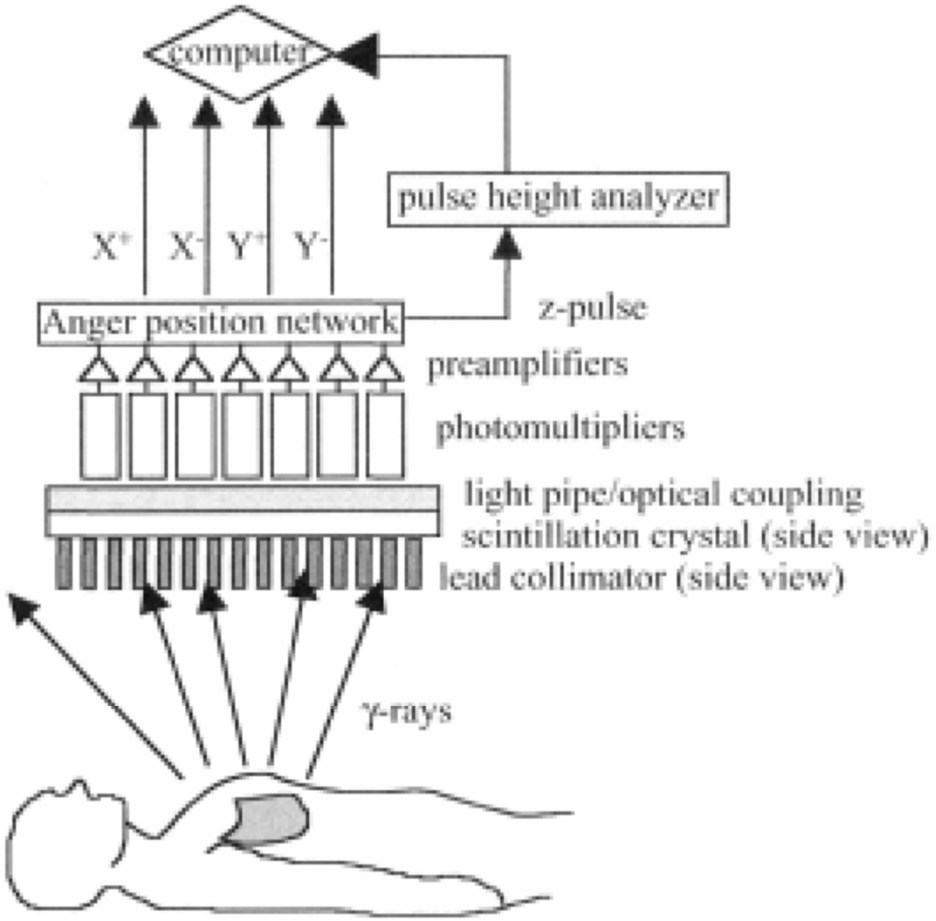

FIGURE 2.4. *Schematic diagram of a gamma camera positioned above the patient. The distribution of the radiopharmaceutical is indicated by the shaded region within the body.*

Conventional Anger Camera

- *PMTs coupled to large, continuous NaI(Tl) crystal*
- *Spatial resolution 3–4 mm FWHM*
- *Energy resolution 8–10% FWHM*
- *Mature technology (DoB ~1957)*
- *Large-area, >40cm x 40cm typical*
- *Simple and cost-effective*

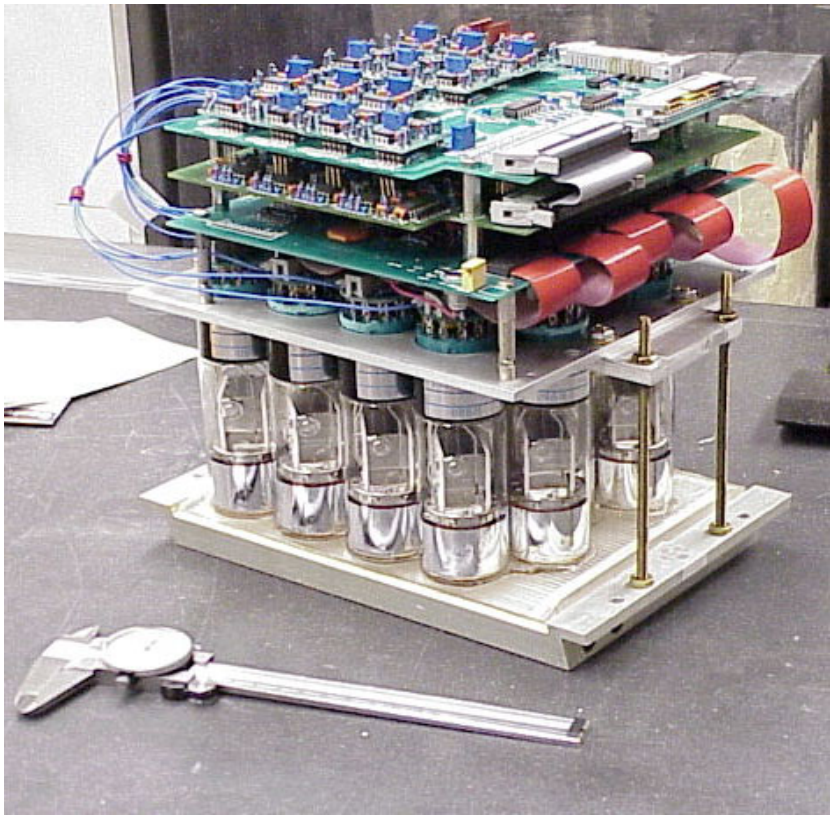

SPRINT II camera module

Scintillation Light

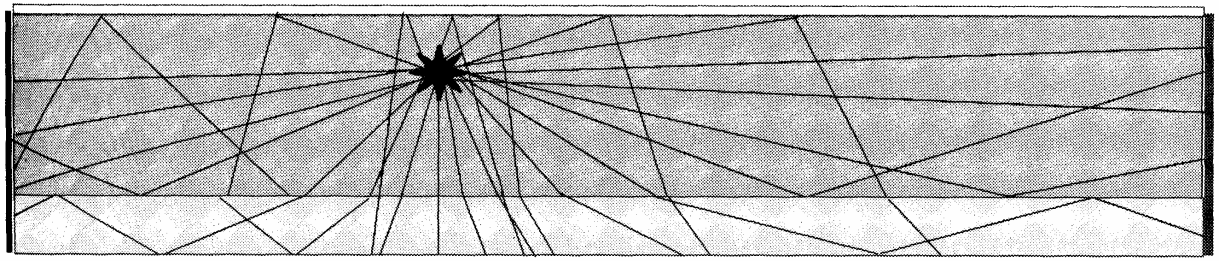

FIGURE 4 Representation of light ray propagation from a point source of light within a scintillation crystal slab with a white diffuse Lambertian reflector on top, absorbing sides, and a light diffuser on the bottom leading into the photodetector.

- *Scintillation light are generated isotropically.*
- *It is difficult to control light propagation inside a continuous bulk scintillator*
- *Light spreading leads to loss in both spatial resolution and energy resolution.*
- *Normally, the best we can do is to provide a better boundary condition for a better light collection efficiency.*

Photoelectric Effect

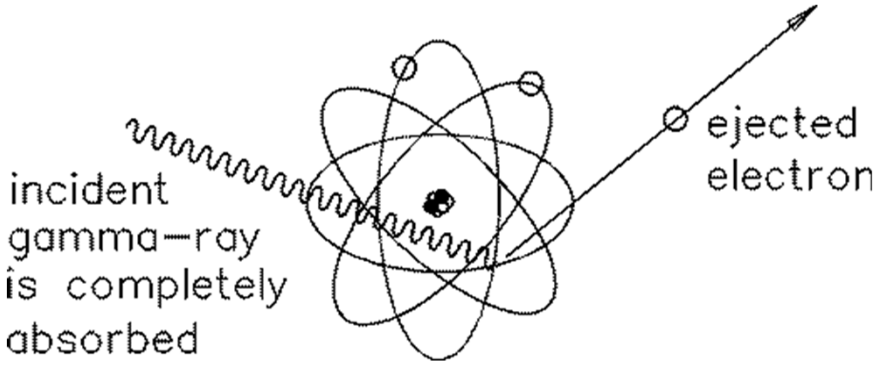

$$E_{e^-} = h\nu - E_b$$

h is the Planck's constant

ν is the frenquency of the photon

- *Photoelectric interaction is* ***with the atom in a whole*** *and can not take place with free electrons.*
- *Photoelectric effect leaves a vacancy in one of the electron shells, which leaves the atom at an excited state.*

Compton Scattering

The incident gamma ray photon may be deflected by an electron in the absorbing material.

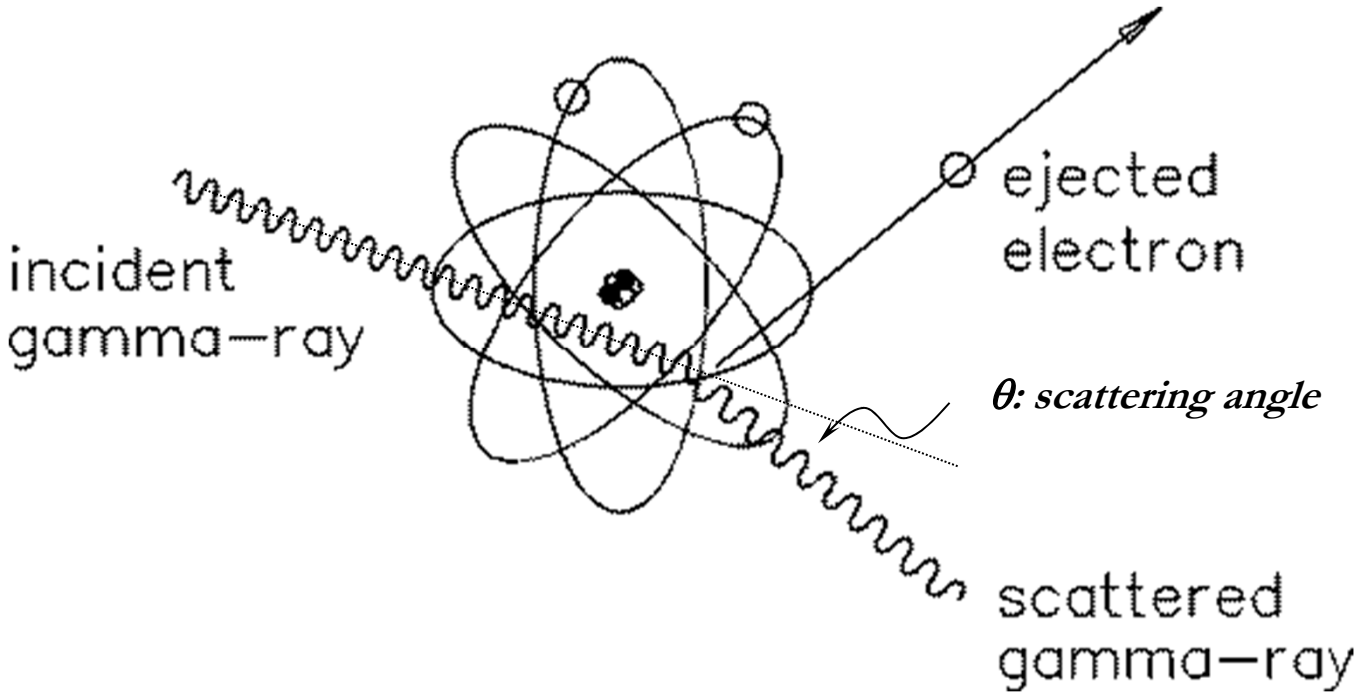

Energy Transfer in Compton Scattering

If we assuming the electron is free and at rest, the scattered gamma ray has an energy

Initial photon energy, v: photon frequency,

h= 6.757704 meter ·kilogram/second, (Planck's constant)

$$h\nu' = \frac{h\nu}{1 + \frac{h\nu}{m_0 c^2}(1 - \cos(\theta))},$$

mass of electron

Scattering angle

and the photon transfers part of its energy to the electron (assumed to be at rest), which is known as a ***recoil electron****. Its energy is simply*

$$E_{recoil} = h\nu - h\nu' = h\nu - \frac{h\nu}{1 + \frac{h\nu}{m_0 c^2}(1 - \cos(\theta))}$$

The one-to-one relationship between scattering angle and energy loss!!

Reading: Page 51, Radiation Detection and Measurements, Third Edition, G. F. Knoll, John Wiley & Sons, 1999.

The Comptel Observatory

- *Compton telescopes are two-level instruments.*
- *Typically sensitive to photons between 300 eV and 30 MeV.*
- *Top level = photon Compton scatters in liquid scintillator.*
- *Bottom level = Scattered photon travels down and is absorbed by crystal scintillator.*
- *PMTs triggered on both levels.*

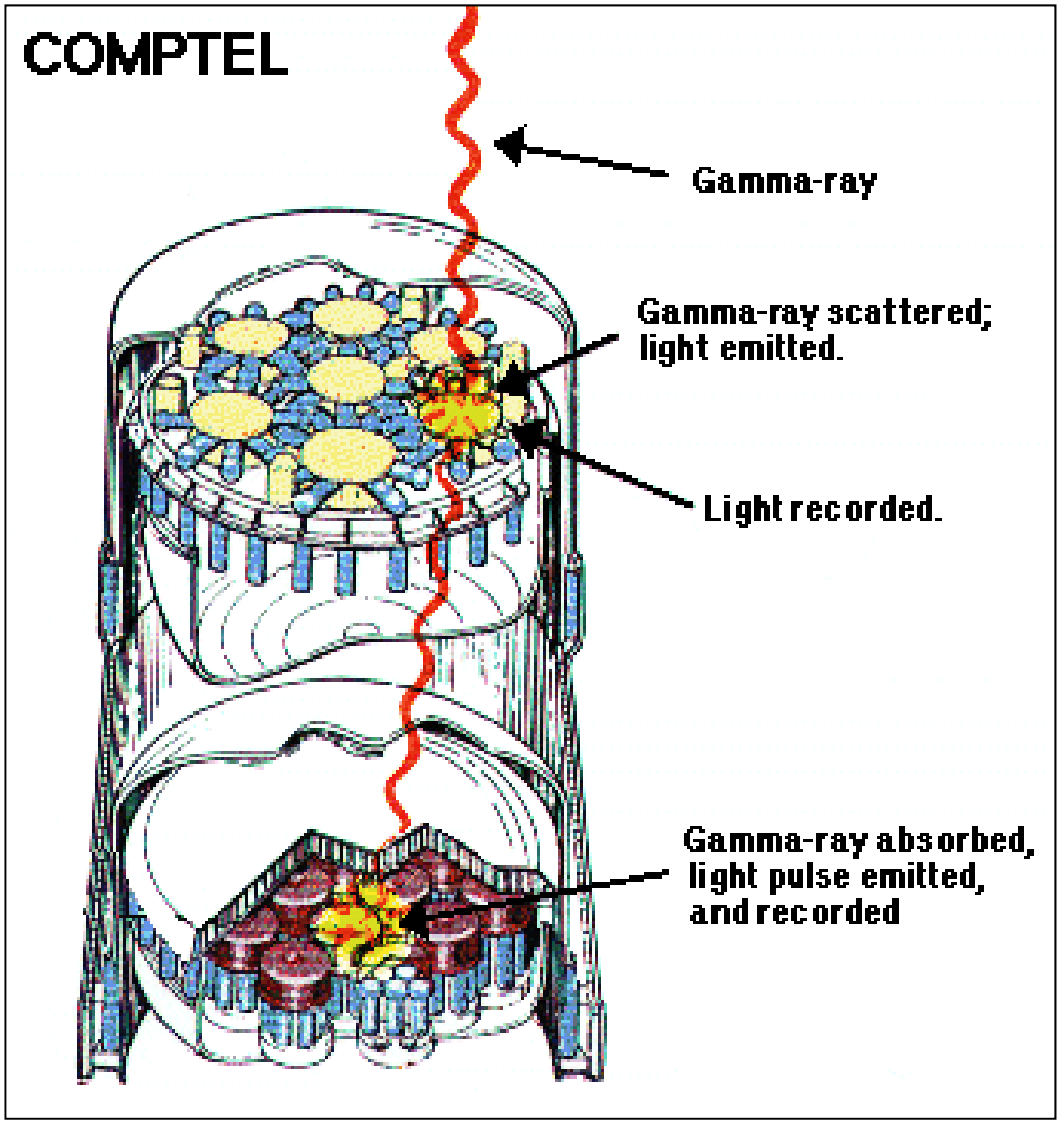

Courtesy of Neal Clinthorne, U. Michigan.

Fundamentals of Positron Emission Tomography (PET)

PET Fundamentals

Ideal Tracer Isotope

- Tracers contain elements of life – perfect for providing the functional information such as metabolism rate.
- Electronic collimation – high sensitivity.
- Easier attenuation correction.

Isotope	half-life (min)	Maximum positron energy (MeV)	Positron range in water (FWHM in mm)	Production method
^{11}C	20.3	0.96	1.1	cyclotron
^{13}N	9.97	1.19	1.4	cyclotron
^{15}O	2.03	1.70	1.5	cyclotron
^{18}F	109.8	0.64	1.0	cyclotron
^{68}Ga	67.8	1.89	1.7	generator
^{82}Rb	1.26	3.15	1.7	generator

Table 2. Properties of commonly used positron emitting radio-isotopes

Annihilation Radiation following Positron Emission

Beta - plus decay or positron decay :

$$ {}^{A}_{Z}X \rightarrow {}^{A}_{Z-1}Y + {}^{0}_{1}\beta + \upsilon $$

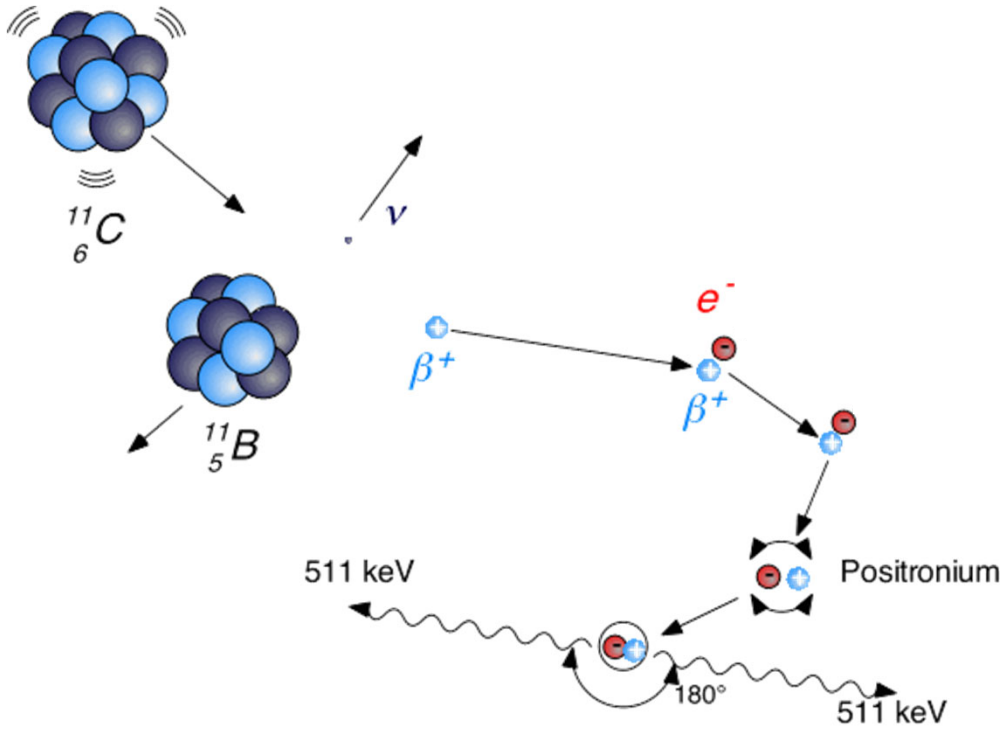

The Tracer Principle Again

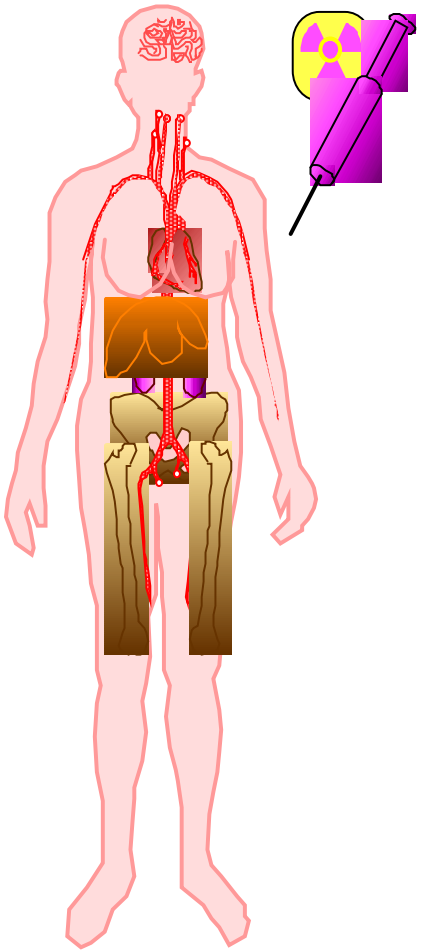

- *Drug is labeled with positron (β^+, anti-particle of an electron) emitting radionuclide.*
- *Drug localizes in patient according to metabolic properties of that drug.*
- *Trace (pico-molar) quantities of drug are sufficient.*
- *Radiation dose fairly small (<1 rem).*

Detect Radioactive Decays

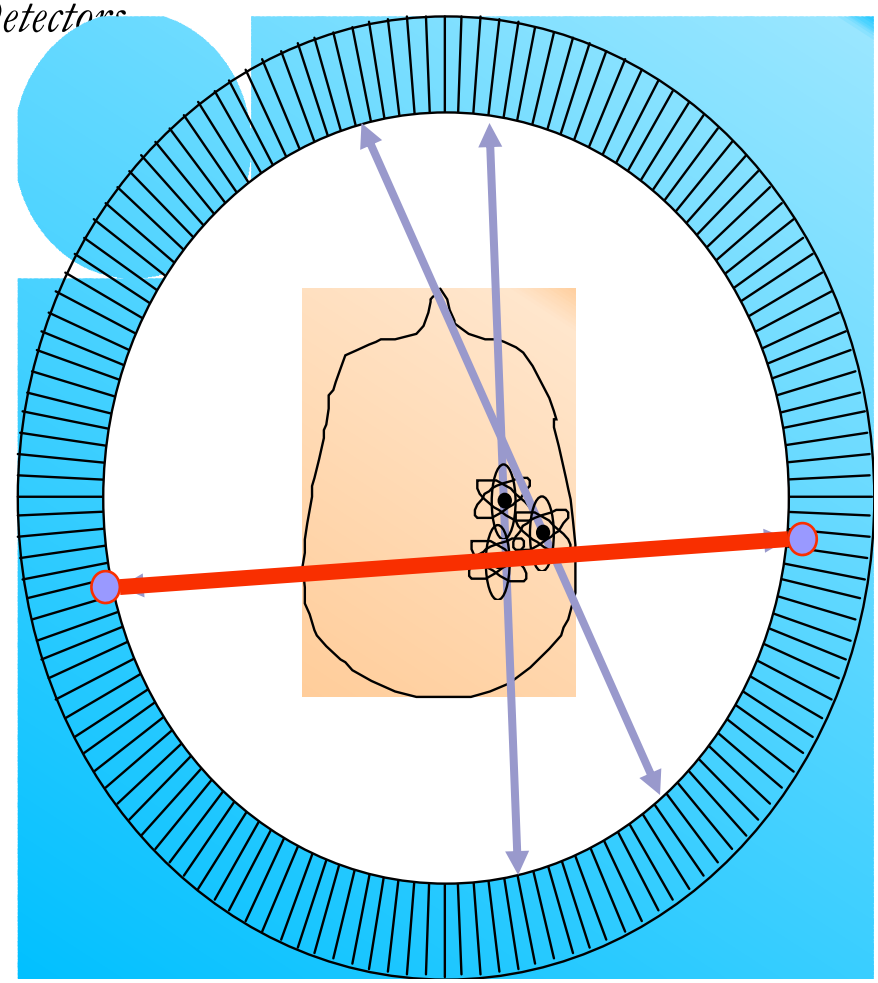

- Radionuclide decays, emitting β^+.
- β^+ annihilates with e^- from tissue, forming back-to-back 511 keV photon pair.
- 511 keV photon pairs detected via time coincidence.
- Positron lies on line defined by detector pair (known as a chord or a line of response or a LOR).

Detect Pair of Back-to Back 511 keV Photons

PET data acquisition

- Organization of data
  - True counts in LORs are accumulated
  - In some cases, groups of nearby LORs are grouped into one average LOR ("mashing")
  - LORs are organized into projections

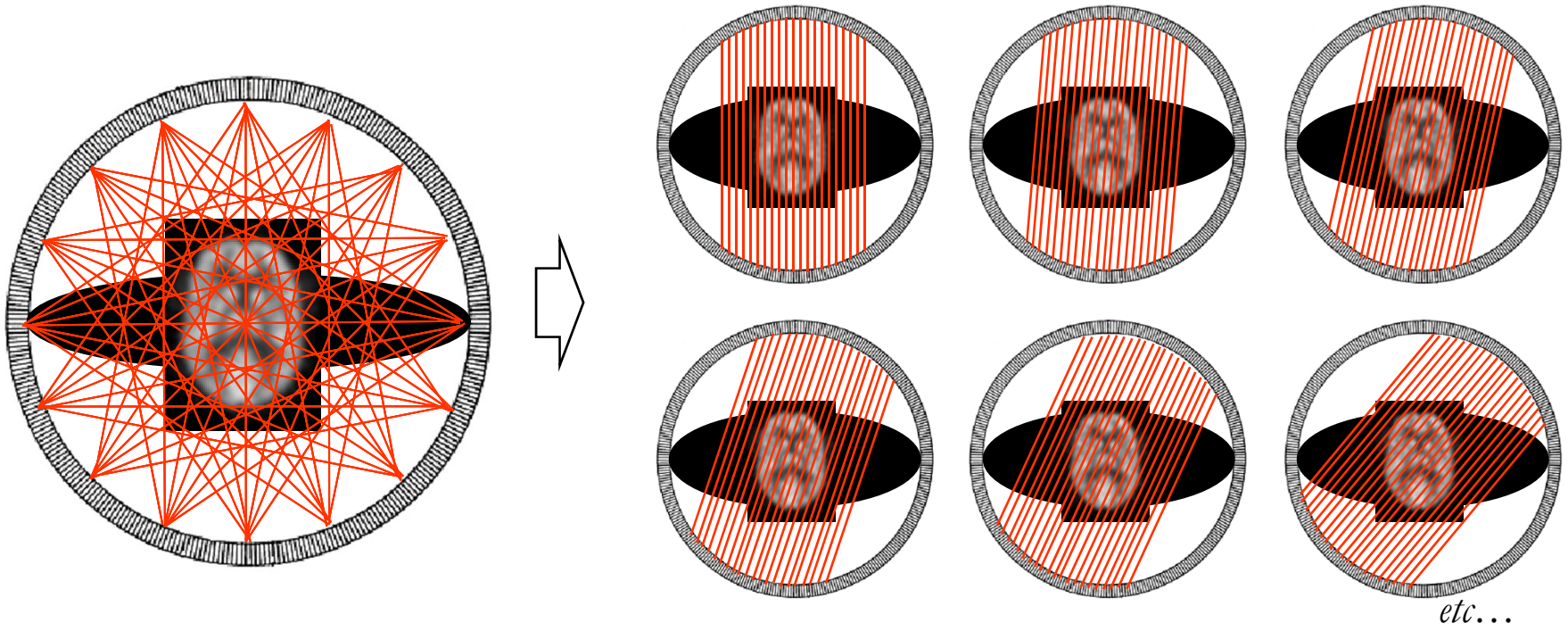

PET data acquisition

- 2D mode vs. 3D mode

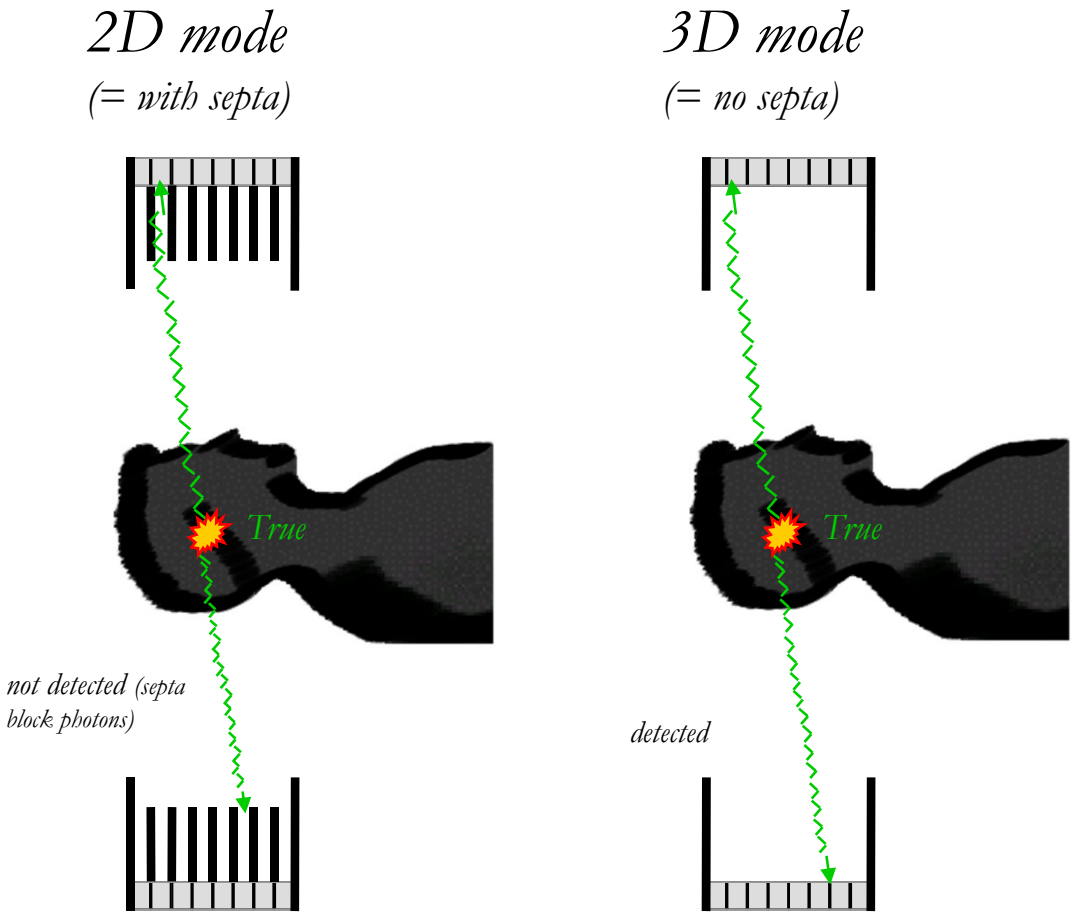

PET data acquisition

- 2D and 3D acquisition modes

2D mode
(= with septa)

3D mode
(= no septa)

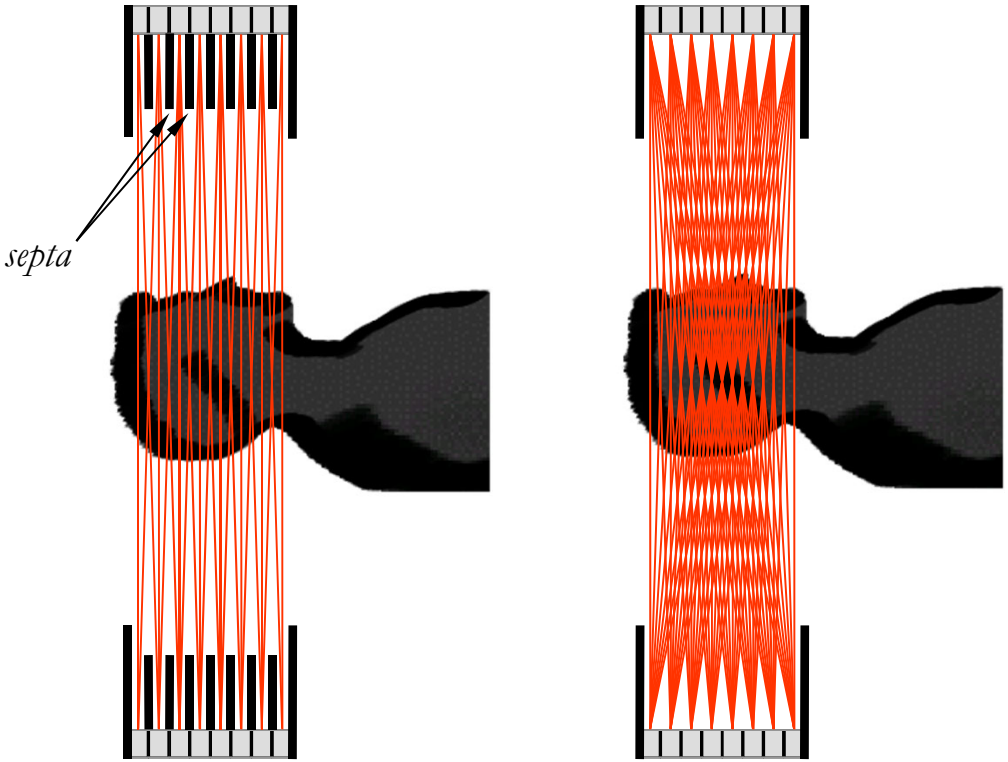

In the 3D mode there are no septa: photons from a larger number of incident angles are accepted, increasing the sensitivity.

Note that despite the name, the 2D mode provides three-dimensional reconstructed images (a collection of transaxial, sagittal and transaxial slices), just like the 3D mode!

Statistical Description of the Projection Data

The probability of a given projection data $\mathbf{g}=(g_1, g_2, g_3, \ldots, g_M)$ *is*

$$p(\mathbf{g}) = \prod_{m=1}^{M} p(g_m) = \prod_{m=1}^{M} \frac{\bar{g}_m^{\,g_m}}{g_m!} e^{-\bar{g}_m}$$

Measured no. of counts on detector pixel m.

where $\bar{g}_m$ is the expected value for the number of counts on detector pixel # m

$$\bar{g}_m = \sum_{n=1}^{N} f_n p_{nm}$$

In the context of emission tomography, p_{nm} *is the probability of a gamma ray generated at a source pixel n is detected by detector element m.*

Remember that

$$\begin{pmatrix} \bar{g}_1 \\ \bar{g}_2 \\ \bar{g}_3 \\ 7 \\ \bar{g}_M \end{pmatrix} = \begin{pmatrix} p_{11} & p_{12} & p_{13} & 6 & p_{1N} \\ p_{21} & p_{22} & p_{23} & 6 & p_{2N} \\ p_{31} & p_{32} & p_{33} & \cdots & p_{3N} \\ 7 & 7 & 7 & 9 & 7 \\ p_{M1} & p_{M2} & p_{M3} & 6 & p_{MN} \end{pmatrix} \begin{pmatrix} f_1 \\ f_2 \\ f_3 \\ \vdots \\ f_N \end{pmatrix}$$

The Maximum Likelihood Reconstruction

Recall that the ***likelihood function,*** $L(\mathbf{f},\mathbf{g})$*, of a possible source function* $\mathbf{f}$ *is*

$$L(\mathbf{f},\mathbf{g}) = p(\mathbf{g} \mid \mathbf{f})$$

So that the maximum likelihood solution (the image that maximizing the likelihood function) can be found as

$$\hat{\mathbf{f}}_{\mathbf{ML}} = \underset{\mathbf{f}}{\operatorname{argmax}}\, L(\mathbf{f},\mathbf{g})$$

or equivalently

$$\hat{\mathbf{f}}_{\mathbf{ML}} = \arg\max_{\mathbf{f}} \log\left[L(\mathbf{f},\mathbf{g})\right] \equiv \underset{\mathbf{f}}{\operatorname{argmax}}\, l(\mathbf{f},\mathbf{g})$$

where $l(\mathbf{f},\mathbf{g})$ is the log-likelihood function

$$l(\mathbf{f},\mathbf{g}) = \log\left[L(\mathbf{f},\mathbf{g})\right]$$

Methods to Estimate the Underlying Image

The Maximum Likelihood Expectation Maximization (MLEM) Algorithm

$$f_n^{(new)} = \frac{f_n^{(old)}}{\sum_{m=1}^{M} p_{nm}} \sum_{m=1}^{M} \frac{g_m}{\sum_{n'=1}^{N} p_{n'm} f_{n'}^{(old)}} p_{nm}, \quad n = 1,2,...,N$$

Why PET?

Element of Life

- Interesting Chemistry

  Easily incorporated into biologically active drugs.

- 1 Hour Half-Life

  Maximum study duration is 2 hours.

  Gives enough time to do the chemistry.

- Easily produced

  Short half life $\Rightarrow$ local production.

^{18}F	*2 hour half-life*
^{15}O, ^{11}C, ^{13}N	*2–20 minute half-life*

glucose, H_2O, NH_3, CO_2, O_2, *etc.*

PET against SPECT

FIGURE 2. (A) Radionuclides that decay by positron emission result in two annihilation photons emitted 180° apart. If both photons are detected, the detection locations define (to within the distance traveled by the positron prior to annihilation) a line along which the decaying atom was located. (B) Radionuclides that decay by emitting single photons provide no positional information, as a detected event could originate from anywhere in the sample volume. (C) For single photon imaging, physical collimation can be used to absorb all photons except those that are incident on the detector from one particular direction (in this case perpendicular to the detector face), defining a line of origin just like the coincident 511-keV photons do following positron emission. To achieve this localization, however, the radiation from the majority of decays has been absorbed and does not contribute to image formation, leading to the detection of many fewer events for a given amount of radioactivity in the object. Absorptive collimation of this kind is the approach used in planar nuclear medicine imaging and in single photon emission computed tomography (SPECT).

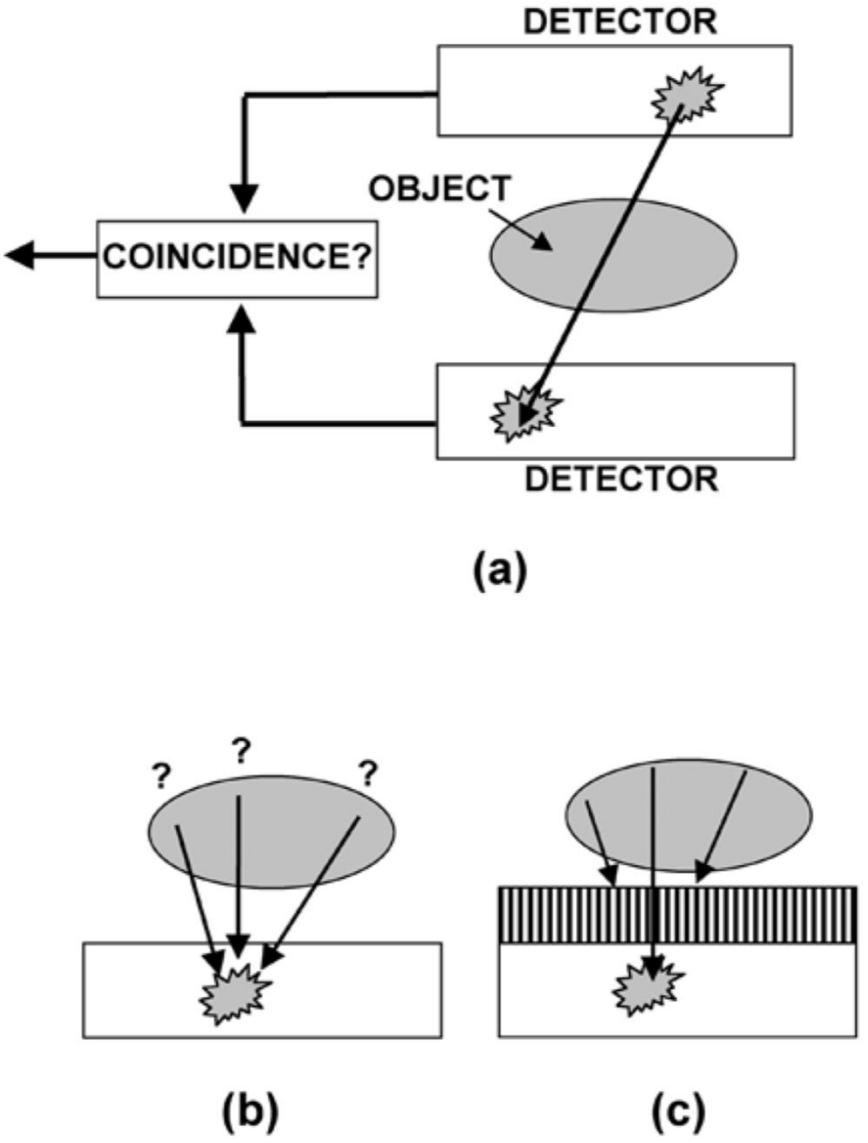

Total-Body PET: Maximizing Sensitivity to Create New Opportunities for Clinical Research and Patient Care

Simon R. Cherry[1,2], Terry Jones[2], Joel S. Karp[3], Jinyi Qi[1], William W. Moses[4], and Ramsey D. Badawi[1,2]

[1]Department of Biomedical Engineering, University of California, Davis, California; [2]Department of Radiology, University of California Davis Medical Center, Sacramento, California; [3]Department of Radiology, University of Pennsylvania, Philadelphia, Pennsylvania; and [4]Lawrence Berkeley National Laboratory, Berkeley, California

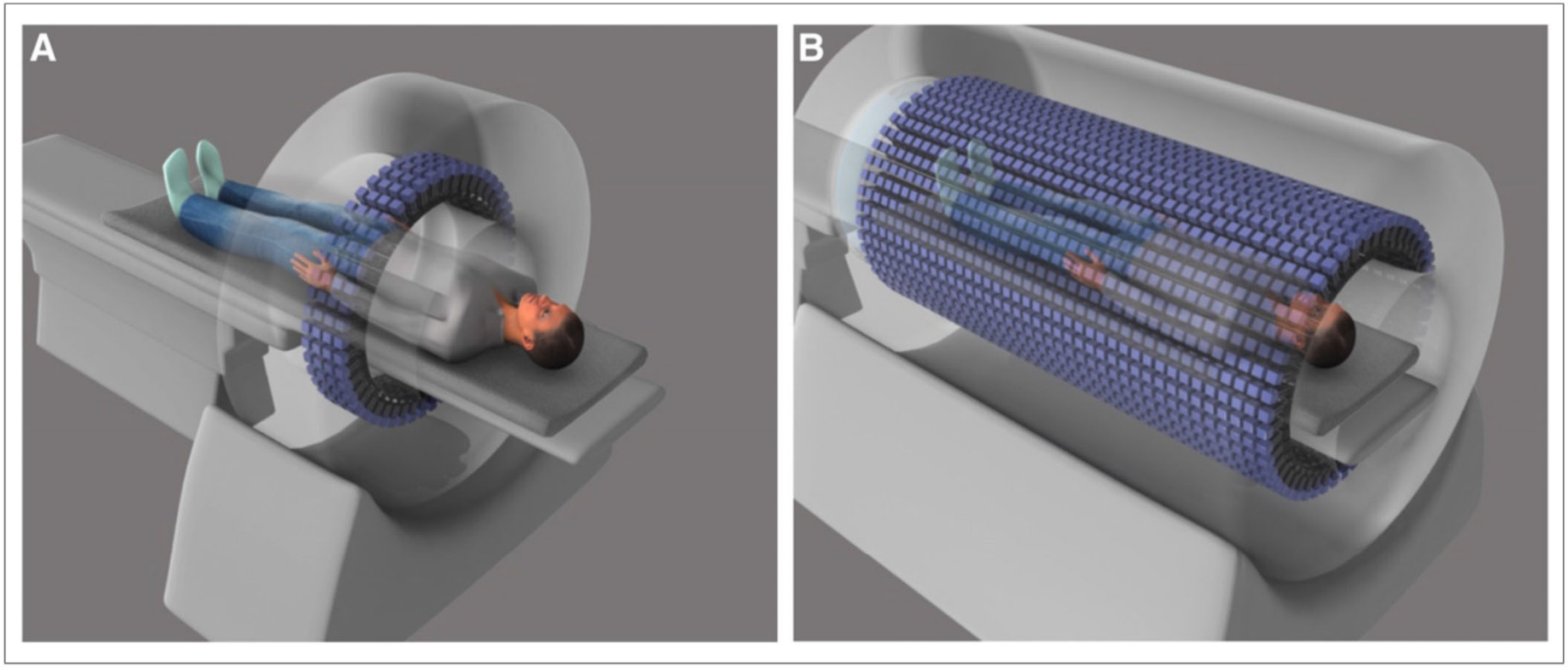

FIGURE 1. Whole-body PET (A) vs. total-body PET (B). (Reprinted with permission of (31).)

$$\mathrm{SNR} \approx k\sqrt{S \times A \times T}, \qquad \text{Eq.1}$$

where k is a constant and S is the effective sensitivity of the scanner. If S is increased by a factor of 40, several consequences

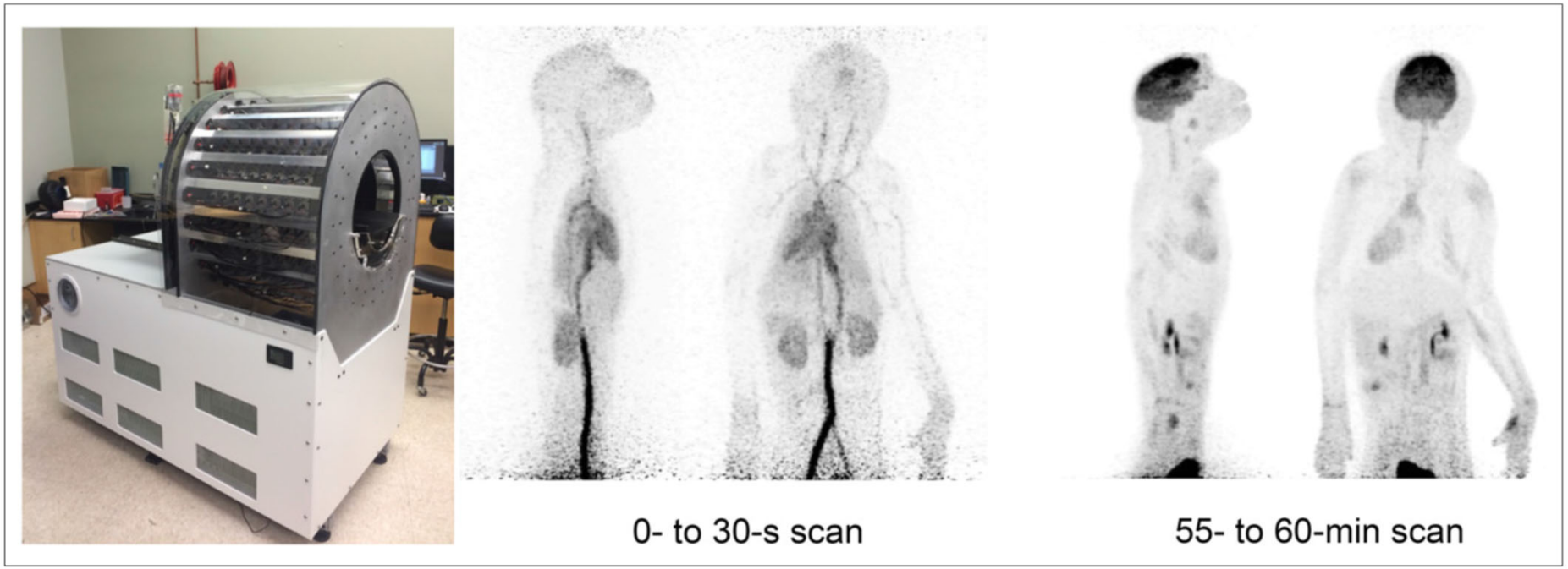

FIGURE 4. Photograph of mini EXPLORER scanner (left) and maximum-intensity-projection images of 2 frames from dynamic total-body imaging study after injection of 8.5 MBq of ^{18}F-FDG ($^{1}/_{10}$ standard activity) in 4.6-kg rhesus macaque (right).

PHILIPS

PET: Impaired Image Quality in Larger Patients

Slim Patient

Large Patient

- *For an equivalent data signal to noise ratio, a 120 kg person would have to be scanned 2.3 times longer than a 60 kg person* [1)]

1) Optimizing Injected Dose in Clinical PET by Accurately Modeling the Counting-Rate Response Functions Specific to Individual Patient Scans. Charles C. Watson, PhD et al Siemens Medical Solutions Molecular Imaging, Knoxville, Tennessee, JNM Vol. 46 No. 11, 1825-1834, 2005

Attenuation Correction ⇒ Quantitation

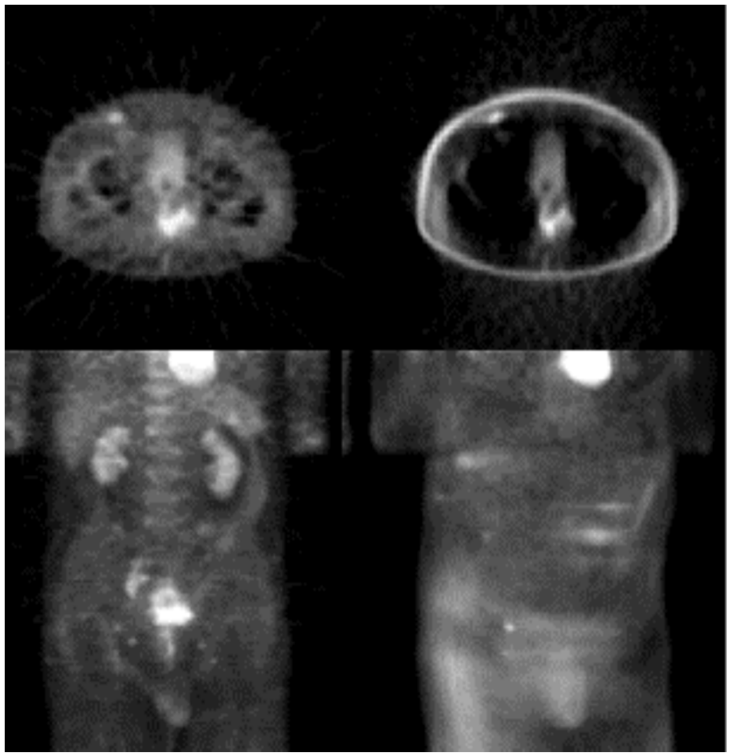

Transverse

Volume Rendered

Corrected *Uncorrected*

**Data courtesy of Duffy Cutler, Washington University*

+	*Accurate Quantitation (μCi/cc) Possible*
–	*Doubles Image Acquisition Time*

Attenuation of Internal Source

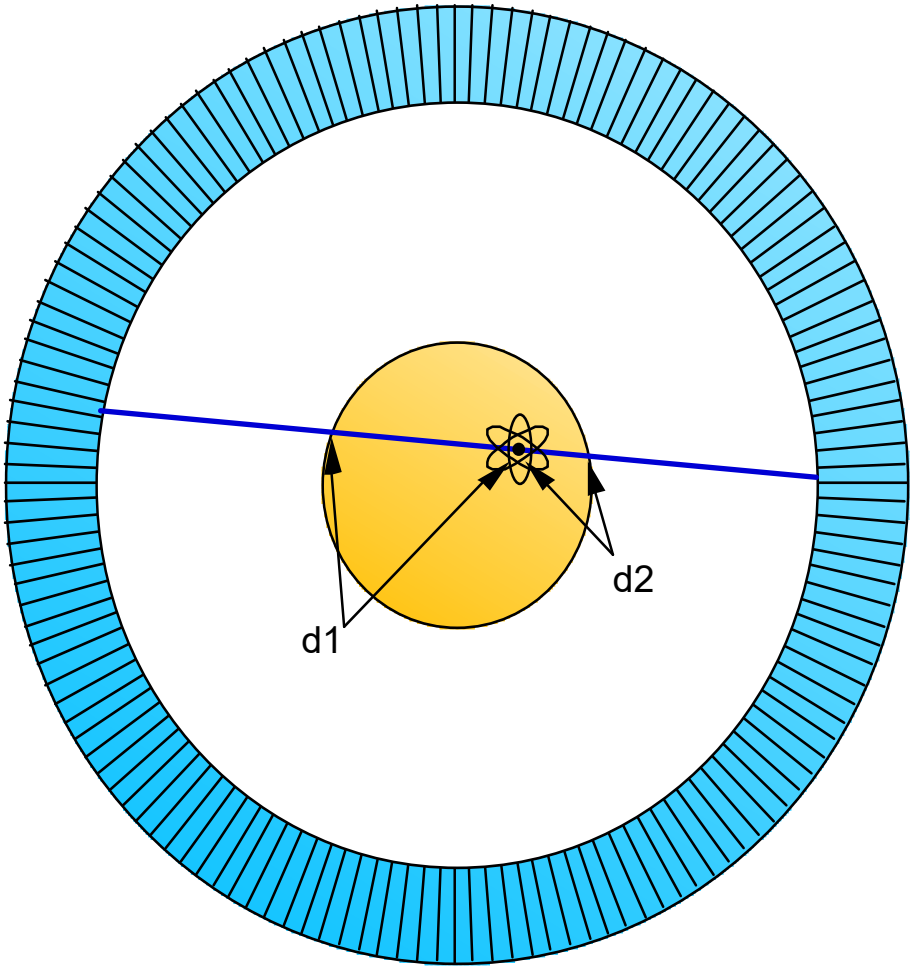

$$P_1 = e^{-\mu \cdot d1} \qquad P_2 = e^{-\mu \cdot d2}$$

$$P = e^{-\mu \cdot (d1+d2)}$$

Event detection probability is product of individual photon detection probabilities.

Clinical Applications

What is [^{18}F]FDG?

GENERAL INFORMATION

Chemical name of **[^{18}F]FDG** is [^{18}F]-2-Fluoro-2-deoxy-β-D-glucopyranose, Chemical Abstract Service registry number 63503-12-8. More commonly it is called [^{18}F]Fluorodeoxyglucose or simply FDG.

This compound is a radioactive derivative of 2-deoxy-D-glucose labelled with positron-emitting isotope $^{18}_{9}$F in the position 2 of the glucose core structure.

Relative molecular mass: 181.15 g/mol

NAMES:

FDG

[^{18}F]FLUORODEOXYGLUCOSE

[^{18}F]-2-Fluoro-2-deoxy-β-D-glucopyranose

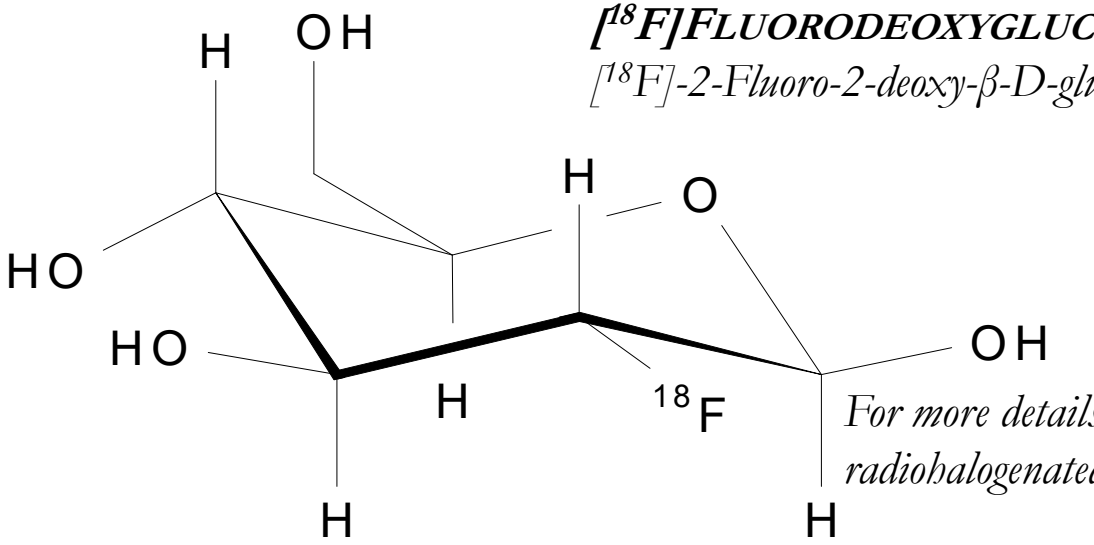

For more details please refer to review article on radiohalogenated sugars.

Why [^{18}F]FDG-PET in tumors?

Elevated glucose metabolism in tumor

[^{18}F]FDG is a glucose analog

[^{18}F]FDG uptake into ***viable neoplastic cells***

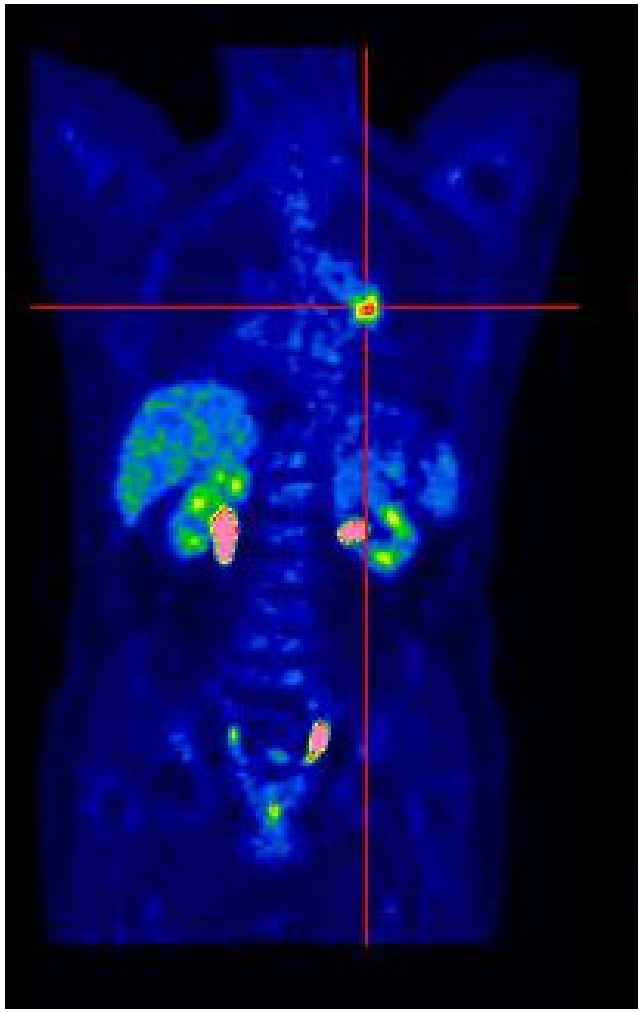

[^{18}F]FDG PET: APPLICATION IN LUNG CANCER

- *Differentiating benign from malignant lesions (SPN)*
- *Staging and re-staging for therapy planning*
- *Predicting and monitoring response to therapy*

Other Clinical Uses

- Brain Dysfunction
  - Tumor vs. Necrosis
  - Alzheimer's Disease
  - Epilepsy
- Heart Tissue Viability

Why Combine PET/SPECT with MRI

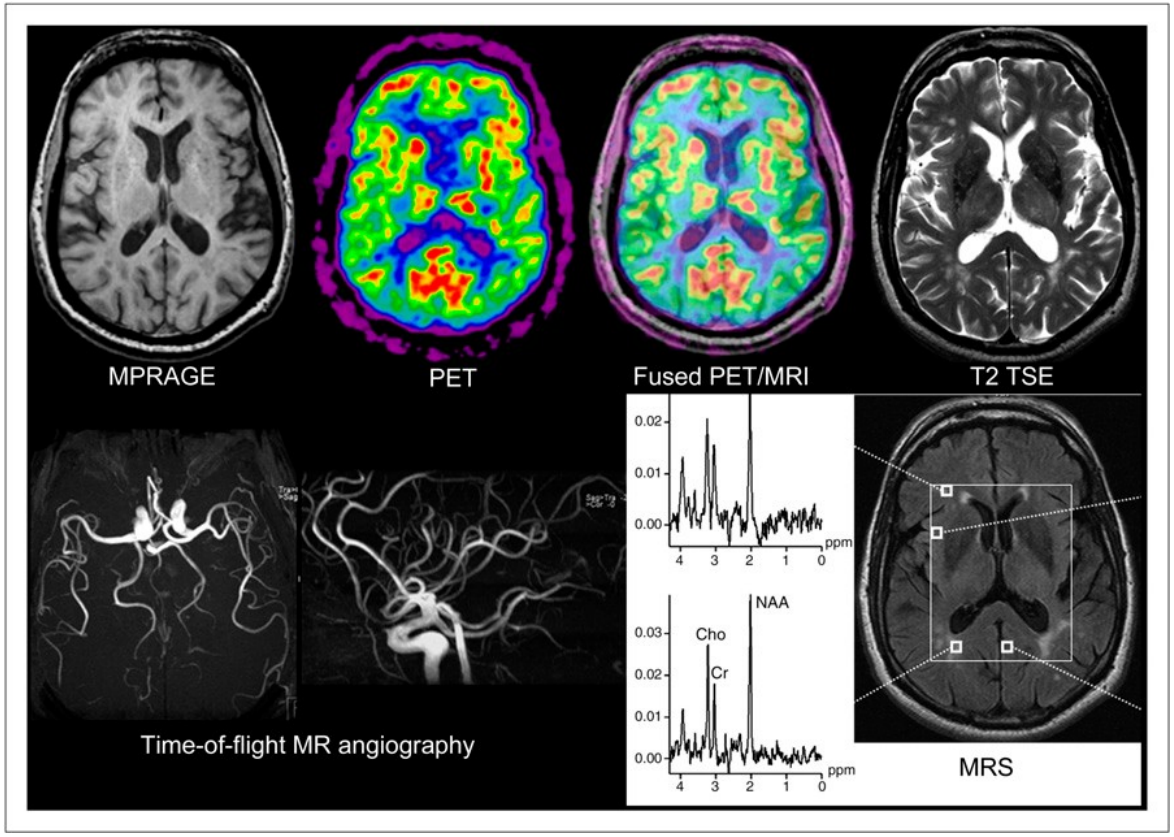

*FIGURE 1. First simultaneous PET/MRI study in 66-y-old healthy volunteer. MRI sequences included T2-weighted turbo spin echo, echo planar, time-of-flight MR angiog- raphy, and MR spectroscopy. PET image displayed was reconstructed from 20-min emission data recorded at steady state after injection of 370 MBq of 18F-FDG. Data were acquired on BrainPET prototype (Siemens). MPRAGE 5 magnetization-prepared rapid gradient echo; MRS 5 MR scintigraphy; TSE 5 turbo spin echo. (**Ciprian Catana et al, Journal of Nuclear Medicine, 2012**)*

Why Combine PET with MRI

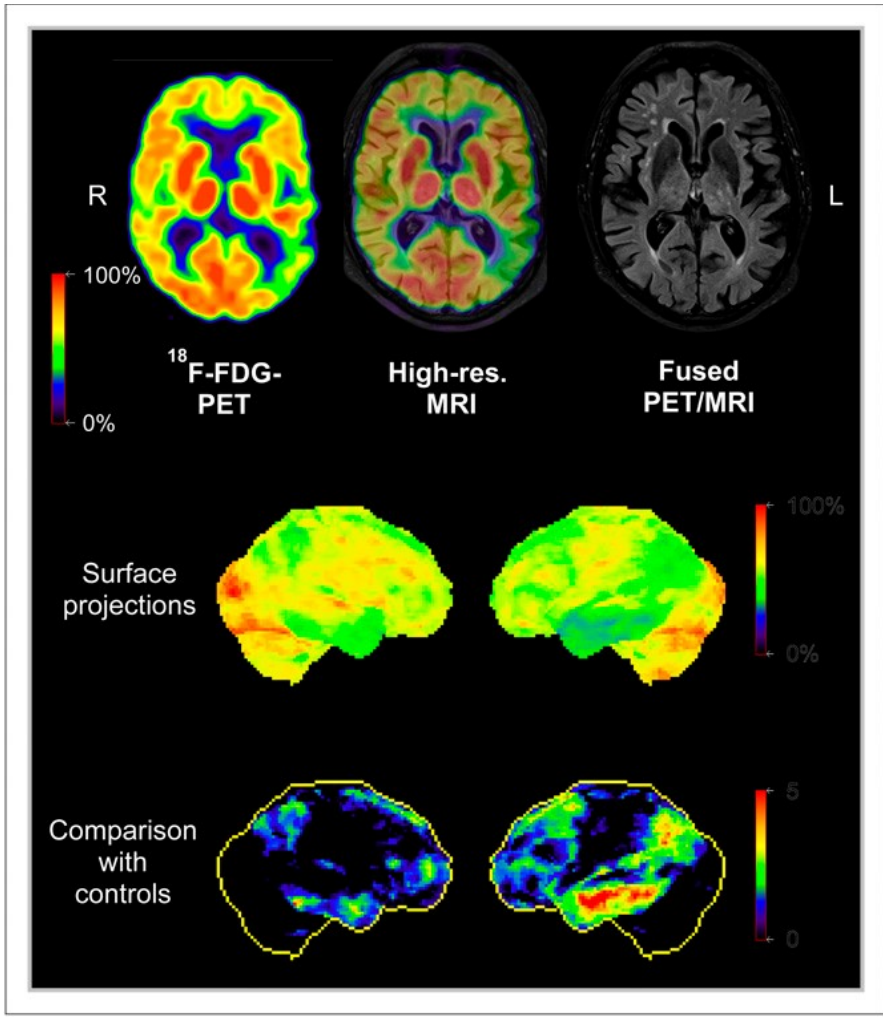

*FIGURE 5. Simultaneous PET/MRI study in Alzheimer disease patient. (Top) Axial 18F-FDG PET, high-resolution MRI, and fusion image. Areas with reduced metabolism (green) representing impaired neuronal function are visible in left temporoparietal cortex. (Middle and bottom) Surface projections of cerebral metabolism and of z score images (comparison with controls). Data were acquired on Biograph mMR scanner. (**Ciprian Catana et al, Journal of Nuclear Medicine, 2012**)*

Fundamental Limitations on PET Imaging Performance

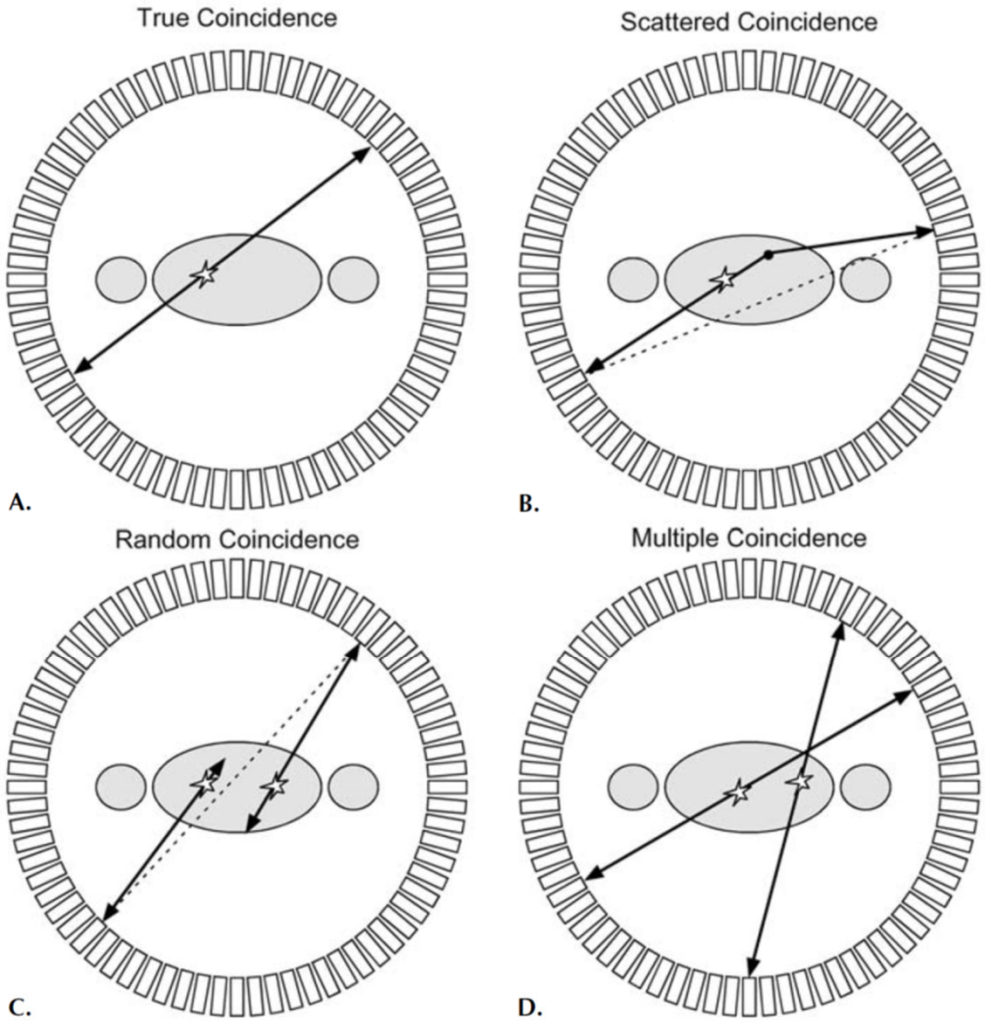

FIGURE 22. Illustration of the four main coincidence event types. A: True coincidence. Both annihilation photons escape the body and are recorded by a pair of detectors. B: Scattered coincidence. One or both of the two annihilation photons interacts in the body prior to detection. This results in a mispositioning of the event. C: Random coincidence: A coincidence is generated by two photons originating from two separate annihilations. These events form a background in the data that needs to be subtracted. D: Multiple coincidence: Three or more photons are detected simultaneously. Due to the ambiguity of where to position the events, these normally are discarded. (Reprinted from *Physics in Nuclear Medicine*, 2nd ed, Cherry SR, Sorenson JA, Phelps ME, W.B. Saunders, New York 1986, with permission from Elsevier.)

PET Data Acquisition

Signal and Noise

PET: Physics, Instrumentation, and Scanners

Simon R. Cherry and Magnus Dahlbom

Positron Range

TABLE 2. Select List of Radionuclides That Decay by Positron Emission and Are Relevant to PET Imaging

Radionuclide	*Half-life*	E_{max}(Mev)	β^+ *Branching Fraction*
^{11}C	20.4 min	0.96	1.00
^{13}N	9.97 min	1.20	1.00
^{15}O	122 s	1.73	1.00
^{18}F	109.8 min	0.63	0.97
^{22}Na	2.60 y	0.55	0.90
^{62}Cu	9.74 min	2.93	0.97
^{64}Cu	12.7 h	0.65	0.29
^{68}Ga	67.6 min	1.89	0.89
^{76}Br	16.2 h	Various	0.56
^{82}Rb	1.27 min	2.60, 3.38	0.96
^{124}I	4.17 d	1.53, 2.14	0.23

Based on data from Table of Nuclides: www2.bnl.gov/ton (accessed October 17th, 2002)

PET: Physics, Instrumentation, and Scanners

Simon R. Cherry and Magnus Dahlbom

Annihilation Radiation following Positron Emission

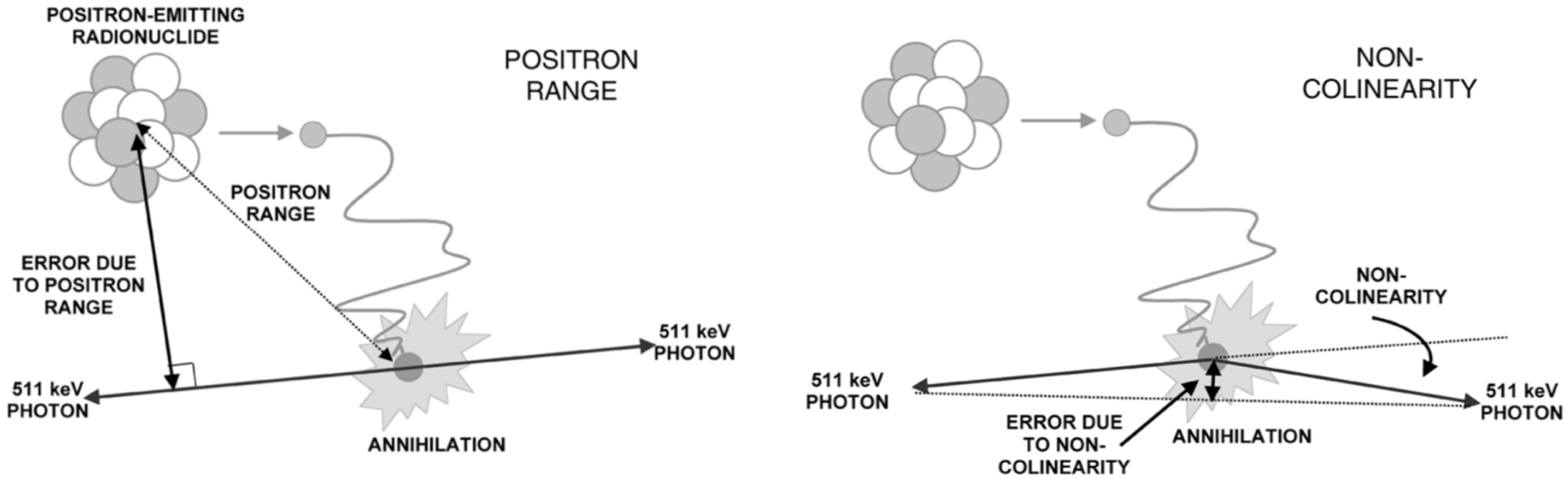

FIGURE 4. Error in determining the location of the emitting nucleus due to positron range (top) and noncolinearity (bottom). The positron range error is dependent on the energy of the emitted positrons. Noncolinearity is independent of radionuclide, and the error is determined by the separation of the detectors. The deviation from noncolinearity is highly exaggerated in the figure; the average angular deviation from 180° is about ± 0.25°. (Reproduced with permission from Cherry SR, Sorenson JA, Phelps ME. *Physics in Nuclear Medicine*, W.B. Saunders, New York, 2003.)

Positron Range

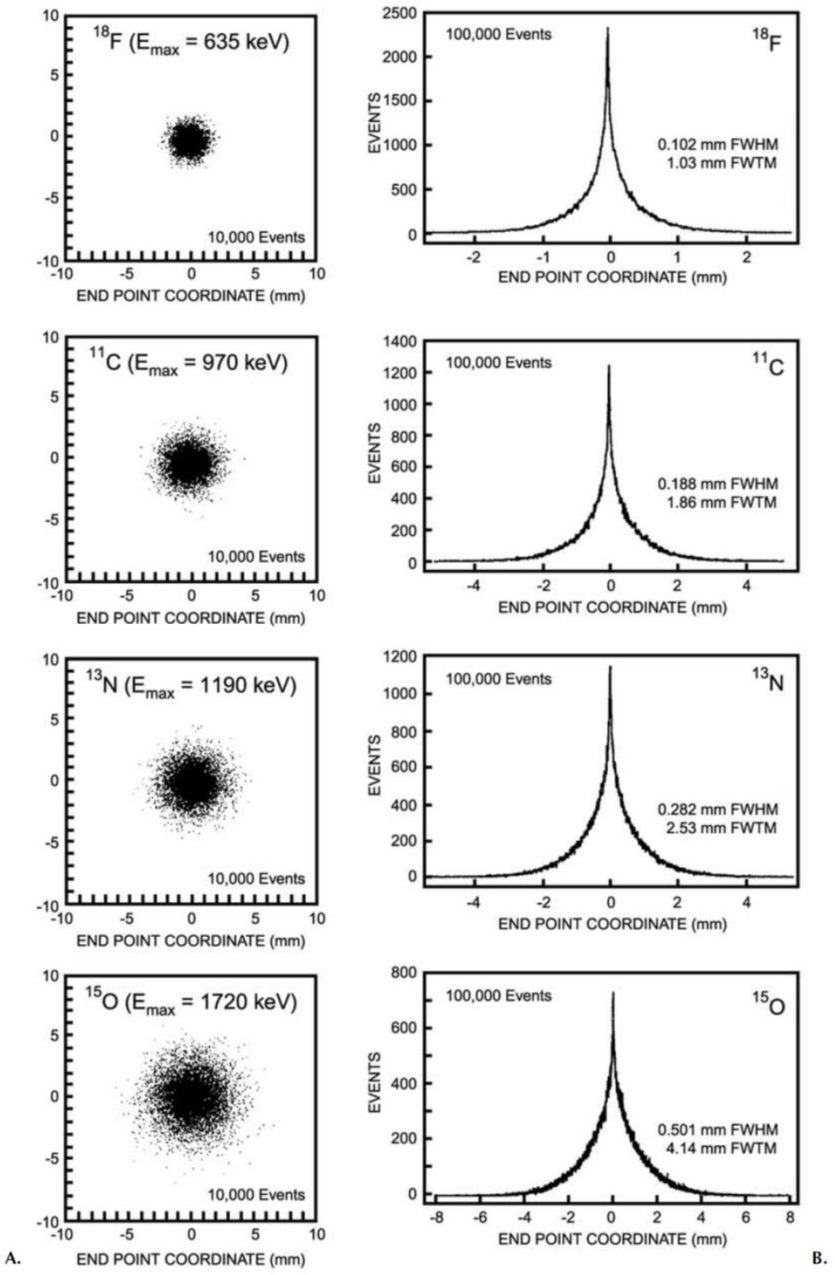

FIGURE 5. A: Simulations for several PET radionuclides showing the distribution of positron annihilation sites in water for positrons emitted at the center of the image (position 0.0 mm). B: Profiles through the simulated distributions showing measured FWHM and FWTM of the distributions. Abbreviations: FWHM, full width at half maximum; FWTM, full width at tenth maximum. (Reproduced with permission from Levin C, Hoffman EJ. *Phys Med Biol* 1999, 44: 781–799.)

Noncollinearity

noncolinearity. This effect is independent of radionuclide because the positrons must lose most of their energy before they can annihilate; hence, the initial energy is irrelevant. The distribution of emitted angles is roughly Gaussian in shape, with a full width at half maximum (FWHM)* of ~0.5°. After detecting the annihilation photons, PET assumes that the emission was exactly back to back, resulting in a small error in locating the line of annihilation (Figure 4 bottom). Assuming a Gaussian distribution and using the fact that the angles are small, the blurring effect due to noncolinearity, Δ_{nc}, can be estimated as:

$$\Delta_{nc} = 0.0022 \times D \tag{10}$$

where D is the diameter of the PET scanner. The error increases linearly as the diameter of the PET scanner increases. Once again, the effect is relatively small compared with the detector resolution in most clinical PET scanners. In PET scanners used for animals, D generally is small, and as illustrated in Example 4, noncolinearity is not a major limiting factor at the present time.

EXAMPLE 4

Calculate the blurring due to photon noncolinearity in an 80-cm diameter PET scanner designed for imaging humans and in a 15-cm diameter PET scanner designed for imaging small animals.

ANSWER

From Equation 10, the blurring is calculated as:

80-cm human scanner:

$$\Delta_{nc} = 0.0022 \times D = 0.0022 \times 800 \text{ mm} = 1.76 \text{ mm}$$

15-cm small-animal scanner:

$$\Delta_{nc} = 0.0022 \times D = 0.0022 \times 150 \text{ mm} = 0.33 \text{ mm}$$

Fundamental Challenges on PET Detector Technology

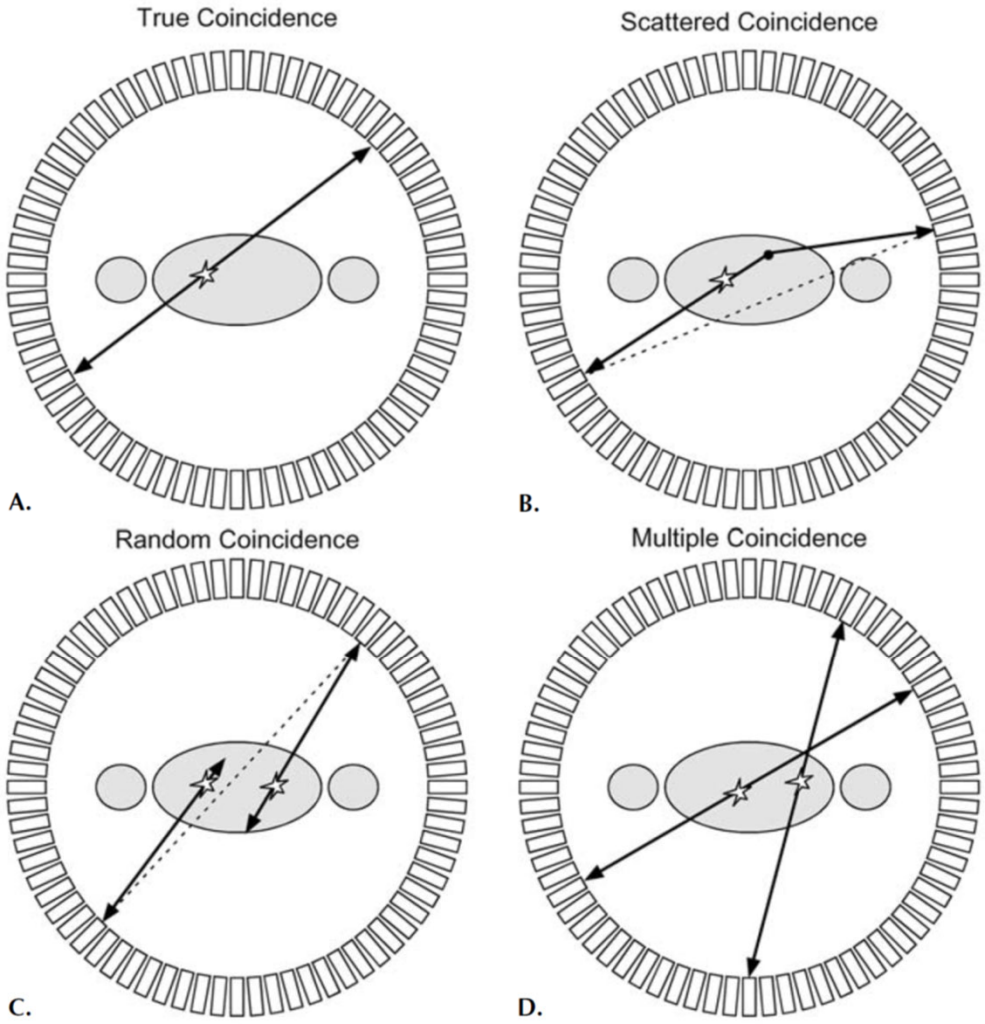

FIGURE 22. Illustration of the four main coincidence event types. A: True coincidence. Both annihilation photons escape the body and are recorded by a pair of detectors. B: Scattered coincidence. One or both of the two annihilation photons interacts in the body prior to detection. This results in a mispositioning of the event. C: Random coincidence: A coincidence is generated by two photons originating from two separate annihilations. These events form a background in the data that needs to be subtracted. D: Multiple coincidence: Three or more photons are detected simultaneously. Due to the ambiguity of where to position the events, these normally are discarded. (Reprinted from *Physics in Nuclear Medicine*, 2nd ed, Cherry SR, Sorenson JA, Phelps ME, W.B. Saunders, New York 1986, with permission from Elsevier.)

PET Data Acquisition

Signal and Noise

PET: Physics, Instrumentation, and Scanners

Simon R. Cherry and Magnus Dahlbom

PET Camera & Detector Design

- *Typical Parameters*
- *Detector Module Design*

What Do We Need for PET Detector?

- *Efficient – 511keV gamma rays are not easily stopped in detector.*
- *Excellent timing accuracy (typically a few ns) – for coincidence measurements.*
- *Capability of a very high counting rate (e.g. 0.5MC/s per cm^2)*
- *High detector spatial resolution – for high imaging resolution. Currently 4 mm × 30mm in commercial clinical PET scanners.*
- *Cost-effective – very large detector volume is needed for practical PET systems.*

Scintillation Crystal Properties

TABLE 1 Properties of Common Scintillation Crystals Used in Small-FOV Imager Designs

Scintillator	Effective Z	Density (g/cc)	Radiation Length (mm)[a]	Relative Light Yield	Refractive Index	Decay Time (ns)	Peak Emission Wavelength (nm)	Hygroscopic?	Rugged?
NaI(Tl)	51	3.67	3.4	100	1.85	230	410	Yes	No
CsI(Tl)	54	4.51	2.2	135	1.79	1000	530	No	Yes
CsI(Na)	54	4.51	2.2	75	1.79	650	420	No	Yes
BGO	74.2	7.13	10.5	15	2.15	300	480	No	Yes
LSO(Ce)	65.5	7.4	11.6	75	1.82	40	420	No	Yes
CaF_2(Eu)[b]	16.9	3.17	N/A	50	1.43	940	435	No	Yes

[a]Radiation lengths for NaI(Tl), CsI(Tl) and CsI(Na) are for 140-keV photons; Values for BGO and LSO are at 511 keV.
[b]CaF_2(Eu) is used in beta imaging.

Lutetium Orthosilicate (LSO) Scintillator

Compared to BGO, LSO has:

Same Attenuation Length:

⇒ *Good Spatial Resolution*

Higher Light Output:

⇒ *Decode More Crystals per Block*

⇒ *Better SNR for "Enhanced" Readout (e.g. Depth of Interaction)*

Shorter Decay Time:

⇒ *Less Dead Time (Allows Larger Block Areas)*

⇒ *Better Timing Resolution*

Reduce Cost OR Increase Performance

PET Cameras

FIGURE 15. Photograph of a large-area NaI(Tl) detector designed for PET applications. The scintillator plate is 50 cm long by 15 cm wide by 2.5 cm thick and is read by thirty, 5-cm diameter PM tubes. Six of these detectors have been used in an hexagonal array to form a PET scanner. (Photograph courtesy of Dr. Joel Karp, University of Pennsylvania.)

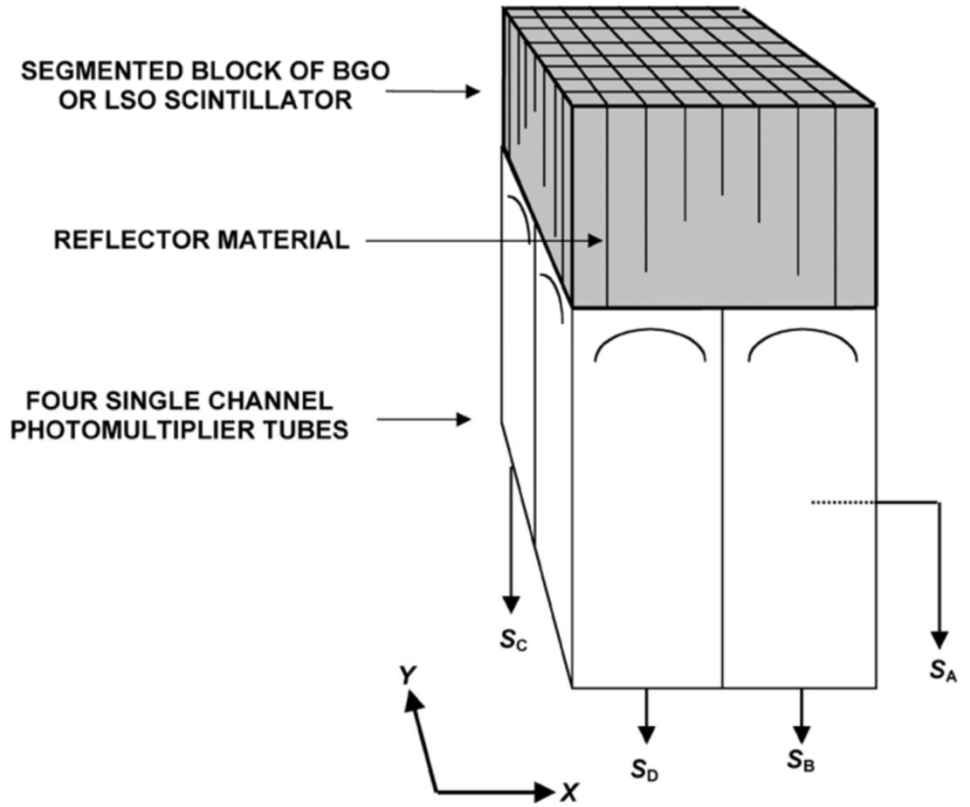

FIGURE 12. Schematic drawing of a typical PET block detector. A block of scintillator is segmented into an 8×8 array using a diamond saw. White reflective material is used in the saw cuts to optically isolate elements. Depth of the saw cuts determines the spread of scintillation light onto four single-channel photomultiplier tubes. By looking at the ratio of signals in the four PMTs, the detector element in which an annihilation photon interacted can be determined. (Reproduced with permission from Cherry SR, Sorenson JA, Phelps ME. *Physics in Nuclear Medicine*, W.B. Saunders, New York, 2003.)

Quadrant Sharing

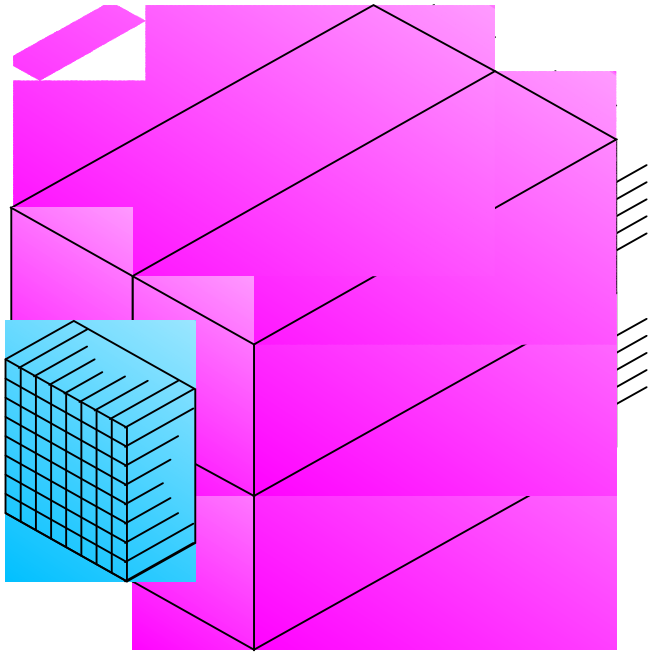

Perspective View

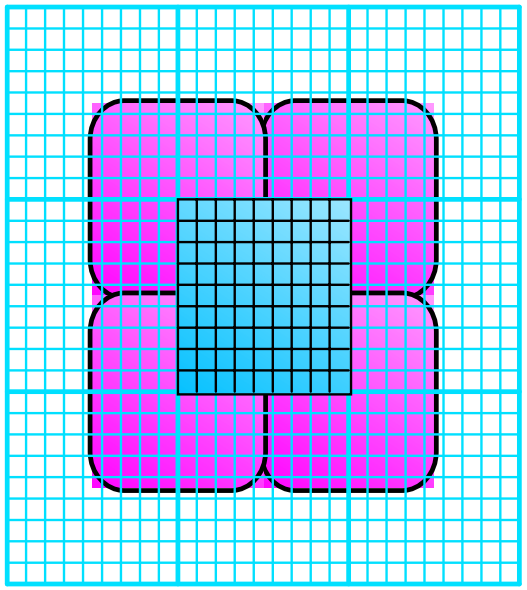

Front View

Each PMT Services 4 Crystal Blocks (Not 1)
(Number of PMTs = Number of Blocks)

\+ *Cost of PMTs Reduced 4x*
– *Dead Time Increased 9x*

Radial Elongation

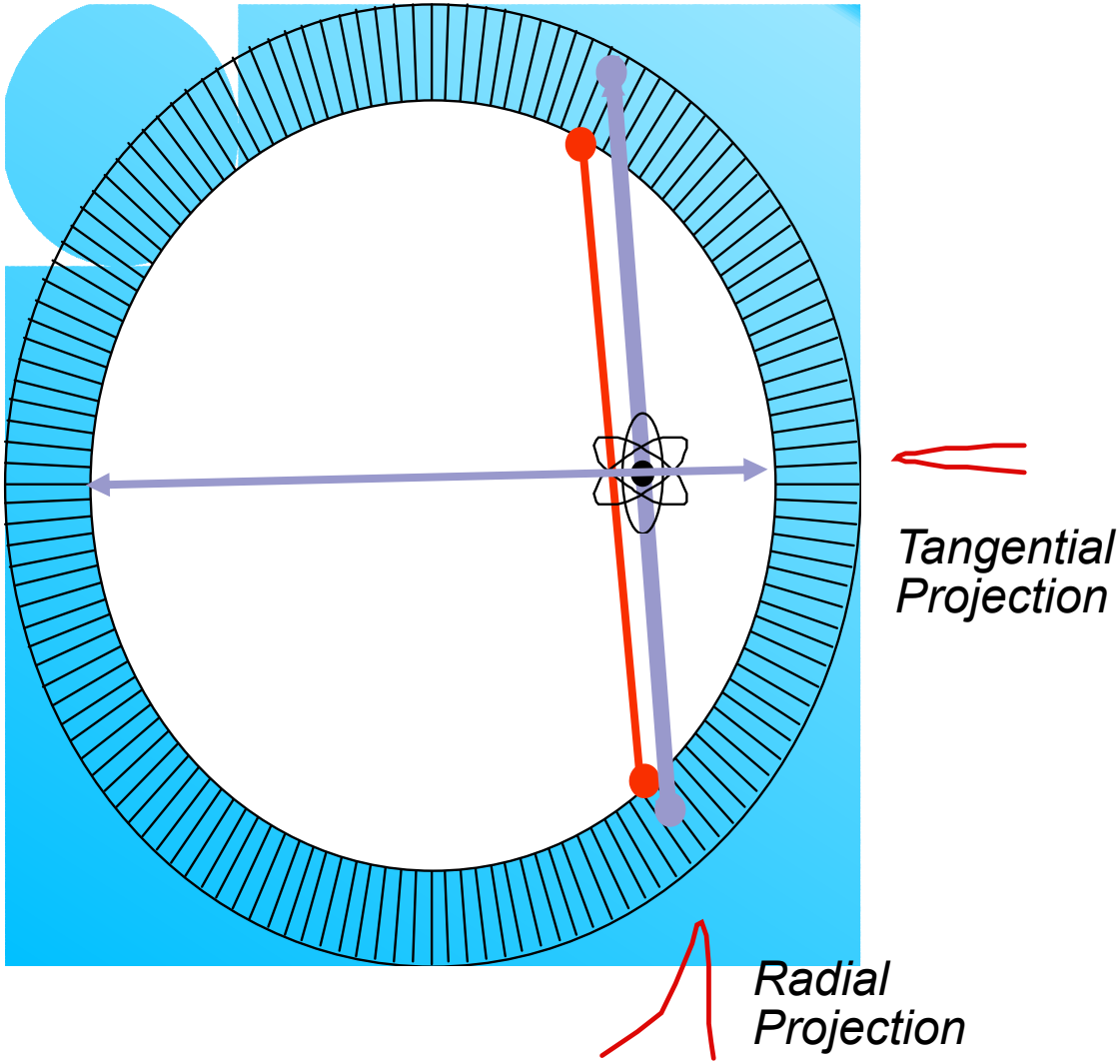

- *Penetration of 511 keV photons into crystal ring blurs measured position.*
- *Blurring worsens as attenuation length increases.*
- *Effect variously known as Radial Elongation, Parallax Error, or Radial Astigmatism.*
- *Can be removed (in theory) by measuring depth of interaction.*

Spatial Resolution

Factor	Shape	FWHM
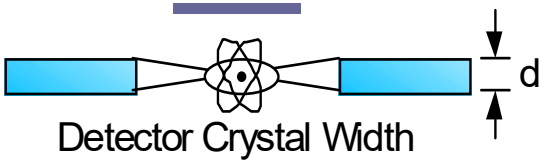 Detector Crystal Width		d/2
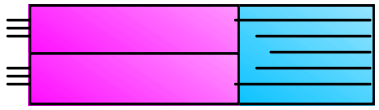 Anger Logic		0 (individual coupling) 2.2 mm (Anger logic)* *empirically determined from published data
180Þ± 0.25Þ 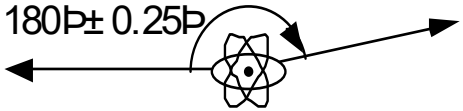 Photon Noncollinearity		1.3 mm (head) 2.1 mm (heart)
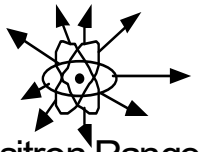 Positron Range		0.5 mm (^{18}F) 4.5 mm (^{82}Rb)
Reconstruction Algorithm	multiplicative factor	1.25 (in-plane) 1.0 (axial)

- *Dominant Factor is Crystal Width*
- *Limit for 80 cm Ring w/ Block Detectors is 3.6 mm*

Spatial Resolution Away From Center

Point Source Images in 60 cm Ring Diameter Camera

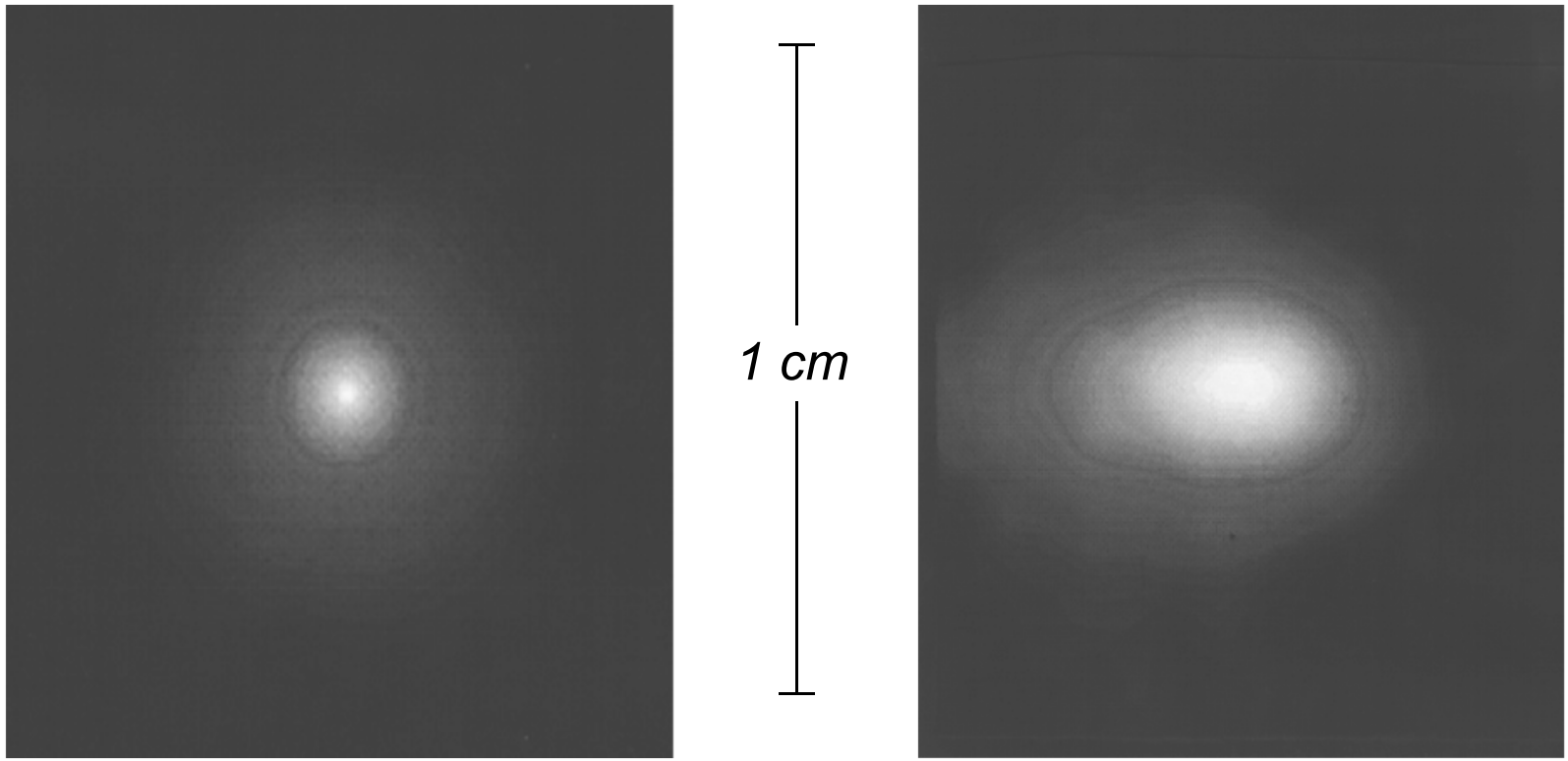

Near Tomograph Center

14 cm from Tomograph Center

Resolution Degrades Significantly...

Loss in Spatial Resolution

Underlying Distribution

Gray / White Ratio = 4:1

Measured Distribution

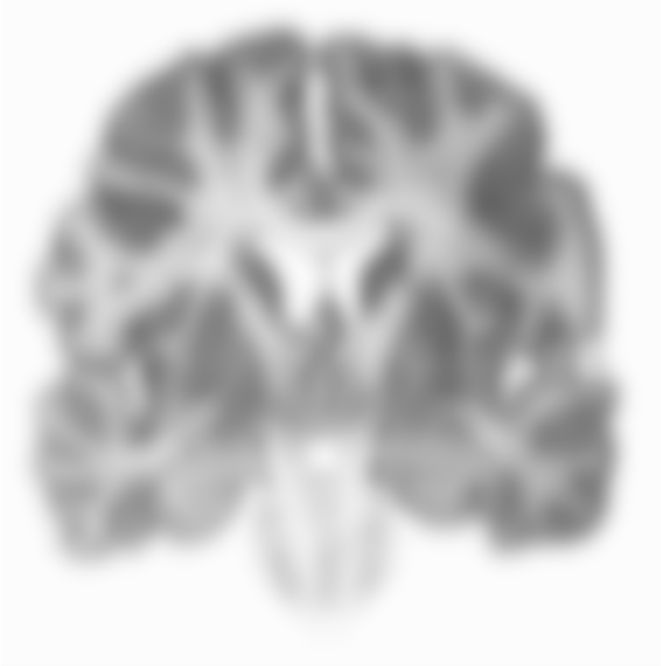

Gray / White Ratio = 2.5:1

Techniques for Extracting DOI Information

FIGURE 17. PET detectors with depth-encoding capability. A: Detector is similar to the standard block detector but is made of two layers of scintillators that have different decay times. An interaction can be assigned to the top or bottom layer, depending on the decay time of the pulse that it generates. This provides one-level (top or bottom) depth of interaction information. (Reproduced from Cherry SR, Sorenson JA, Phelps ME. *Physics in Nuclear Medicine*, 3rd ed, W.B. Saunders, New York, 2003, with permission from Elsevier). B: An array of scintillator elements has photodetectors at both ends. A silicon PIN photodiode is used to determine which crystal the interaction took place in, and the single-channel PMT at the back of the array is used to generate the fast timing signal necessary for PET and a high signal-to-noise measure of the deposited energy. The ratio of the signal in the photodiode and PMT gives an indication of the depth of interaction within the detector element.[25] This provides continuous depth of interaction information but requires careful calibration of the depth information. Abbreviations: LSO, lutetium oxyorthosilicate.

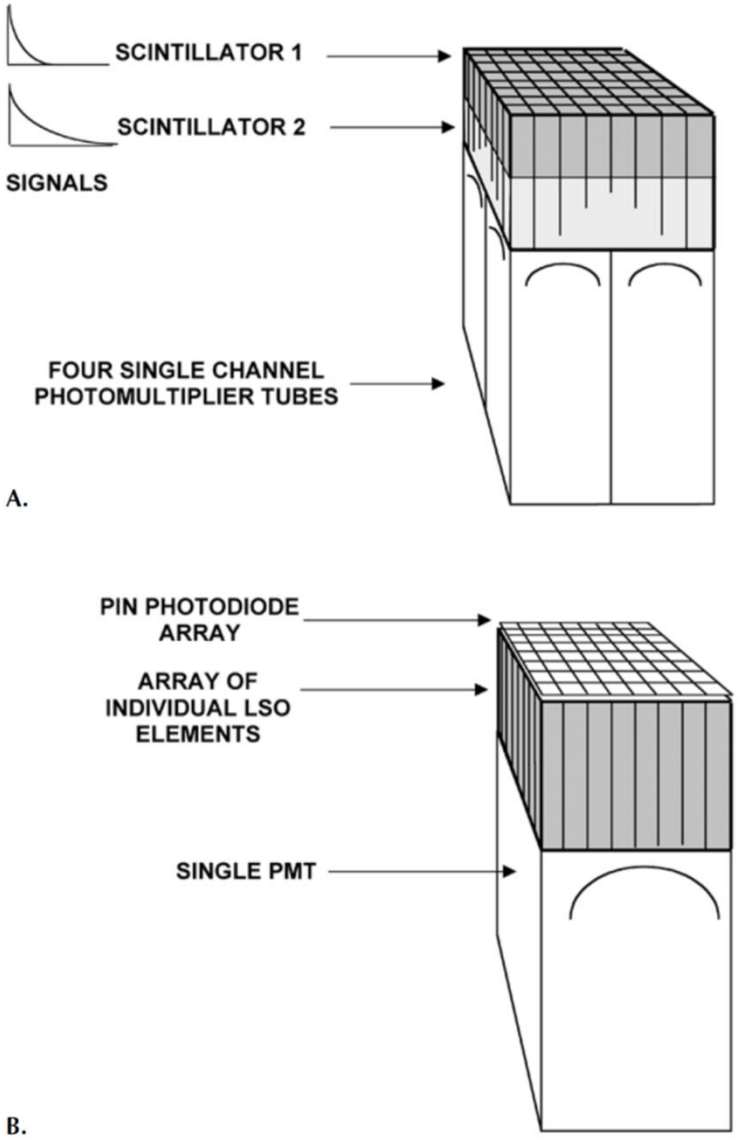

Timing Resolution of a PET Scatter and Radom Coincidence

Imperfections in PET Image Acquisation

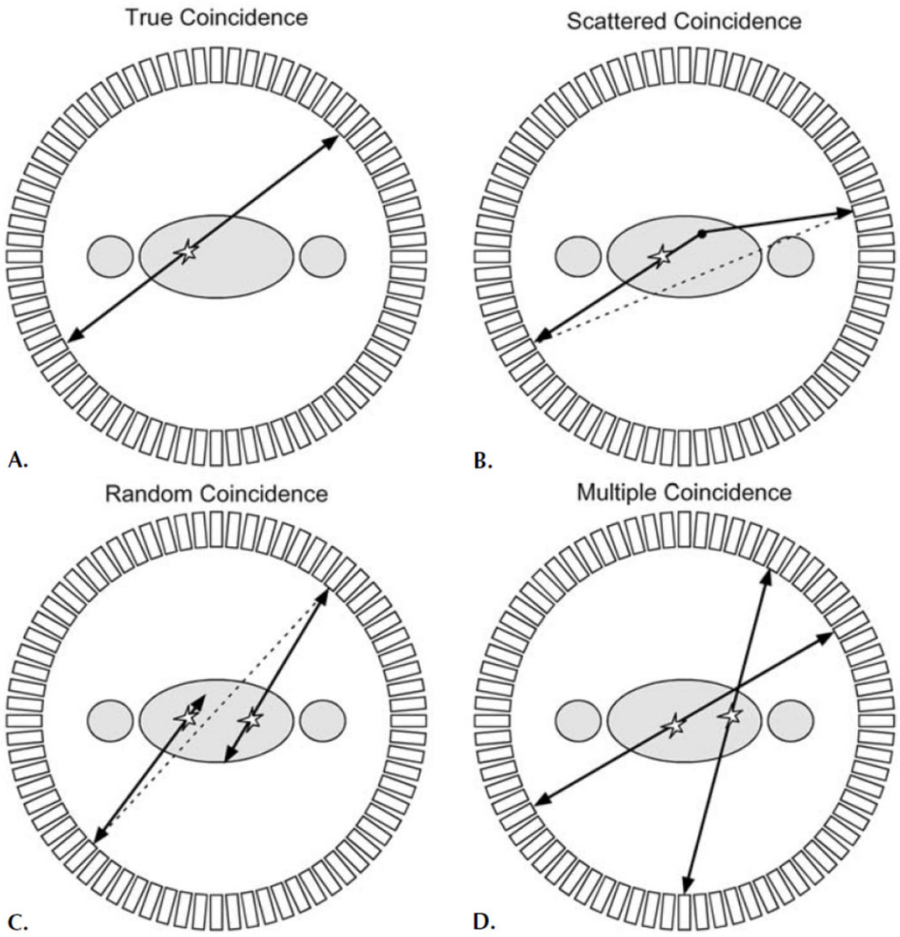

FIGURE 22. Illustration of the four main coincidence event types. A: True coincidence. Both annihilation photons escape the body and are recorded by a pair of detectors. B: Scattered coincidence. One or both of the two annihilation photons interacts in the body prior to detection. This results in a mispositioning of the event. C: Random coincidence: A coincidence is generated by two photons originating from two separate annihilations. These events form a background in the data that needs to be subtracted. D: Multiple coincidence: Three or more photons are detected simultaneously. Due to the ambiguity of where to position the events, these normally are discarded. (Reprinted from *Physics in Nuclear Medicine*, 2nd ed, Cherry SR, Sorenson JA, Phelps ME, W.B. Saunders, New York 1986, with permission from Elsevier.)

Noise Equivalent Count Rate (NECR)

$$NECR = \frac{T^2}{T + S + R}$$

T: true count-rate, S: scattered count-rate, R: random count rate

NECR Properties:

- *Like a Signal / Noise Ratio (Sensitivity only Includes Signal).*
- *Includes Noise from Backgrounds.*
- *Statistical Noise Variance ∝ NECR.*

Maximize NECR to Minimize Image Noise

NECR Depends On Activity Density

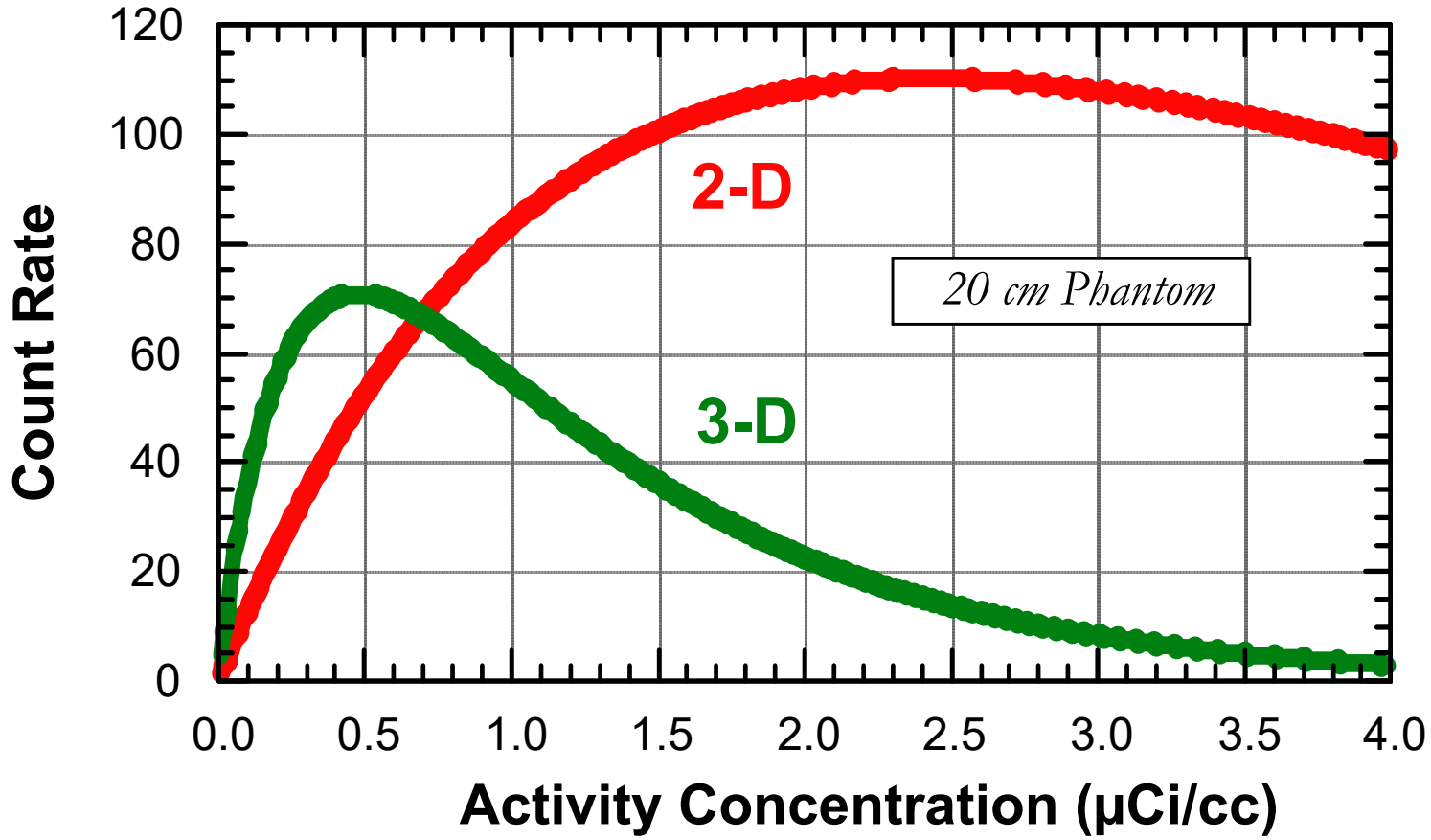

- *At Small Activities, 3-D has Higher NECR*
- *Peak NECR in 2-D > Peak NECR in 3-D*
- *Very Sensitive to Scanner, Definitions, & Phantom Size!*

Coincidene Measurement in PET Image Acquisation

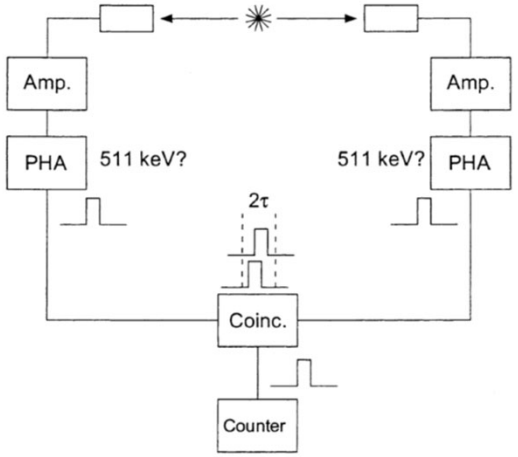

FIGURE 20. Diagram of a basic coincidence circuit. The two scintillation detectors with are connected to individual amplifiers (Amp) and pulse height analyzers (PHA). When a photon interacts in either of the detectors, the signals are amplified and analyzed to determine if the energy is above a certain threshold. If the energy criterion is satisfied, a logic pulse is generated by the PHA. These pulses are fed into a coincidence module (Coinc), which determines if there is an overlap of two pulses from the individual channels. An overlap occurs if both pulses occur within a time period of 2τ (e.g., they differ from each other in time by $\leq \tau$), where τ is the width of the pulse. If this is the case, a coincidence has been detected and the coincidence circuit generates a logic pulse that is fed into a counter for registration of the event. In a PET imaging system, the memory location corresponding to the two detectors in which the interaction occurred is incremented by one.

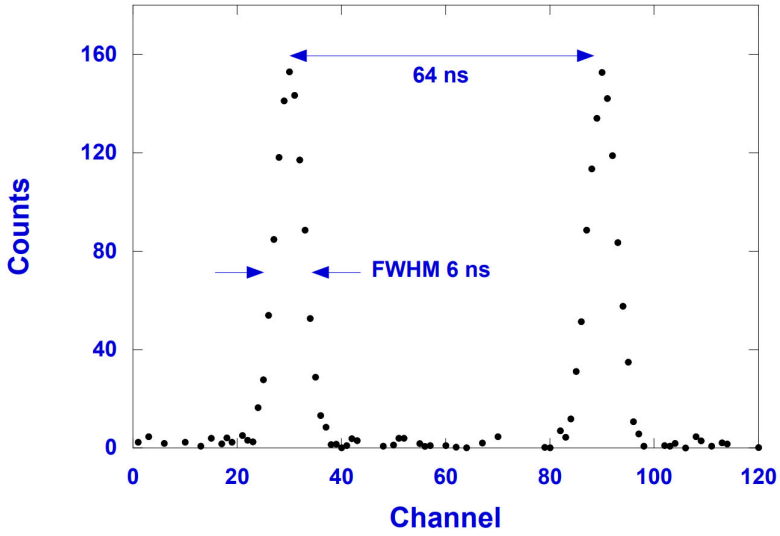

Timing spectrum showing the PHA trigger time variation for a pair of BGO detectors in coincidence. The two peaks corresponds to two separate measurements where an additional delay of 64 ns of the stop pulse for channel-to-time calibration.

Coincidene Measurement in PET Image Acquisation

For a uniform distribution of activity, a formula for the random count rate per ring has been established:

$$C_R = \tau f C_s^2 \qquad \left(\frac{\text{counts}}{\text{sec}} \cdot \frac{\mu\text{Ci}}{\text{cm}^3}\right) \tag{8-2}$$

where C_s is the single count rate for the entire ring, τ is the coincidence resolving time, and f represents the coincidence fraction of a given phantom (which is the ratio of the number of detectors in a fan to the total number of detectors in the ring, each of which is in coincidence with any one of the detectors on the opposite side). The value of f for a ring system is given by

$$f = \left(\frac{2}{\pi}\right)\sin^{-1}\left(\frac{d}{D}\right) \tag{8-3}$$

Fundations of Medical Imaging, Z. H. Cho.

Time-of-Flight PET

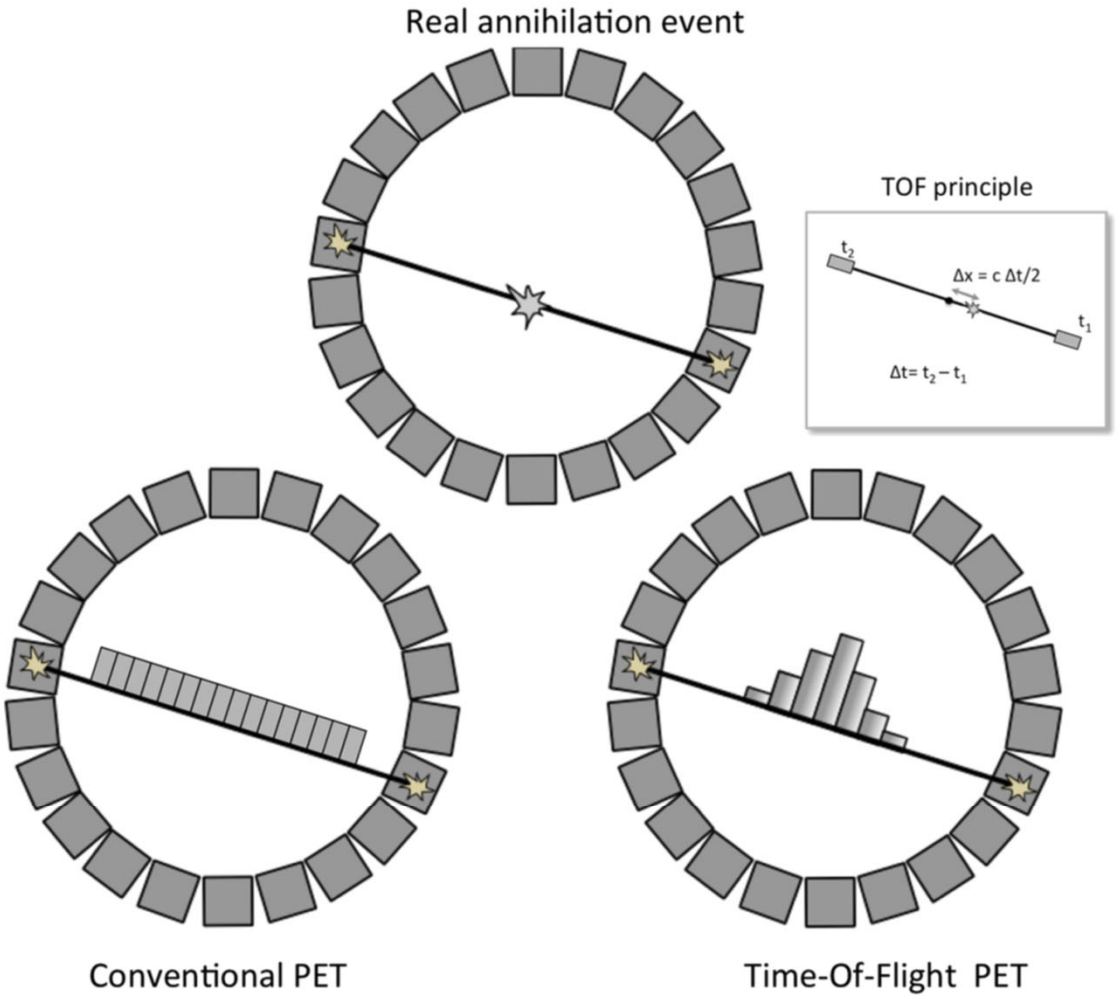

Fig. 1 Compared to conventional PET, the estimated time-of-flight difference (Δt) between the arrival times of photons on both detectors in TOF-PET allows localization (with a certain probability) of the point of annihilation on the line of response. In TOF-PET, the distance to the origin of scanner (Δx) is proportional to the TOF difference via the relation: Δt: $\Delta x = \frac{c\Delta t}{2}$, where c is the speed of light. t_1 is the arrival time on the first detector, and t_2 is the arrival time on the second detector

Eur J Nucl Med Mol Imaging (2011) 38:1147–1157
DOI 10.1007/s00259-010-1711-y

REVIEW ARTICLE

Focus on time-of-flight PET: the benefits of improved time resolution

Maurizio Conti

Table 1 Time resolution, spatial uncertainty and estimated TOF gain for a 40-cm effective diameter patient

Time resolution (ns)	Δx (cm)	TOF NEC gain	TOF SNR gain
0.1	1.5	26.7	5.2
0.3	4.5	8.9	3.0
0.6	9.0	4.4	2.1
1.2	18.0	2.2	1.5
2.7	40.0	1.0	1.0

In particular, the SNR in a TOF image improves with decreasing time resolution Δt (or the corresponding spatial uncertainty Δx) and it is larger for larger patients (being related to the effective diameter D). The TOF SNR is proportional to the non-TOF SNR, through the following relationship [1, 2, 4, 14–20]:

$$SNR_{TOF} = \sqrt{\frac{D}{\Delta x}} \cdot SNR_{non-TOF} \qquad (2)$$

Clinical Benefit of Time-of-Flight PET

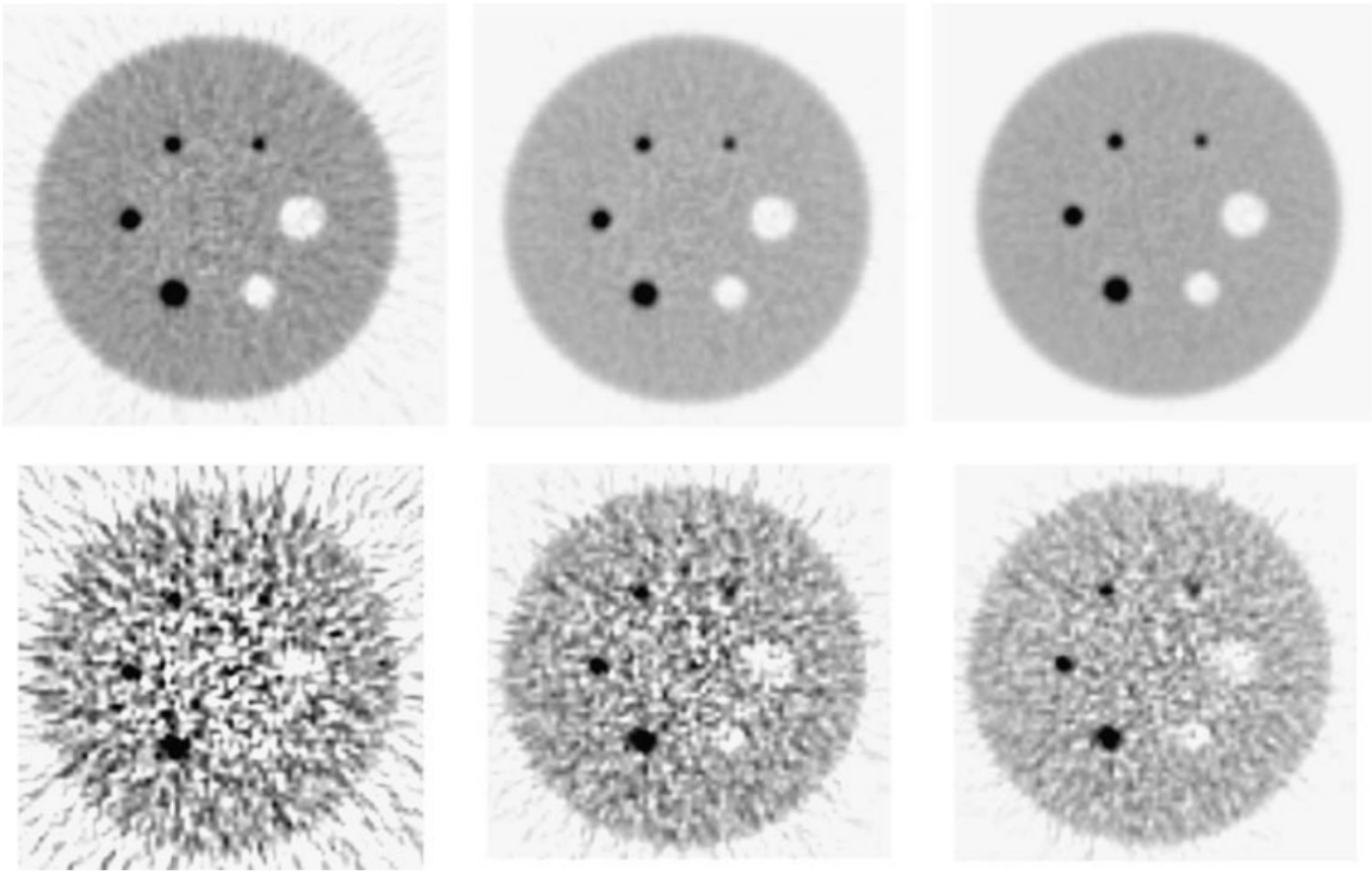

Fig. 7 Monte Carlo simulation of a uniform cylinder with spheres of diameter 10, 13, 17 and 22 mm at a contrast ration of 4:1 and two spheres of diameter 28 and 37 mm filled with water with no activity: high statistics, 356×10^6 counts in the total volume (*top*); low statistics, 10×10^6 counts (*bottom*). Filtered back-projection was used for non-TOF reconstruction (*left*), for TOF reconstruction with 600 ps time resolution (*centre*), and for TOF reconstruction with 300 ps time resolution (*right*)

Clinical Benefit of Time-of-Flight PET

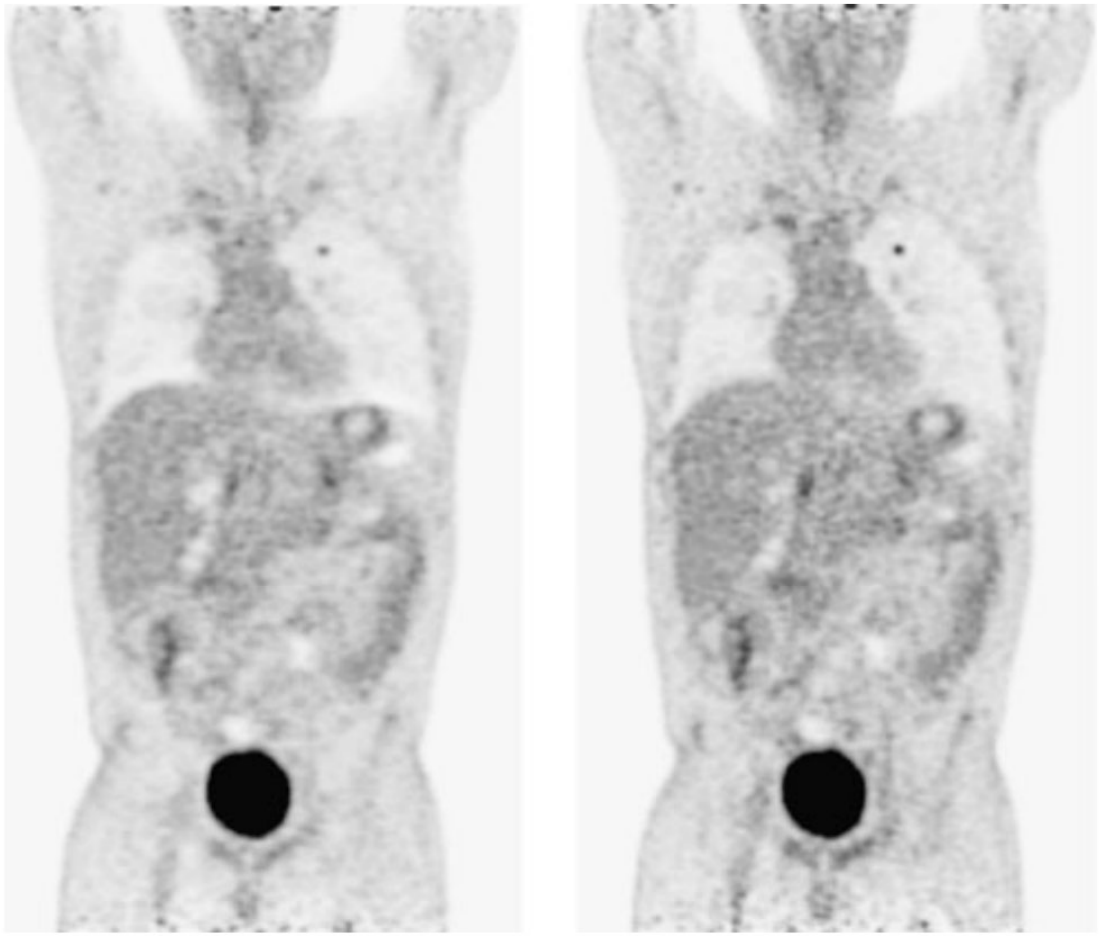

Fig. 1 Coronal images reconstructed from a non-TOF scan (*left*) and a TOF scan (*right*) in a patient with lung cancer. The acquisition time was 3 min per bed position for both images. At the same number of counts, the image quality is better with the TOF reconstruction

Clinical Benefit of Time-of-Flight PET

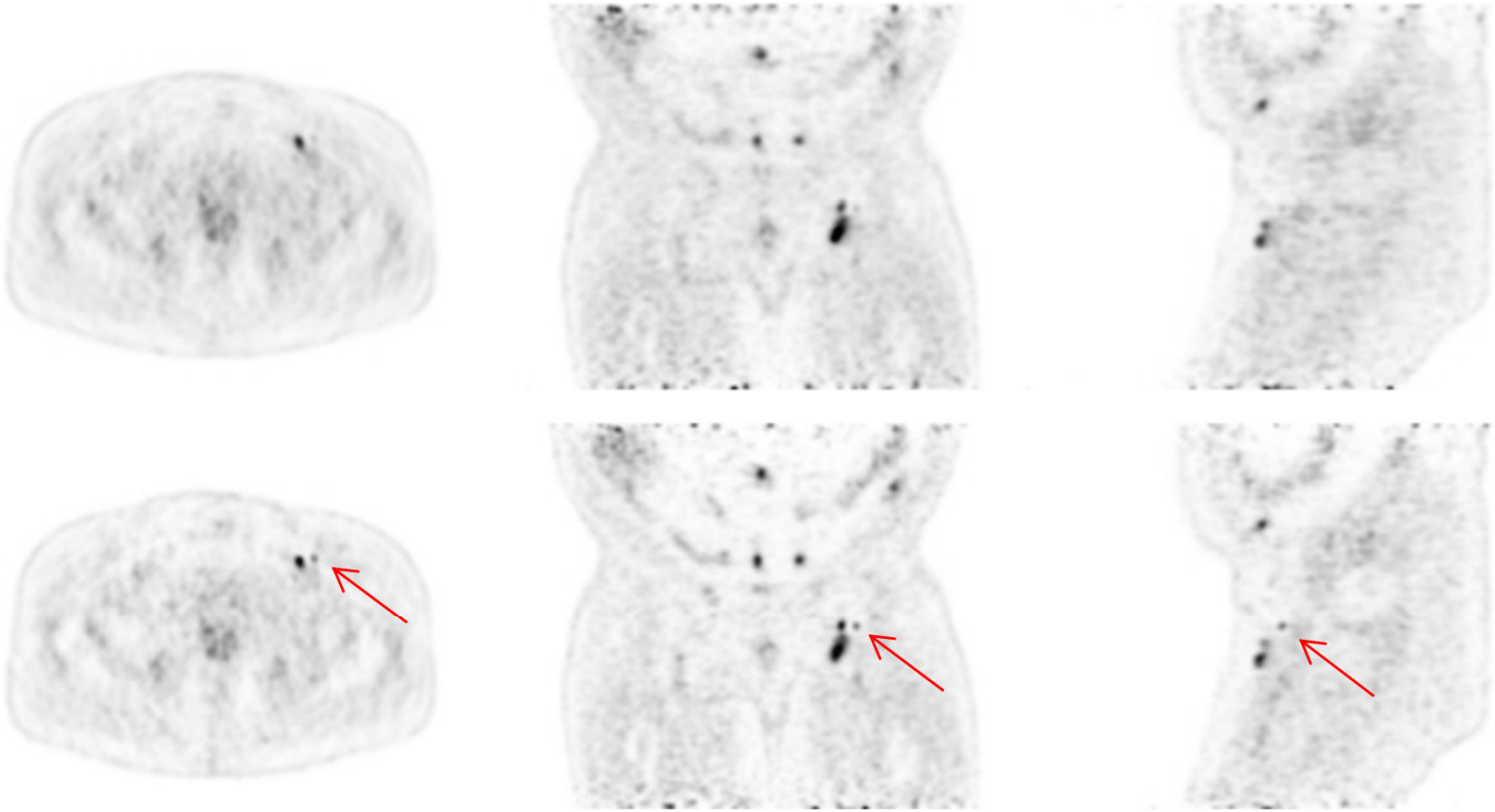

Fig. 3 Transaxial, coronal and sagittal images in a patient with nodules in the pelvic region showing FDG uptake (*top* non-TOF image, *bottom* TOF image). *Arrows* uptake focus not visible in the non-TOF images